Alma Mater Studiorum – Università di Bologna

DOTTORATO DI RICERCA IN

CHIMICA

Ciclo XXXII

Settore Concorsuale: 03/B1

Settore Scientifico Disciplinare: CHIM/03

SPECTROSCOPIC STUDY ON DIVERSE PHOTOCATALYTIC SYSTEMS FOR ORGANIC TRANSFORMATIONS

Presentata da: Ewelina Magdalena Kuna

Coordinatore Dottorato **Supervisore**

Prof. Domenica Tonelli **Prof. Giacomo Bergamini**

Esame finale anno 2020

„Niczego w życiu nie należy się bać, należy to tylko zrozumieć”

Nothing in life is to be feared, it is only to be understood

Maria Skłodowska-Curie

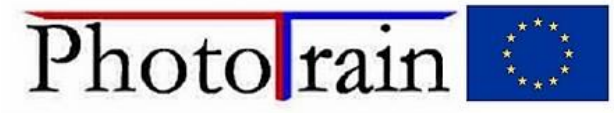

This work was realized with financial support of project (G.A No: 722591) funded by the Marie Skłodowska-Curie Actions of the European H2020 programme, PHOTOTRAIN is an Innovative Training Network (ITN).

Acknowledgements

I gratefully acknowledge the funding received towards my PhD from the PHOTOTRAIN ITN PROJECT realised in the framework of Marie Skłodowska-Curie Action.

Most of all, I would like to thank to my supervisor Prof. Giacomo Bergamini for his guidance, continuous support and possibility to pursue my PhD work in his research group. His immense knowledge, motivation and patience have helped me in all the time of research and writing of this thesis. My sincere thanks also go to my co-supervisor Prof. Paola Ceroni for support and encouragement, which I have received from her since the beginning of my study at the University of Bologna.

I am sincerely thankful to Dr. Francesca Di Maria and Dr. Chiara Gualandi for the fruitful collaboration and their contribution to this work.

I am grateful to Prof. Johan Hofkens and Prof. Maarten Roeffaers, who provided me an opportunity to join their team as intern, and who gave access to the laboratory and research facilities. Without it would not be possible to conduct this research.

I thank all the members of the PHOTOTRAIN project for the stimulating discussions, knowledge sharing and wonderful time we spent together during our meetings, workshops and conferences.

Special thanks go to former and current labmates, especially colleagues for my research group, who created a friendly and helpful atmosphere during my PhD study. I would like to thank for your collaboration and support.

Invaluable thanks to all the international people, who made me feel in Bologna like at home. I appreciate all the good time we had together during last 3 years.

I am utterly grateful to all my colleagues and friends, who made throughout my time during this “PhD journey”. Particularly, thanks to my best friend for his help, good advice and criticism, which helped me to finish writing this thesis.

Last but not the least, I am grateful to my parents, siblings and relatives who remembered me in their prayers for the ultimate success. Particularly, I would like to thank my mother who gave me enough moral support, encouragement and motivation to accomplish my personal goals. Dziękuję!

ABSTRACT

The present doctoral dissertation was dedicated to select and develop an integrated photocatalytic system, which can be applied in organic reactions performed at liquid-liquid (homogenous reaction system) or liquid-solid (heterogenous reaction system) interface inside the microfluidic channels. The scientific strategy included (i) examination of potential photocatalysts upon various reaction conditions, (ii) selection of stable photocatalytic system and (iii) its implementation towards flow photochemistry by design an exemplar prototype of microfluidic devices for chemical transformations. Demonstrated strategy consist of consecutive protocols precisely described in subsequent chapters of this thesis.

First part of the discussion is concentrated on the selection of photoactive organic molecule, which can act as photocatalyst for further organic transformation. The significant efforts have been made to understand all the factors which affect the formation of stable and efficient photocatalytic system. On that basis, benzothiadiazole derivative compound is proposed as an environmentally friendly photocatalyst applicable in a simple dehalogenation and C-C bond formation reactions of thiophene compounds, as well as in photo-controlled polymerization reaction of methacrylate monomers.

Subsequently, to expand the scope of the photoredox catalysis towards flow technologies, the extensive spectroscopic studies on selected photocatalytic system, forming at the liquid-liquid and the solid-liquid interfaces inside the microchannel, were performed. This study allowed to design an exemplar prototype of microfluidic device, which can work upon homogenous and heterogeneous reaction conditions.

At the end, the potential application of inorganic photocatalyst towards flow photochemistry is briefly discussed. The ruthenium ($Ru(bpy)_2CN_2$) complex with cyanide ligands (CN^-) is consider as a potential molecular module that may provide desire architecture of photocatalytic systems, especially under microfluidic conditions due to its self-assembling properties.

Contents

ABSTRACT 6

CHAPTER 1: INTRODUCTION AND THEORETICAL BACKGROUND 10

Introduction 11

Theoretical background 12

1.1 Light and molecule interaction 13

1.2 Electronically excited state 14

1.3 The deactivation processes of excited state and quenching measurement 15

1.4 The energy and electron transfer 18

1.5 Photocatalysis and photoredox catalytic cycle 21

1.6 Photoredox catalyst 22

References: 24

CHAPTER 2: ORGANIC PHOTOREDOX CATALYSIS 25

2.1 Theoretical part 26

2.1.1 Organic photocatalyst 26

2.1.2 Thiophene-based compounds for photocatalytic application 27

2.2 Experimental part I: Selection of reagents 27

2.2.1 Potential organic photocatalyst 27

2.2.2 Sacrificial agent 31

2.2.3 Halogen compounds 33

2.3 Experimental part II: Debromination reaction 35

2.3.1 Light-mediated non-photocatalytic reaction pathway of debromination reaction 37

2.3.2 Side product formation 39

2.3.3 Influence of amine 42

2.3.4 Influence of the photocatalyst in the EDA photoreaction 43

2.3.5 Photocatalytic reaction pathway of debromination reaction 44

2.4 Experimental part III: Coupling reaction 45

2.4.1 Photocatalytic reaction system for C-C bond formation 46

2.4.2 Optimization study 47

2.5 Conclusion 49

Reference: 50

ANNEX 2 51

Annex 2.1 Catalyst selection 51

Annex 2.2 Halogen compounds 52
Annex 2.3 Side product formation 53
Annex 2.4 Influence of amine 55
Annex 2.5 Influence of photocatalyst in the EDA photoreaction 56
Annex 2.6 Photocatalytic reaction pathway of debromination reaction 57
Annex 2.7 Coupling reaction 58
CHAPTER 3: PHOTOPOLYMERIZATION 59
3. Theoretical part 60
3.1.1 Photochemistry in the polymer synthesis 60
3.1.2 Photoinitiated polymerization reaction 60
3.1.3 Photoredox catalysis for polymer synthesis 62
3.1.4 Photo-controlled polymerization 62
3.2 Experimental part 63
3.2.1 Selection of the reagent 64
3.2.2 Mechanistic studies 66
3.2.3 Influence of the light 68
3.2.4 Molecular weight and polydispersity 69
3.3 Conclusion 73
Reference 74
ANNEX 3 75
Annex 3.1 Stability of the photocatalytic system 75
Annex 3.2 Polymerization reaction procedures 75
Annex 3.3 Characterization 76
Annex 3.4 ^{1}H NMR spectra of isolated polymer 78
Annex 3.5 The molecular weight distribution of isolated polymer 79
CHAPTER IV: FLOW PHOTOCHEMISTRY 80
4.1 Theoretical part 81
4.1.1 Basic concepts of flow photochemistry 81
4.1.2 Continuous-flow technology for photocatalytic application 83
4.1.3 Photochemical reactor materials selection 86
4.2 Experimental part 87
4.2.1 Microfluidic channels 87
4.2.2 Liquid-liquid interface formation 87
4.2.3 Channel modification 93

4.2.4 Solid-liquid interface 95
4.2.5 Continuous-flow reaction in the bithiophene immobilized microreactor 97
4.3 Conclusion 99
4.4 Inorganic photocatalytic system: perspectives 100
Reference: 104
ANNEX 4 106
Annex 4.1 Pressure influence 106
Annex 4.2 Fluorescence lifetime calculation 107
Annex 4.3 Profile of fluorescent lifetime and intensity 109
Annex 4.4 Channel modification 110
Annex 4.5 Selection of chromophore immobilization method 111
SUMMARY 112
Chemicals 113
Instruments and photocatalytic reaction setup 115

CHAPTER 1: INTRODUCTION AND THEORETICAL BACKGROUND

Introduction

Inspired by nature, mankind has learned that sunlight is one of the most powerful sources of energy on the Earth. Since then, the conversion of light energy from one form to another became a challenging goal of the modern photochemistry science (Figure 1.1) [1,2]. A comprehensive study of the interaction between light and matter allows to design a wide range of artificial systems in which light energy can be converted into chemical energy *via* a photoinduced electron process [2]. However, the efficiency and stability of the photoactive artificial systems leave a lot to be desired, since the overall photosynthetic process reaches a conversion efficiency of a few percent at best [3]. The effective conversion of light into a usable form of energy is mainly limited due to non-efficient charge separation and poor light harvesting architecture, which can be improved by the proper selection of individual components [4]. Following the key concepts of photochemistry, it is possible to design an artificial system in which selected photoactive components, with precise spatial and energy organization, allow to convert incoming light into exploitable reactive species [4,5].

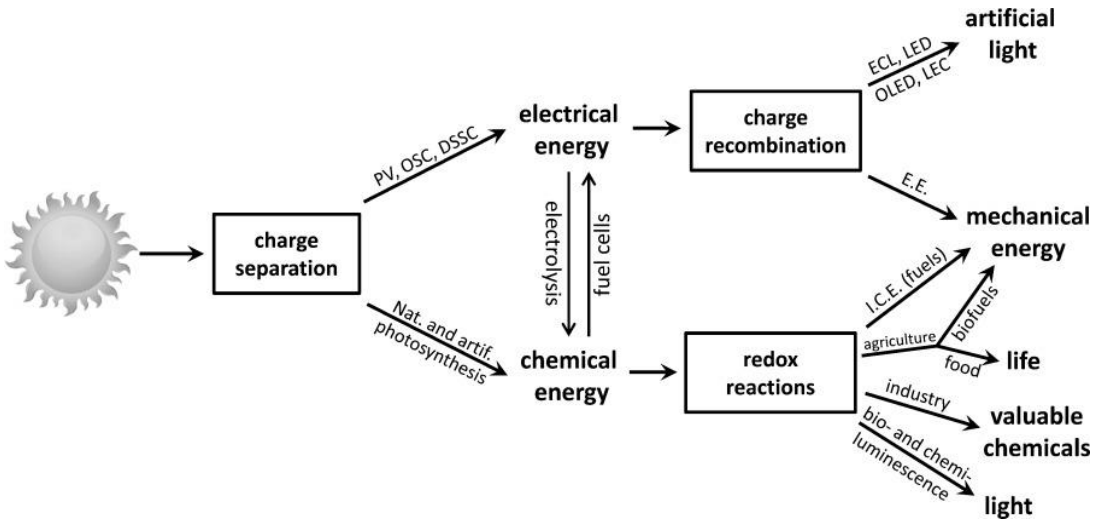

Figure.1.1. Schematic representation of light energy conversion. Reprinted from [2] with permission.

The photoinduced electron transfer chemistry may drive a diverse range of free radicals and radical ions reactions giving complex product mixtures. Hence, the selection of a photoactive molecule, which meets all the requirements to become a photocatalyst,

plays a crucial role in the selective activation of organic reagents that do not absorb the energy of visible light by themselves [6]. Numerous examples show that photoredox catalysis can be successfully applied in sustainable free-radical-mediated processes for organic synthesis (*i.e.* for bond-forming and bond-cleavage) [7]. In these cases, the proper selection of a photoactive catalyst provides high conversion and yield, upon well-selected conditions, and allows to avoid rather toxic and hazardous reagents employed in the classical synthetic methodology [8].

However, the undoubted potential of photoredox catalysis in synthetic chemistry must face some limitations. First of all, the industrial implementation and scale up process may be hindered due to the high cost of the commonly employed transition metal-based photocatalysts (*i.e*. ruthenium/ iridium complexes). Secondly, a homogenous catalytic reaction system requires a remarkable effort to separate the final product and re-cycle the photocatalyst. Finally, due to the short-range light penetration in standard batch reactors, photoinduced redox processes requires special photoreactors (such as flow reactors) to achieve an efficient photon and mass transfer [9].

In order to address these limitations, the presented dissertation is focused on the formation of a photocatalytic system that can be created at the liquid-liquid (homogenous reaction system) or solid-liquid (heterogenous reaction system) interfaces inside a microfluidic channel, starting from the selection of a stable photocatalyst for the organic transformation (*i.e*. reductive dehalogenation, coupling or polymerization reaction).

Therefore, the research goals of this work included: (i) selection of a suitable photocatalyst for organic transformation, (ii) selection of a stable photocatalytic reaction system (iii) study of the photoinduced electron- transfer processes of the selected photocatalytic system upon static (stationary batch system) and dynamic (microfluidic) conditions and (iv) evaluation of the microfluidic prototypes.

Theoretical background

To understand the mechanism of a photocatalytic process is necessary to know some fundamental concepts of photophysics and photochemistry. Nevertheless, since a comprehensive description requires more than one chapter [10], herein a brief overview of the most relevant aspects in the context of photocatalytic applications is described.

The following subsections provide information about: (i) the changes occurring in a molecule upon the absorption of the light; (ii) properties of the molecule upon the light excitation related to its electronically excited state; (iii) intramolecular and intermolecular deactivation processes of excited state which might initiate a photochemical reaction by energy or electron transfer; (iv) the mechanism of photoinduced electron transfer involved in the photocatalytic process and (v) the requirements to make an efficient photocatalyst.

1.1 Light and molecule interaction

A phenomenon in which radiation transfers to matter which traverses some of or all its energy is called absorption (IUPAC definition) [11]. The absorption of a photon can promote a molecule from the ground electronic state to an electronically excited state only if the energy change and the frequency of the light is related to the Bohr equation (1.1) [10]:

$$h\nu = E_f - E_i \tag{1.1}$$

where E_f is the energy of the excited state and E_i is the energy of the ground state. Consequently, the energy gained by light-absorbing molecule causes an electron to be promoted to a higher electronic orbital, changing the electronic structure of the molecule.

The physico-chemical properties of each molecule in its ground state (like the energy content, bond lengths, spatial structure, charge distribution, electron affinity or ionization potential) depend on the electronic structure [12]. Therefore, the molecule in its ground state has different properties than in its excited state.

The electronically excited state has an extra amount of energy and different electronic distribution compared to the ground state and hence might be considered as a new chemical reactive species, which offers a different reaction pathway compare with a classical thermal reaction.

Nevertheless, due to the high energy content, the excited state is an unstable species and hence undergo fast deactivation process, by the photophysical process (in which the excited states of the original molecule leading back to the ground state) or by photochemical processes (with formation of other species) [10].

1.2 Electronically excited state

The photophysical deactivation process of the electronic excited states is illustrated by the Jabłoński diagram (including light absorption; Figure 1.2).

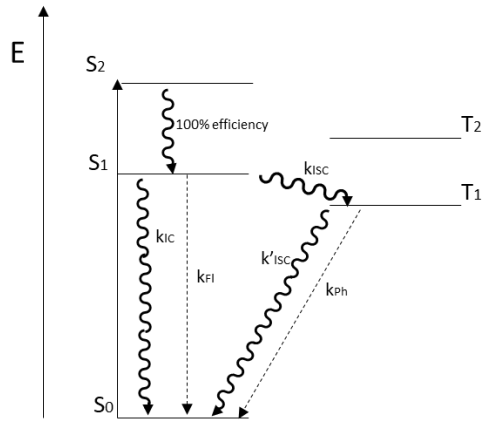

Figure 1.2. Jabłoński diagram for an organic molecule (where: S_n is a singlet state, T_n is a triplet state, k_{ISC} is an intersystem crossing rate constant, k_{IC} is an internal conversion rate constant, k_{FI} is a fluorescence rate constant and k_{Ph} is a phosphorescence rate constant).

The diagram indicates the electronic states (represented by horizontal lines) of a molecule, and transitions between them (represented by the arrows). It is assumed, at least for organic molecules, that the ground state (S_0) of a molecule is a singlet state [10]. Whereas, excited states are either singlets ($S_{n\geq1}$) or triplets ($T_{n\geq1}$). Singlet and triplet states are defined by the total electron spin quantum number[†]. In principle, the transitions between electronic states which have the same spin value (multiplicity) are allowed, while transitions between states of different multiplicity are forbidden. Therefore, the electronic absorption bands (observed in the UV-visible spectrum) of molecules usually correspond to S_0 to $S_{n\geq1}$ transitions.

The transitions between excited states can be induced by **radiative** (absorption or emission) or by **non-radiative processes**. For instance, a molecule in an upper singlet excited state (*i.e*. $S_{n\geq2}$), usually undergoes a rapid and efficient non-radiative deactivation (*i.e.* internal conversion) to the lowest excited singlet state (*i.e*. S_1). This lowest singlet state (S_1) undergo further deactivation *via* three competing processes like: (i) a non-radiative decay to the ground state (*i.e*. internal conversion (k_{IC})); (ii) a radiative decay to the ground state (**called fluorescence** (k_{FI})) and (iii) conversion to the lowest triplet state (*i.e*.

intersystem crossing (k_{ISC})). In its turn, the excited triplet state (T_1) subsequently undergo radiationless deactivation *via* intersystem crossing ($k_{'ISC}$)) or by radiative decay to the ground state (**called phosphorescence** (k_{Ph})) [10].

The photophysical deactivation process proceeds according to first order kinetics, in which the reaction rate depends linearly on the molecule concentration. Hence, the reciprocal of the sum of the first order deactivation rate constants describes one of the most important characteristics of the excited state, the **lifetime (τ)**:

$$\frac{1}{\tau} = k_r + k_{nr} \tag{1.2}$$

where k_r is the rate constant of radiative process and k_{nr} is the rate constant of competitive non-radiative process.

Although, the kinetic constants of the deactivation processes usually cannot be measured directly, the excited state lifetime can be estimated by measuring the decay of a property (*e.g.* emission intensity) which is proportional to the excited state concentration [10,13].

Another measurable quantity, which characterises the probability of a radiative deactivation process like fluorescence or phosphorescence is the **quantum yield (Φ).** The quantum yield is defined as the number of emitted photons relative to the number of absorbed photons and might be described by the following equation [13]:

$$\Phi = \frac{k_r}{k_r + k_{nr}} = k_r \tau \leq 1 \tag{1.3}$$

where k_r is the rate constant of the radiative process; k_{nr} is the rate constant of the competitive non-radiative process and τ is the lifetime.

In other words, the quantum yield could address how exploitable will be an excited state to promote photoinduced processes, whereas the lifetime allows for a careful evaluation of the kinetics of unimolecular and bimolecular processes of the lowest excited states, helping in predicting the photochemical behaviour. Therefore, the **lifetime** and **quantum yield** are very important characteristic, which should be considered during the selection of a suitable photocatalyst (Chapter 2.2.1).

1.3 The deactivation processes of excited state and quenching measurement

The deactivation process of the excited states might occur not only *via* intramolecular processes, which does not cause any change in the chemical composition

(called photophysical processes), but also by a variety of chemical processes. The chemical processes occur with (*e.g*. decomposition reaction) or without changes (*e.g*. isomerisation reaction) in the chemical composition of the molecule and usually, they are not shown in the Jabłoński diagrams [10].

In general, three unimolecular processes like radiative deactivation (k_r), non-radiative deactivation (k_{nr}), and chemical reaction (k_p), might compete for the deactivation of any excited state of a molecule as shown in Figure 1.3.

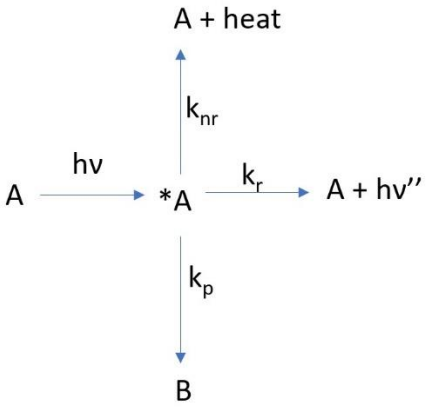

Figure 1.3. Schematic representation of the intramolecular deactivation processes of the excited state (*A).

Furthermore, deactivation process of excited state might also take place by intermolecular process. The intermolecular deactivation process of the excited state (A*) occurs by the electron or energy transfer, which might take place *via* encounters of another molecule (called quenchers) (Figure 1.4A) or by an interaction with a nearby component unit of the same molecular system (*i.e.* in a supramolecular system) (Figure 1.4B) [10].

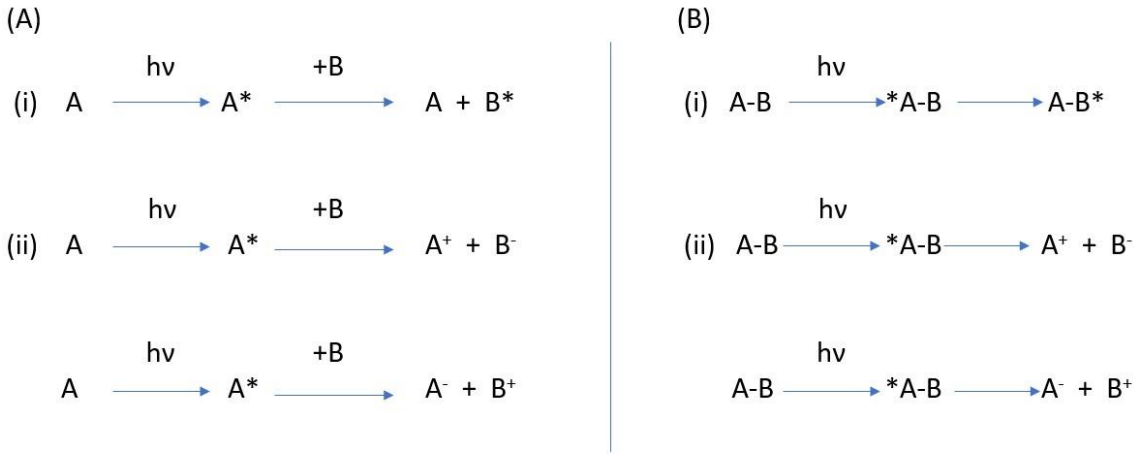

Figure 1.4. Schematic representation of the deactivation processes: (A) in a bimolecular system consisting of molecule A and molecule B as a quencher; (B) in a supramolecular system consisting of A and B component units. In both cases, the deactivation process is induced by (i) energy transfer or by (ii) electron transfer.

As shown in Figure 1.4A, the energy transfer results in the formation of an excited state (B*), which might further undergo deactivation process, including luminescence (called sensitized luminescence) and chemical reaction (called sensitized reaction). Whereas, electron transfer is rather involved in an oxidation or reduction of the excited state. In both cases, the luminescence of the species (A*) is quenched.

The term ''quenching'' refers to any deactivation process that reduces the radiative quantum yield and hence results in the reduced fluorescence of molecule [13]. However, here is discussed in the context of bimolecular reaction taking place in solution. The molecular interaction between molecules can be dynamic (if caused by collisional quenching) or static (if caused by the complex formation). In static quenching, the complex formed between molecule and quencher is non-fluorescent. In the dynamic quenching process, the quencher diffuses towards the excited state species and undergoes bimolecular reaction, in which the molecule returns to its ground state. To identify the nature of the quenching process, time-resolved spectroscopic methods (*e.g.* single photon lifetime measurements) and steady-state techniques (*e.g*. fluorescence spectroscopy) are commonly applied. Nevertheless, the static quenching is most clearly demonstrated using steady-state techniques. Since, the static interaction between molecule and quencher does

not decrease the decay time of the uncomplexed chromophore (only the unquenched chromophore is observed) [13,14].

The nature of the quenching process provides important information about the photocatalytic reaction system and allows to understand the interaction between the photocatalyst and the other reagents, therefore the quenching measurements are further discussed in the Chapter 2.2.3.

1.4 The energy and electron transfer

The energy and electron transfer processes are the driving force for photochemical reactions. Hence, understanding the nature of these process allows to design an efficient photocatalytic system. Nevertheless, since the great majority of organic substrates absorb at higher energy (the energy transfer is forbidden), the photocatalytic reactions are mainly driven by the electron transfer process [12,15].

The photoinduced electron transfer process requires an electronic interaction between molecules and obeys the same rules, which describe an electron transfer between the ground state (Marcus equation and related quantum mechanical elaborations) [10,15].

As a reminder, the favourable thermodynamics of electron-transfer process occurs when the free energy of electron transfer $\Delta G<0$ [15,16]. Therefore, the redox potential of molecule A (in its excited state (A*)) and redox potential of molecule B (in its ground state) are crucial parameters which determine an efficient photoinduced electron transfer reaction (Figure 1.5).

For a ground state electron transfer reaction in solution (Figure 1.5), the free energy change is obtained from the oxidation potential of the donor (A), and the reduction potential of the acceptor (B). Whereas, for the electron transfer reaction in which an excited state (A*) is involved, an extra free energy contribution should be considered [10].

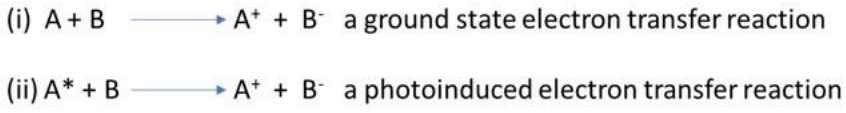

Figure 1.5. Scheme of electron transfer reaction in bimolecular system involving (i) ground and (ii) excited state of molecule A.

The redox potential of an excited state couple may be calculated from the potential of the related ground state couple and the one-electron potential corresponding to the zero-zero excited state energy ($E_{o,o}$), according to the equations [10,16]:

$$E^*_{ox}\left(A^{\bullet+}/_{A^*}\right) = E_{ox}\left(A^{\bullet+}/_{A}\right) - E_{o,o} \quad (1.4)$$

$$E^*_{red}\left(A^{*}/_{A^{\bullet-}}\right) = E_{red}\left(A/_{A^{\bullet-}}\right) + E_{o,o} \quad (1.5)$$

where E^*_{ox} is oxidation potential of excited state, E^*_{red} is reduction potential of excited state, E_{ox} is oxidation potential in the ground state and E_{red} is reduction potential in the ground state.

The free energy of photoinduced electron transfer (ΔG_{PET}) (after the omission of the electrostatic work term *w*, which accounts for solvent-depended Coulombic interactions) might be defined by the equations (1.5 and 1.6). For a photoinduced reaction involves reduction of the excited state (A*) [16]:

$$\Delta G_{PET} = -N_A e\left(E^*_{red}\left(A^{*}/_{A^{\bullet-}}\right) - E_{ox}\left(B^{\bullet+}/_{B}\right)\right) \quad (1.6)$$

where N_A- Avogadro's number; e is the electronic charge; E_{ox} is oxidation potential of molecule B. For a photoinduced reaction involves oxidation of the excited state (A*):

$$\Delta G_{PET} = -N_A e\left(E_{red}\left(B/_{B^{\bullet-}}\right) - E^*_{ox}\left(A^{\bullet+}/_{A^*}\right)\right) \quad (1.7)$$

where N_A- Avogadro's number; e is the electronic charge; E_{red} is reduction potential of molecule B.

To simplify, a photoinduced oxidation reaction of molecule B is possible, when reductive potential of molecule A in its excited state (E^*_{red}) is more positive than oxidation potential of molecule B (E_{ox}). Similarly, a photoinduced reduction reaction of B might occur when the oxidative potential of molecule A in its excited state (E^*_{ox}) is more negative than reductive potential of B (E_{red}) [16].

For a reversible redox process, the redox potential values might be simply measured using electrochemical techniques. Whereas, for an irreversible process, the direct experimental measurements are not possible. In this case, the redox potential might be estimated from other parameters. Nevertheless, is difficult to predict if the actual electron transfer will occur under the selected experimental conditions [12].

In practice, the simplest way to estimate if an efficient electron transfer between the molecules takes place is the fluorescence quenching measurement. For the photoinduced electron transfer process, quenching measurements allow to estimate the reaction pathway. Especially, in the case where the efficient electron transfer occurs between the photocatalyst and more than one reagent. For instance, if the photocatalyst in its excited state might trigger an oxidation reaction of substrate A and a reduction reaction of substrate B (or both in redaction reaction), the Stern-Volmer study gives important information about the bimolecular quenching constant. Since, the bimolecular quenching constant determines which reaction is dominant, Stern-Volmer study will be further discussed to predict a photochemical reaction pathway (Chapter 2.2.3).

1.5 Photocatalysis and photoredox catalytic cycle

The term “photocatalysis” might be referred to any reaction that requires the simultaneous presence of a catalyst and light [10]. In principle, the catalyst is a molecule which increases the rate of a chemical reaction without undergoing any permanent chemical change and is restored at the end of reaction [17]. In a photocatalytic reaction system, catalyst (C) absorbs the light, and in its excited states (C*) activates the substrates *via* energy or electron transfer [10,17]. Nevertheless, as previously mentioned, a photoinduced electron transfer process is involved more frequently in the photocatalytic reactions than energy transfer process.

Photocatalyst might undergo oxidation or reduction reaction (Figure 1.6), which results in the formation of product X` and modified (oxidized or reduced) catalyst C’ [14]. These two reactive species X` and C` diffuse away from each other, however (if any of them cannot escape the solvent cage fast enough), back electron transfer reaction may take place and stop desired chemical transformation [14,15]. Once formed, X` is not a final reaction product and might undergo secondary reaction (*e.g.* with other substrates) before it ends in stable products P_X. To close catalytic cycle and recover catalyst, C` must react with an intermediate of the reaction or another molecule Y (called sacrificial agent). The reaction with the sacrificial agent provides mainly side products, where in the ideal case both P_X and P_Y are high value-added compounds [14].

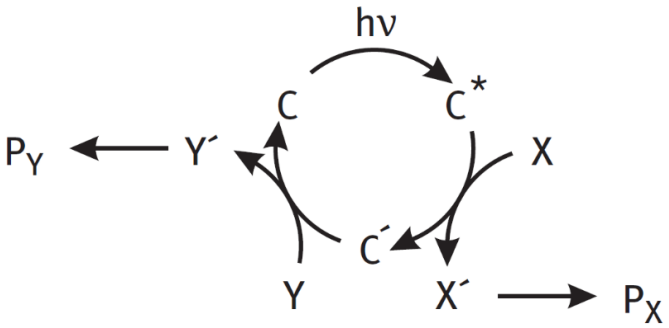

Figure 1.6. Photocatalytic reaction cycle. Reproduced from [14] with permission.

The photochemical synthetic strategy is limited to reagent which can absorb light. Therefore, if any of reagent cannot absorb the light addition of photocatalyst is required.

1.6 Photoredox catalyst

A suitable photocatalyst for photoredox transformation should: (i) strongly absorbs the light in the required spectral region, (ii) be stable upon reaction conditions, (iii) have a prolonged lifetime of excited state in the range nano- to microseconds, (iv) exhibit a reversible redox behaviour with redox potential of ground and excited state efficient for given reaction and (v) should be simply tuned by synthetic modifications in order to tailor its reactivity [15].

Not surprisingly, among commonly applied photocatalysts we can distinguish a wide range of the photoactive transition metal complexes (like ruthenium (Ru), iridium (Ir) or chromium (Cr)) (Figure 1.7), which meet all the criteria mentioned above.

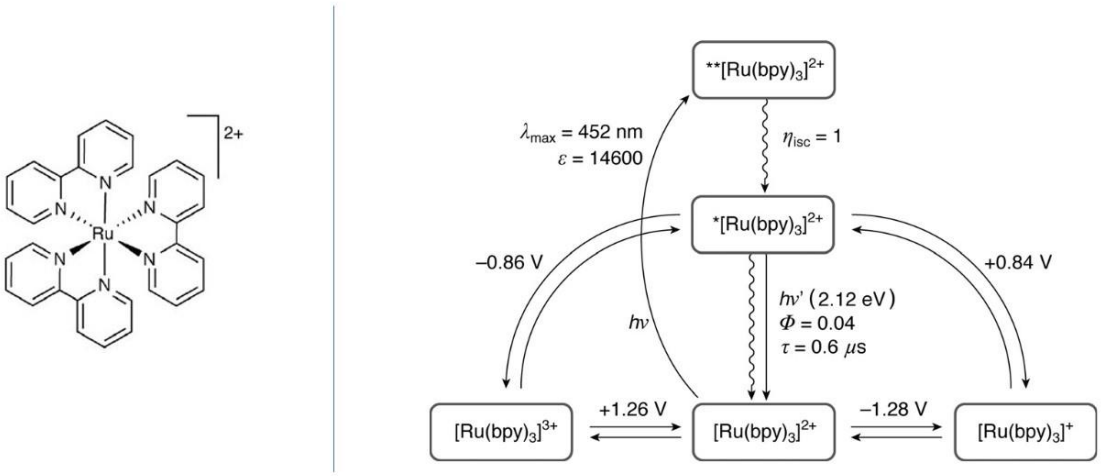

Figure 1.7. Example of a transition metal complex based on ruthenium bipyridine $[Ru(bpy)_3]^{2+}$ as suitable photocatalyst; (**[$Ru(bpy)_3]^{2+}$ indicates the spin-allowed excited state reached by the absorption of light and *$[Ru(bpy)_3]^{2+}$ the lowest spin-forbidden luminescent excited state). Reproduced from [18] with permission.

The ruthenium metal complexes are probably the most common photoactive transition metal complexes applied towards photocatalytic transformation. Their phosphorescence quantum yield efficiency reaches almost 100% [15,19] and the lifetime of excited state persists long enough to perform a photocatalytic reaction (approximately from 300ns to 6μs) [20]. Additionally, the ruthenium photocatalysts are stabile upon

various reaction conditions and display a reversible redox behaviour. The redox potentials of these metal complexes (of both the ground and excited states) are usually broad enough to provide an oxidation and reduction transformation of various compounds (Figure 1.7) [21,22]. Whereas, the electrochemical potential might be easily adjusted by the proper selection of metal and ligands. In most cases, the electron donating ligands provide more facile oxidation of metal center and in opposite electron withdrawing ligands facilitate its reduction [23]. The ligand exchange allows to control not only electrochemical and optical properties but also self-assembling properties of photoactive metal complex. This feature will be further discussed (Chapter 4.4), considering their potential application towards flow photochemistry inside the microchannel.

Although, the role of the transition metal complexes in photocatalysis is undoubted, their further catalytic application is questioned due to a high cost and toxicity of metals [24]. Consequently, enormous efforts have been made to scope the field of photoactive organic dyes that might act as an alternative class of photoredox catalysts (Chapter 2).

References:

[1] G. Ciamician, *Science*, 1912, 36(926), 385.

[2] V. Balzani, G.Bergamini, P. Ceroni, *Angew. Chem.*, 2015, 54, 11320.

[3] T.P.J. Krüger, R. Grondelle, *J Phys B-At Mol Opt.*, 2017, 50(13), 1320.

[4] C.C. Chua, D.M. Bassani, Photochem. *Photobiol. Sci*., 2008, 7, 521.

[5] S. Archer, J.A. Weinstein, *Coord. Chem. Rev*., 2012, 21-22, 2530.

[6] C. Stephenson, T. Yoon, *Acc. Chem. Res*., 2016, 49 (10), 2059.

[7] D. Staveness, I. Bosque Corey, R. J. Stephenson, *Acc. Chem. Res*., 2016, 49, 10229.

[8] C.D. Mc Tiernan, S.P. Pitre, J.C. Scaiano, *ACS Catal*., 2014, 411, 4034.

[9] T.V. Gerven, G. Mulc, J. Moulijn, A. Stankiewicz, *Chem Eng Process*., 2007, 46, 781.

[10] V. Balzani, P. Ceroni, A. Juris, (2014), *Photochemistry and Photophysics: Concepts, Research, Applications,* Wiley-VCH.

[11] A. D. McNaught, A. Wilkinson. Blackwell (1997), *Compendium of Chemical Terminology,* Scientific Publications, Oxford.

[12] V. Balzani, G.Bergamini, P. Ceroni, *P. Rend*. *Fis. Acc. Lincei*, 2017, 28, 125.

[13] J.R. Lakowicz, (2006), *Principles of Fluorescence Spectroscopy*, Springer US.

[14] B. Konig, (2013), *Chemical Photocatalysis*. De Gruyter.

[15] D. M. Arias-Rotondo, J.K. McCusker, *Chem. Soc. Rev*., 2016 ,45, 5803.

[16] N.A. Romero, D.A. Nicewicz, *Chem. Rev.*, 2016, 116, 1710075.

[17] C. Michelin, N. Hoffmann, *ACS Cata*l., 2018, 8, 12046.

[18] V. Balzani, A. Juris, *Coord. Chem. Rev*., 2001, 211, 97.

[19] N. Sutin, C. Creutz, *Pure Appl. Chem*., 1980, 52, 2717.

[20] A. Juris, V. Balzani, F. Barigelletti, S. Campagna, P. Belser, A. von Zelewsky, *Coord. Chem. Rev.*, 1988, 84, 85.

[21] J.M.R. Narayanam, C.R.J. Stephenson, *Chem. Soc. Rev.*, 2011, 40, 102.

[22] M.H. Shaw, J. Twilton, D.W. C. MacMillan, *J. Org. Chem*., 2016, 81, 6898.

[23] J.W. Tucker, C.R.J. Stephenson, *J. Org. Chem*., 2012, 77, 1617.

[24] C. Li, Y. Xu, W. Tu, G. Chenb, R. Xu, *Green Chem*., 2017, 19, 882.

[†] comment: *singlet state having a total electron spin quantum number equal to 0; triplet state having a total electron spin quantum number of 1*

CHAPTER 2: ORGANIC PHOTOREDOX CATALYSIS

2.1 Theoretical part

2.1.1 Organic photocatalyst

Organic chromophores (Figure 2.1) have gained increasing attention in the photoredox catalysis, since they are considered as a green alternative to inorganic photocatalysts (*i.e.* toxic and expensive transition metal complexes). The structural diversity of organic chromophores provides a wide range of diverse photophysical and electrochemical properties and hence influences their reactivity in the photoinduced electron transfer reactions. Consequently, organic chromophores allow to perform a broad spectrum of chemical transformation in similarity to their metal counterparts [1]. Furthermore, due to the low cost and accessibility of photoactive organic dyes [2], the industrial implementation and scale up process of photocatalytic reaction system are much more affordable. Nevertheless, some of these organic chromophores might exhibit limited photocatalytic stability, due to prolonged exposure to the irradiation and chemical reagents [3,4]. Hence, selection of suitable reaction conditions is the key to obtain stable and efficient photocatalytic systems.

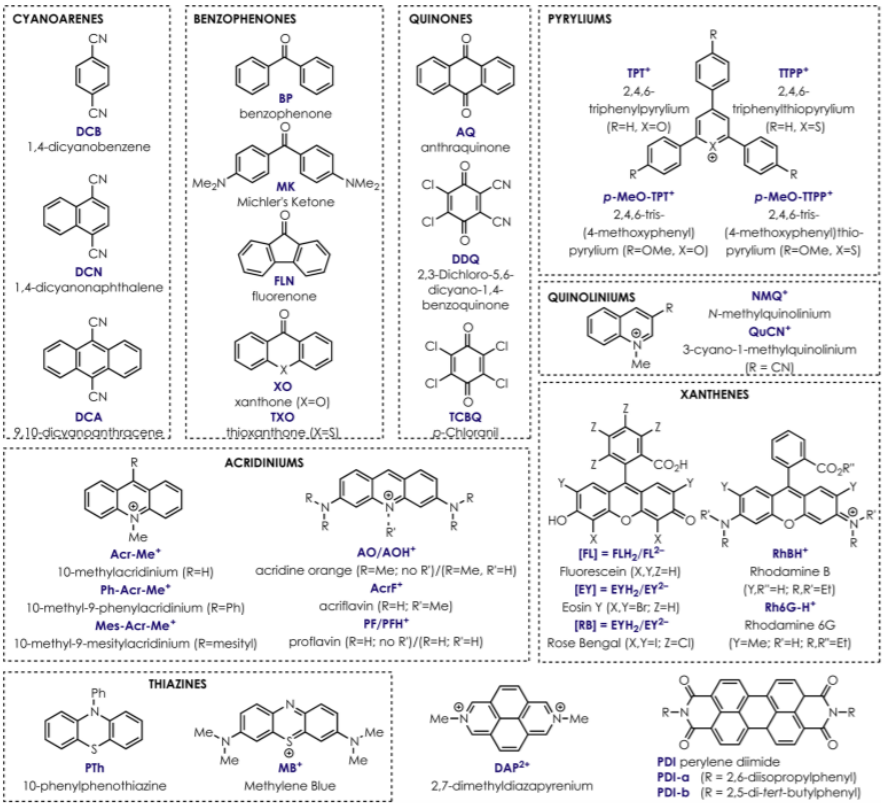

Figure 2.1. Organic chromophores commonly applied in the photoredox catalysis. Reprinted with permission from [1]. Copyright (2016) American Chemical Society.

2.1.2 Thiophene-based compounds for photocatalytic application

Thiophene-based derivatives belong to the class of heterocyclic sulfur compounds displaying properties of organic semiconductors (*i.e*. charge conduction) and chromophores (*i.e*. light-harvesting properties). Therefore, thiophene-based materials like oligomers or polymers are commonly applied in a wide range of fields from organic solar cells, light emitting diodes to fluorescent markers for biological application. Importantly, the structure of thiophene-based compounds might be simply modified by the ring functionalization, where their synthesis leads to desired characteristic [5]. Flexible design allows to tune the photophysical and electrochemical properties and hence control the photocatalytic activity.

Nevertheless, the amount of scientific papers related to implementation of thiophene-based compounds towards photoredox catalysis is rather limited. In 2014, the potential application of thiophene derivatives (such as α-sexithiophene) towards reductive dehalogenation of vicinal dibromide compounds was described by Scaiano [6,7]. Further studies on the organic semiconductors (like benzothiadiazole derivatives) have been performed by Zhang et al. [8]. As is demonstrated, the suitable structural design of benzothiazole compounds allows to provide a new class of metal-free photocatalyst, which photocatalytic activity towards debromination and coupling reactions is reported in detail in the corresponding references [8,9,10]. Those examples were considered as a good motivation for further work on the potential application of thiophene compounds in the photoredox catalysis.

2.2 Experimental part I: Selection of reagents

2.2.1 Potential organic photocatalyst

To explore the possibility of using a metal-free catalyst, which possess photophysical and electrochemical properties suitable for photoredox catalysis, an extensive study on selected thiophene derivatives (Figure 2.2) was carried out.

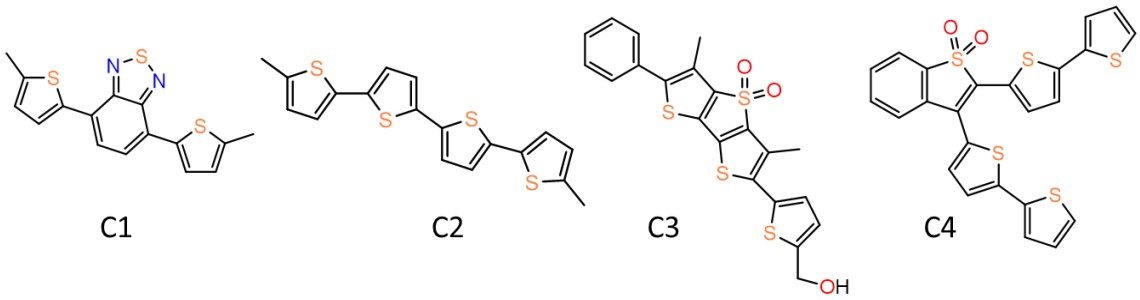

	Name of compound
C1	4,7-bis(5-methylthiophen-2-yl)benzo[c][1,2,5]thiadiazole
C2	5,5'''-dimethyl-2,2':5',2'':5'',2'''-quaterthiophene
C3	2-(5-(hydroxymethyl)thiophen-2-yl)-3,5-dimethyl-6-phenyldithieno[3,2-b:2',3'-d]thiophene 4,4-dioxide
C4	2,3-di([2,2'-bithiophen]-5-yl)benzo[b]thiophene 1,1-dioxide

Figure 2.2 Potential organic photoactive catalyst. Synthesized by Dr. Francesca Di Maria (CNR-ISOF, Bologna, Italy).

Initially, the absorption and emission spectra of the selected compounds were registered in acetonitrile solution to identify the maximum absorption (λ_{max}) and emission (λ_{em}) wavelengths. To describe how efficiently the photoactive molecule absorbs the light at a given wavelength, the molar absorption coefficient (ε) was calculated based on the Lamber-Beer law:

$$A = ln\frac{I_0}{I} = \varepsilon * l * C \quad (2.1)$$

where A – is absorbance, I_0 – is the intensity of light incident upon sample cell, I – is the intensity of light leaving sample cell, l – is the length of sample cell and C – is the concentration of the compound.

Secondly, fluorescence lifetime (τ) of the organic dyes were measured using a time correlated single photon counting (TCSPC) technique (Table 2.1), where all the experiments were carried out at room temperature on deareated acetonitrile solution to avoid quenching process by molecular oxygen. The lifetime (τ) value was calculated using the single-exponential decay based on the following equation:

$$I = I_0 + Ae^{\frac{-t}{\tau}} \quad (2.2)$$

where I- is the intensity at time t, I_0- is the initial intensity, A- is a normalization term (the pre-exponential factor and t - is the time at which the intensity has decayed to $1/e$ of the original value.

Table 2.1. Photophysical characterization of organic dyes.

Compound	Lifetime (τ)	Maximum absorption Wavelength (λ_{max})	Emission wavelength (λ_{em})	Molar absorption coefficient (ε)
	[ns]	[nm]	[nm]	[$cm^{-1}M^{-1}$]
C1	**14.72**	**310/460**	**590**	**12983**
C2	1.49	356	469	24000
C3	6.13	276/425	540	20079
C4	1.35	316/426	530	11900

Since, the selected compounds exhibited a high molar absorptivity in the UV-Vis range (320-490 nm) and a strong emission in the visible range (420-720 nm) (Annex 2.1), all of them were considered as a potential photocatalyst and consequently tested under various reaction conditions. The absorption and emission spectra of the organic dyes were monitored during irradiation to estimate their stability in the presence of other reagents. Keeping in mind a further application of examined photocatalytic system towards C-C bond formation, acetonitrile and toluene were selected as solvents which tend to favor coupling reaction.

Performed experiments indicated that irradiation of compound (C2) and compound (C3) leads to their decomposition in an aprotic polar media such as acetonitrile (Annex 2.1), which limited their further application in the selected photocatalytic system. Especially, the potential application in microfluidic devices (fabricated using polydimethylsiloxane; referred in Section 4.1.3), which require a polar reaction media to carry out chemical transformations. Nevertheless, both compounds can still be considered as potential photocatalysts, since they are stable in non-polar solvents as toluene. The compounds (C1) and (C4) exhibit extended stability under irradiation in both solvents.

Nevertheless, only compound (C1) has a prolonged lifetime of the excited states, which is a crucial parameter determining the final performance of the photocatalytic system. The prolonged lifetime of excited state results in higher probability to encounter and be quenched by the other regents and, consequently, increase efficiency of the photocatalytic activity. Hence, among the potential candidates **compound (C1)** *i.e.* the *4,7-*

bis(5-methylthiophen-2-yl)benzo[c][1,2,5]-thiadiazole (hereafter called **T_3BTCH_3**) was selected as promising metal-free photocatalyst.

As shown in Figure 2.3, the intensity decay profiles of T_3BTCH_3 do not exhibit any changes in the aerated and non-aerated solution, indicating that the excited state of T_3BTCH_3 is not quenched in the presence of molecular oxygen. Consequently, T_3BTCH_3 does not decrease the potential photocatalytic activity in the presence of air, allowing its application towards scale up processes, where the maintenance of inert atmosphere is challenging.

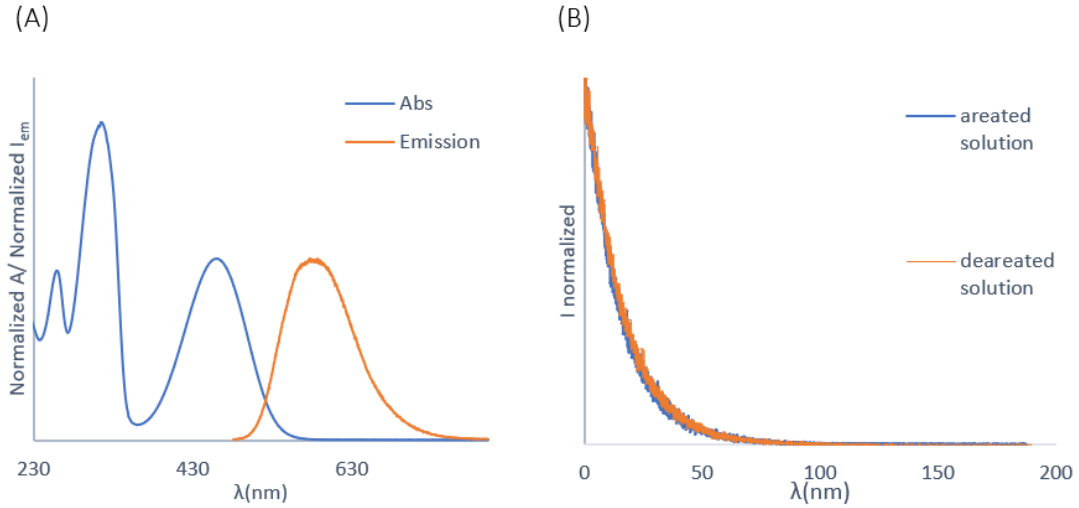

Figure 2.3. (A) Normalized absorption and emission spectra of T_3BTCH_3 (*4,7-bis(5-methylthiophen-2-yl)-2,1,3-benzothiadiazole)* in ACN (B) Fluorescence delay spectra of T_3BTCH_3 collected at the maximum fluorescence.

To define how efficiently the selected photocatalyst converts the excitation light into fluorescence, the quantum yield of T_3BTCH_3 was calculated using the relative method with anthracene (ϕ_{em} = 0.27; λ_{em}=357nm), according to equation:

$$QY = QY_{ref} \frac{\eta^2}{\eta_{ref}^2} \frac{I}{A} \frac{A_{ref}}{I_{ref}} \quad (2.3)$$

where QY - represents the fluorescence quantum yield, I - is the absorption intensity, A - is the area under fluorescence intensity, and η - is the refractive index of the solvent (etanol η=1.3421; acetonitrile η= 1.3617).

The high value of quantum yield (estimated at **ϕ= 0.83**) indicates favourable radiative deactivation (discussed in Chapter 1.2).

Finally, since the electrochemical potential (-1.15eV/ +1.12eV vs. SCE) of T_3BTCH_3 was found [10] sufficient to carried out oxidative and reductive transformations, further photocatalytic activity of T_3BTCH_3 was examined towards reductive dehalogenation and coupling reaction.

2.2.2 Sacrificial agent

The formation of a high-efficient photocatalytic system starts with the careful selection of reagents, where at least one of the substrates should possess strong tendency to accept or to donate electrons towards an excited state of the photocatalyst (PC*). If any of the substrates cannot provide an efficient electron transfer, the addition of a sacrificial quencher (Q) is required. The sacrificial agent can act as electron donor or electron acceptor and provide reduced ($PC_{red}^{\bullet-}$) or oxidized ($PC_{ox}^{\bullet+}$) photocatalytic species, which further interact with individual reaction reagents (D/A) closing the whole catalytic cycle (Figure 2.4) [11].

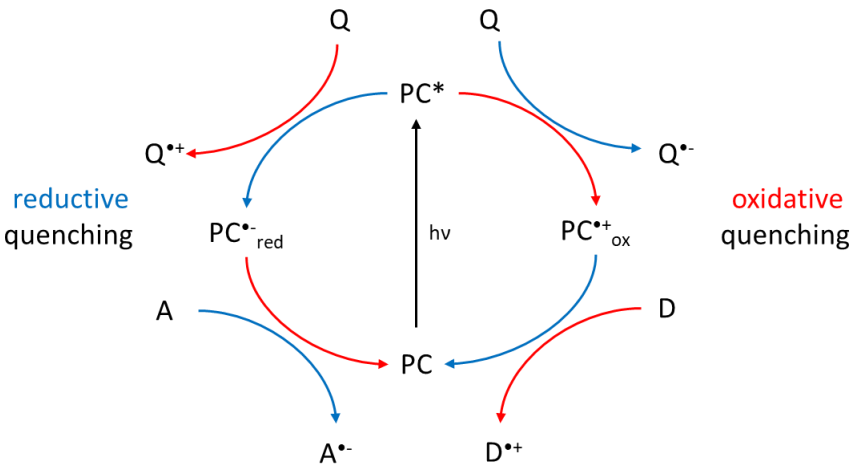

Figure 2.4. Scheme of a photoredox catalytic cycle. The oxidative cycle is shown on the right; the reduction cycle is shown on the left (PC is a photocatalyst, Q is a quencher, D is an electron donor, A is an electron acceptor). Reproduced with permission [12].

As previously discussed (Chapter 1.4), suitable fitting between the redox potential of sacrificial agent (measured in the ground state) and the redox potential of photocatalyst in its excited state, is the key step to provide an efficient electron transfer and perform a photocatalytic reaction. In practical terms, even if the redox potential of the compounds is

not well-known, the effective photoinduced electron transfer, between a sacrificial agent and the excited state of the photocatalyst, might be estimated by fluorescence spectroscopy (since an efficient fluorescence quenching process is provided *via* electron transfer). Therefore, the quenching of T_3BTCH_3 by selected sacrificial agent was monitored through the fluorescence spectroscopy and lifetime measurements.

Among the most common sacrificial agents used for reductive dehalogenation reactions [13], ***N,N-diisopropylethylamine*** **(DIPEA)** was chosen as an efficient electron-donor. The changes of lifetime and emission intensity of T_3BTCH_3 were registered for a series of experiments performed with an incremental amount of DIPEA. As shown in Figure 2.5, increasing the amount of amine results in decreased fluorescence of photocatalyst and decreased lifetime of its excited state, which indicates that photoinduced electron transfer, between DIPEA and T_3BTCH_3, occurs *via* collisional quenching. The concentration of the sacrificial agent (DIPEA) required for an effective quenching of fluorescence, was estimated based on the Stern-Volmer equation:

$$\frac{I_o}{I} = 1 + \tau_0 \, k \, [Q] \tag{2.4}$$

where I_o - is the fluorescence intensity of the chromophore without the quencher; I - is the fluorescence intensity of the chromophore with the quencher, τ_0 is the lifetime of the emissive excited state of T_3BTCH_3 without the presence of the quencher, k - is the quencher rate coefficient.

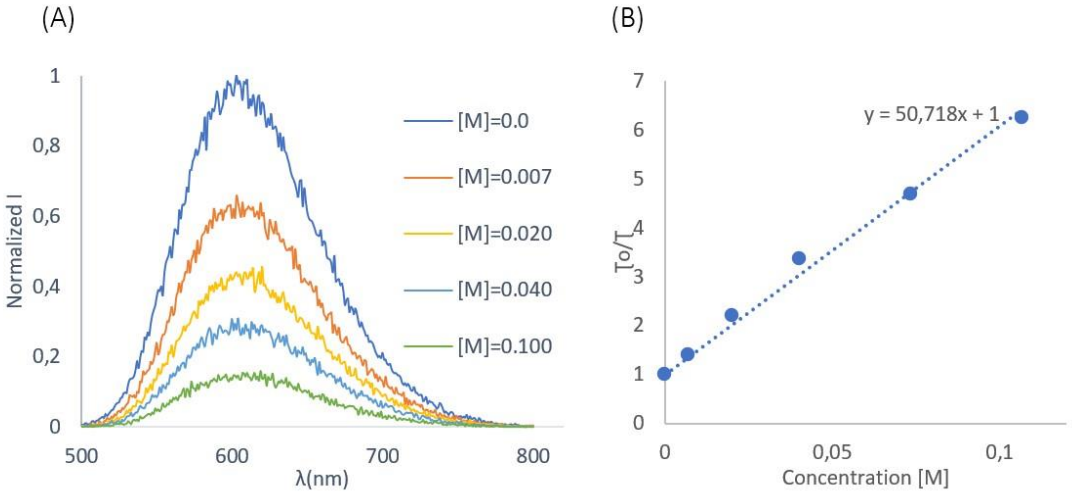

Figure 2.5. (A) Fluorescence quenching of T_3BTCH_3 upon addition of *N,N-Diisopropylethylamine* (B) the rate of T_3BTCH_3 quenching ($k=3.0\times10^8\ M^{-1}s^{-1}$) as a function of concentration *N,N-Diisopropylethylamine* in acetonitrile.

The concentration of DIPEA, which provides 90% of an effective quenching of T_3BTCH_3, was estimated at 0.1M and further applied to carry out organic transformations.

2.2.3 Halogen compounds

The thiazole and thiophene derivatives (Figure 2.6) were selected as potential substrates for further debromination reaction. As previously mentioned, the effective quenching of photocatalyst might be provided by both reaction reagents (*i.e.* the sacrificial agent and substrate). In the present case, the reductive quenching leading by amine, is in competition with the oxidative quenching, leading by halogen molecules. To understand the pathway of the photoinduced electron transfer between the reaction reagents and photocatalyst, spectroscopic studies were performed.

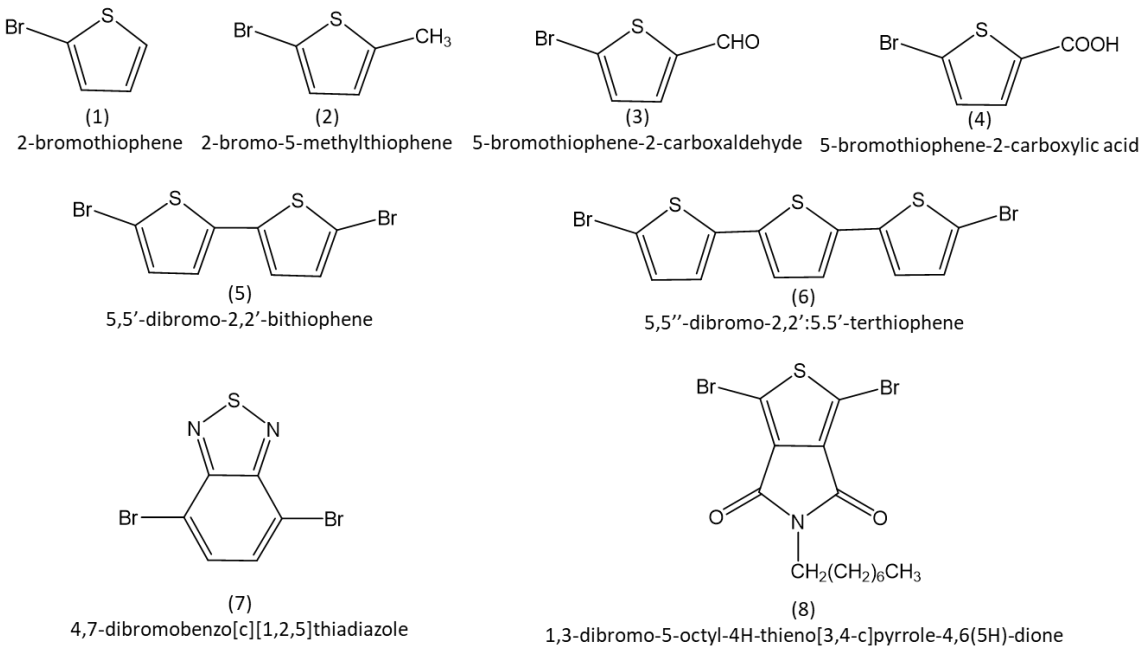

Figure 2.6. Examined halogenated compounds.

The absorption and emission spectra of photocatalyst were registered upon addition of the halogen compounds. In all cases, the addition of selected reagents does not provide any changes in the absorption spectra of T_3BTCH_3. The fluorescence quenching measurements do not show emission quenching of the photocatalyst, in the presence of *2-bromo-thiophene* and *2-bromo-5-mehtylthiophene* (compounds 1 and 2; Figure 2.6). Whereas, the remarkable decrease of the fluorescence intensity of T_3BTCH_3 is provided

upon the addition of all the other thiophene derivatives and the thiadiazole compound (Annex 2.2). Moreover, performed fluorescence lifetime measurements prove that the collisional quenching, which affects the lifetime of the excited states, occurs only in the presence of *4,7-dibromobenzo[c][1,2,5]thiadiazole* (compound 7; Figure 2.6). For all the remaining molecules, the deactivation of fluorescence occurs *via* static quenching (fluorescence quenching occurs without changing the lifetime of T_3BTCH_3). In static quenching, the fluorescence of photocatalyst is reduced due to the formation of a non-fluorescent ground-state complex between photocatalyst and reaction reagents. Comparison between the dynamic and static quenching of T_3BTCH_3 is presented in Figure 2.7.

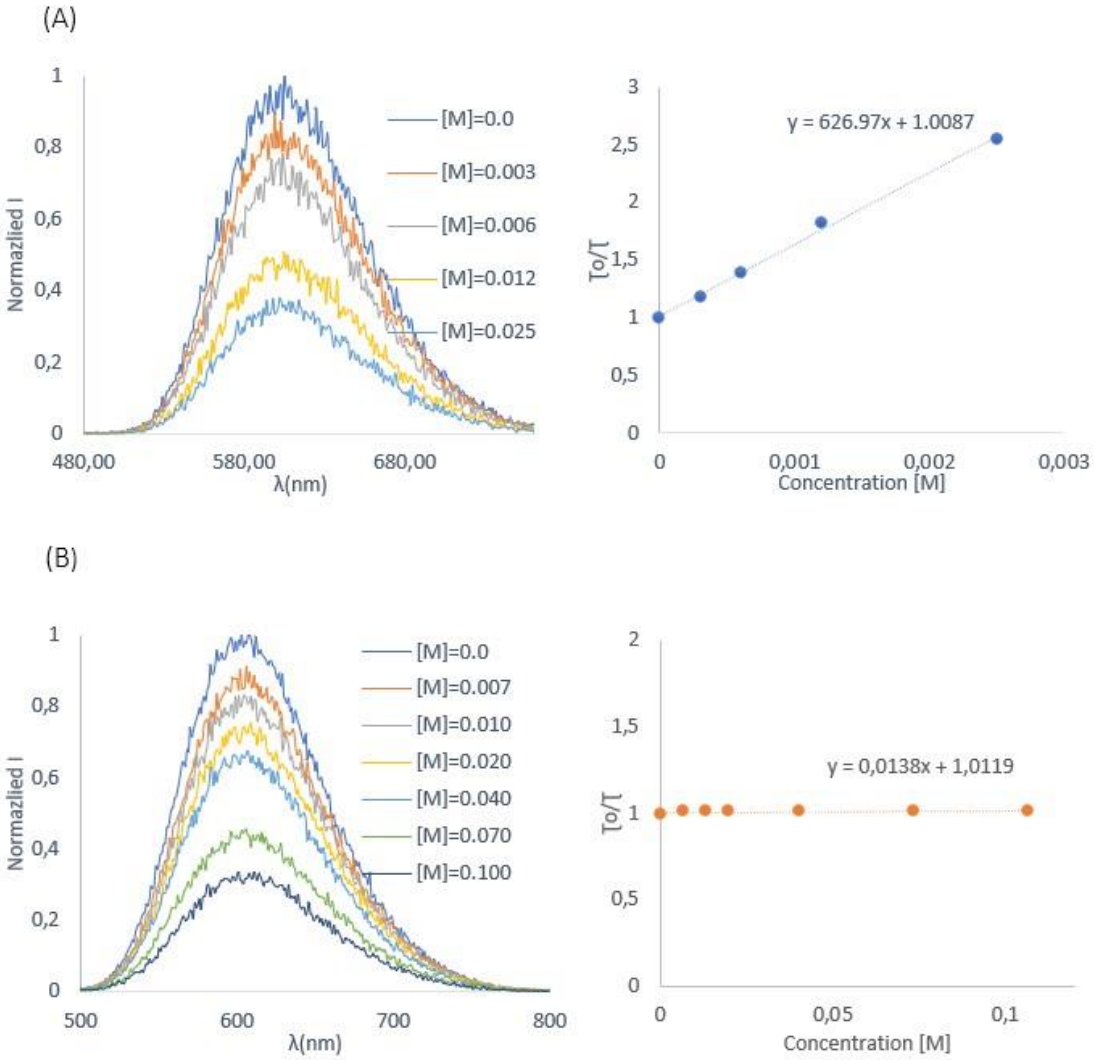

Figure 2.7. Exemplar comparison between (A) the dynamic quenching of T_3BTCH_3 upon addition of compound (7) *4,7-dibromobenzo[c][1,2,5]thiadiazole* and (B) static quenching of T_3BTCH_3 upon addition of compound (3) *5-bromothiophene-2-carboxyaldehyde*

measured in acetonitrile solution. The inset shows the normalized intensity changes at 605 nm. The sample was excited: for emission measurement at λ_{ex}=420nm and for the lifetime measurements at λ_{ex}=405 nm.

The fluorescence quenching rates, calculated based on the Stern-Volmer equation for **compound (7)** *4,7-dibromobenzo[c][1,2,5]thiadiazole* and sacrificial agent **DIPEA**, are presented in Table 2.2. The higher value of quencher rate coefficient (DIPEA), indicates that a more efficient photoinduced electron transfer occurs through the reductive quenching led by amine. The quencher rate coefficient will be further discussed to estimate the potential photocatalytic pathway.

Table 2.2 Quencher rate coefficient of substrate (compound 7) and sacrificial agent (DIPEA).

Quencher	Quencher rate coefficient k [$M^{-1}s^{-1}$]
4,7-dibromobenzo[c][1,2,5]thiadiazole	$2.3x10^7$
N,N-Diisopropylethylamine (DIPEA)	$3.0x10^8$

2.3 Experimental part II: Debromination reaction

The dehalogenation reaction of the examined halogen molecules was carried out in an anhydrous acetonitrile solution, except for bithiophene and terthiophene soluble in toluene. Since the presence of oxygen could interfere in radical reaction, the screw cap cuvette was charged with the photocatalyst, substrate and sacrificial agent under inert atmosphere. Afterwards, the reaction mixture was irradiated with a LED light source (λ_{ex}=460nm) for 6 hours (Figure 2.8). The changes in the absorption spectra during irradiation were monitored by the UV-Vis spectroscopy, where the final product formation was roughly evaluated using gas chromatography-mass spectrometry (GC-MS) technique.

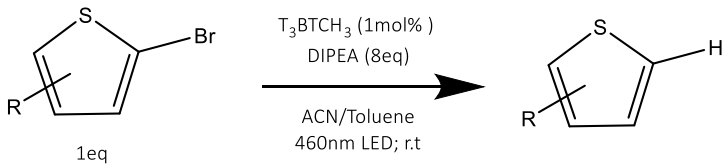

Figure 2.8. Standard reaction condition applied for dehalogenation reaction: concentration of photocatalyst (C_C =1.6x10^{-4} M), halogen compound (C_S =1.6x10^{-2}M) and DIPEA (C_A=1.3x10^{-1} M), inert atmosphere (glovebox conditions <200ppm O_2; <0.5ppm H_2O), room temperature (30℃).

A cross-check of the absorption spectra and GC-MS chromatograms, indicates that the successful debromination reaction is performed only in the presence of *5-bromothiophene-2-carboxyaldehyde* (compound 3); *4,7-dibromobenzo[c] [1,2,5]-thiadiazole* (compound 7) and *1,3-dibromo-5-octyl-4H-thieno[3,4-c]pyrrole-4,6(5H)-dione* (compound 8).

Consequently, to understand the role of the photocatalyst and obtain more insight into the reaction mechanism, the debromination reactions were carried out also without the presence of photocatalyst. Performed control experiments prove that the debromination reaction of compound (7) is driven by the photocatalytic reaction pathway, given that no debromination reaction is reported without the presence of T_3BTCH_3. Whereas, a low conversion of compound (3) and (8) into the debrominated product is registered also in the absence of the photocatalyst. Importantly, in all the cases non-reaction is observed without the presence of light, what indicates a photochemical reaction pathway, where the absorption of the light might occur by photocatalyst (Figure 2.9B) or by one of the reaction reagents (Figure 2.9A).

(A) (B)

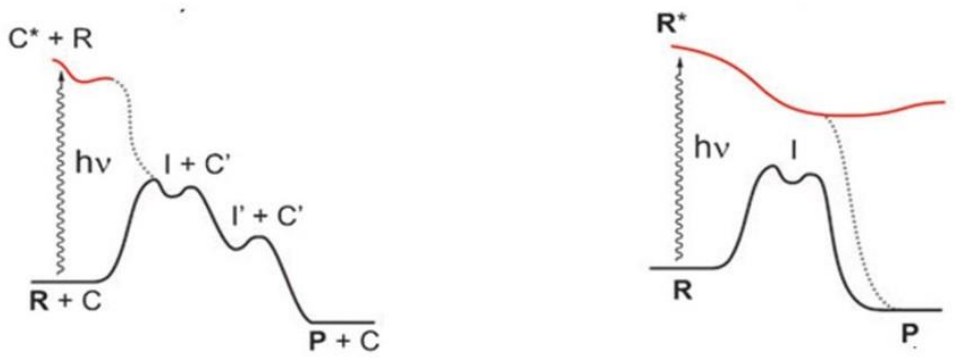

Figure 2.9. Photoinduced reaction pathway : (A) provided by excited state of photocatalyst (C*) (B) provided by excited state of one of reagents (R*); (C-photocatalyst, R-reagents, I-intermediates, P- product). Reproduced with permission [14].

Considering the previously mentioned fluorescence quenching measurements (Chapter 2.2.2/2.2.3), one may suspect that an efficient debromination, which occurs *via* photocatalytic reaction pathway, is provided only when the electron transfer between the photocatalyst and both reaction reagents (reduction of halogenated compound/oxidation of sacrificial agent) takes place. Otherwise, dehalogenation reaction might be caused by direct interaction between amine and reaction reagent, where the addition of the catalyst may trigger or block further transformations, depending on the substrates.

2.3.1 Light-mediated non-photocatalytic reaction pathway of debromination reaction

The photoinduced electron reaction pathway, which occurs *via* direct excitation of substrates, is proposed for debromination reaction of **compound (3)** and **(8)** (Figure 2.10).

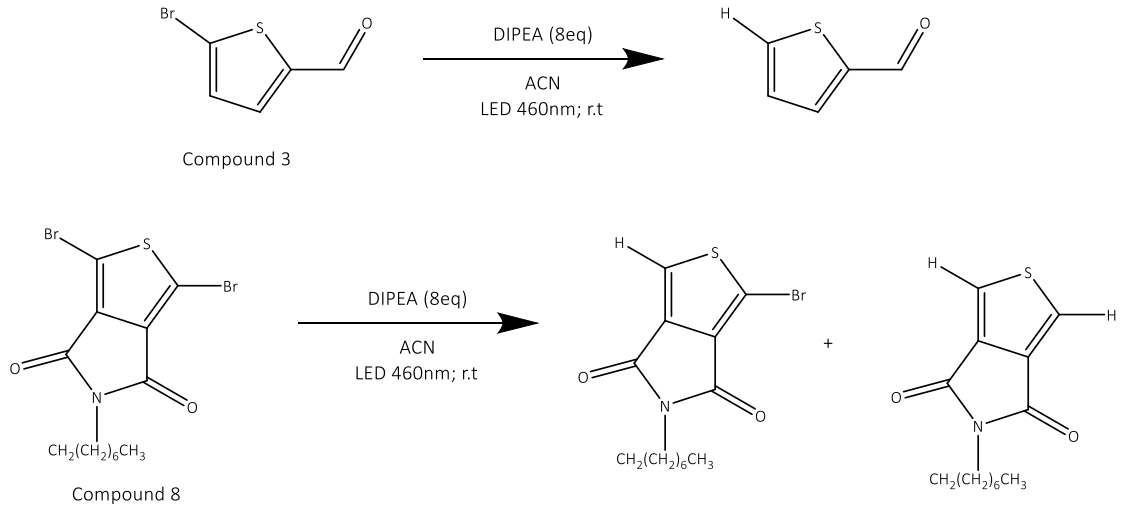

Figure. 2.10. General scheme of the light-mediated debromination reaction of compound (3) and (8).

To confirm this hypothesis, further spectroscopic studies on the interaction between the **compounds (3) and (8)** and the **sacrificial agent (DIPEA)** were performed. Initially, the absorption spectra of the individual compounds were measured upon the

addition of the sacrificial agent (at the concentration of reaction mixture). As shown in Figure 2.11, the registered spectra display remarkable changes of their absorption upon the addition of progressively increasing equivalents of amine. Especially, in the case of compounds (3), where the generation of significant extinction in the visible part of the spectrum, might indicate the formation of an electron donor-acceptor (EDA) complex. The EDA complex might be formed in-situ by bromine and amine [15]. If this is the case, the debromination reaction might be caused by direct excitation of bromide compounds (slightly absorb in the visible region) or more likely *via* irradiation of a formed *in-situ* EDA complex halogen-bonded.

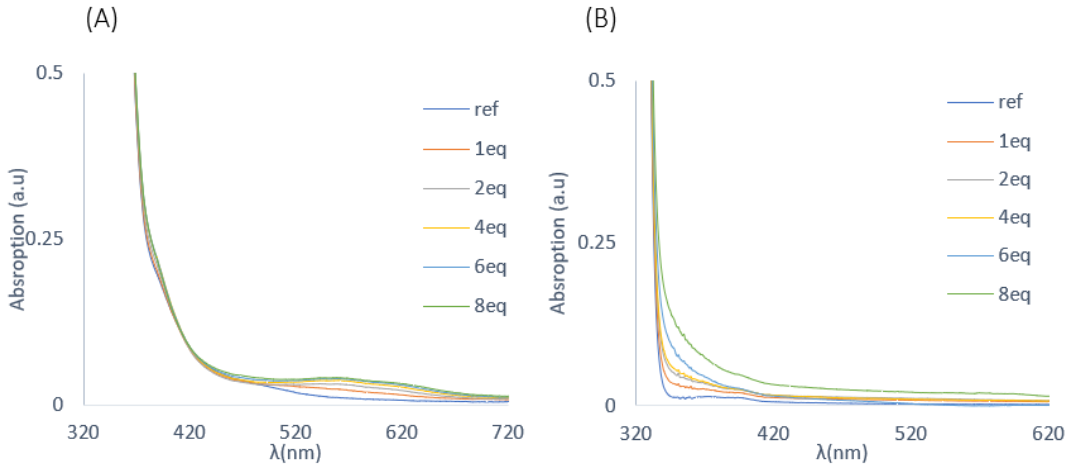

Figure 2.11. Changes in the absorption spectra of (A) compound 3 and (B) compound 8 upon the addition of DIPEA.

As already reported in literature [7], an excited EDA complex cleaves to form a radical pair ($D^{+\bullet}/A^{-\bullet}$), which can subsequently provide various reaction pathways including additions, eliminations or rearrangements transformation (Figure 2.12a). Unless, as foreseen in the discussed debromination reaction, the electron acceptor (halogen compound) is transferred into a neutral radical ($B^{\bullet}$) along with an anion (L^{-}) (*e.g.* halide anion). If is the case, neutral radical might further interact with the electron donor (amine) and provides the final debromination product (Figure 2.12b).

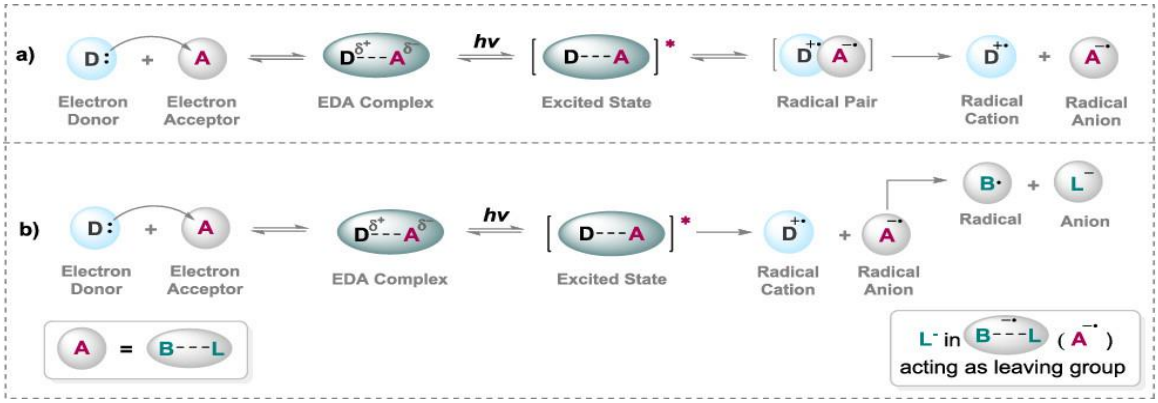

Figure 2.12. Proposed mechanistic pathway include formation of electron donor-acceptor complex. Reprinted with permission from [16]. Copyright (2019) American Chemical Society.

2.3.2 Side product formation

Irradiation of halogen compounds after the addition of DIPEA results in the formation of new absorption bands, at ʎ=370 nm for **compound (3)** and at ʎ=360 nm for **compound (8)**, significantly increasing during the irradiation time (Figure 2.13). Therefore, since the final debromination compounds do not absorb light in that region, the new absorption bands indicate a formation of a side-products during irradiation, which could have been proved by the complementary analysis to GC-MS spectroscopy. Hence, further evolution of the selected reactions was followed by ^{1}H NMR analysis.

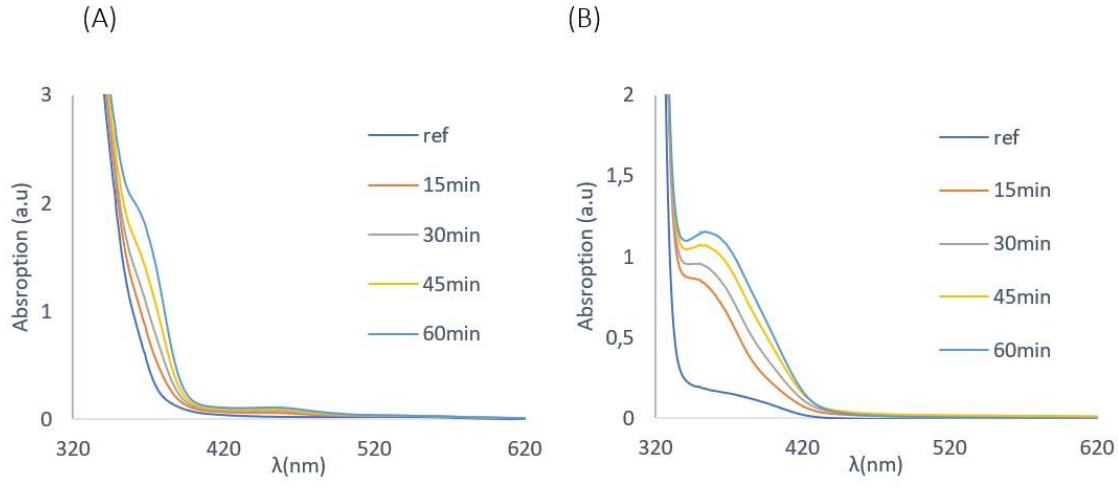

Figure 2.13. The absorption spectra of (A) compound 3 and (B) compound 8 in the presence of DIPEA registered during irradiation.

To monitor the reaction changes in-situ, the debromination were carried out directly in the NMR tube (charged with $5x10^{-5}$moles of the reaction reagent, $4x10^{-4}$ moles of the DIPEA and 0.75mL of acetonitrile-d3), where the ^{1}H NMR spectra were registered before and after irradiation. In the first approximation conversion rate and selectivity to debrominated product were calculated based on the integrals of specify moieties, using the residual peak of the deuterated solvent as reference, followed the equations:

$$Conversion = (1 - \frac{I_{a_{24h}}}{I_{a_0}}) * 100\% \quad (2.5)$$

$$Selectivity = \frac{I_{a*}}{(I_{a_0} - I_{a_{24h}})} * 100\% \quad (2.6)$$

where I_{a_0} – is the integration of the proton at 9.79 ppm before irradiation; $I_{a_{24h}}$ – is the integration of the proton at 9.79 ppm after 24h irradiation; I_{a*}– is the integration of the proton at 9.94 ppm coming from debromination product.

The representative ^{1}H NMR spectra (for compound 3) is reported in Figure 2.14.

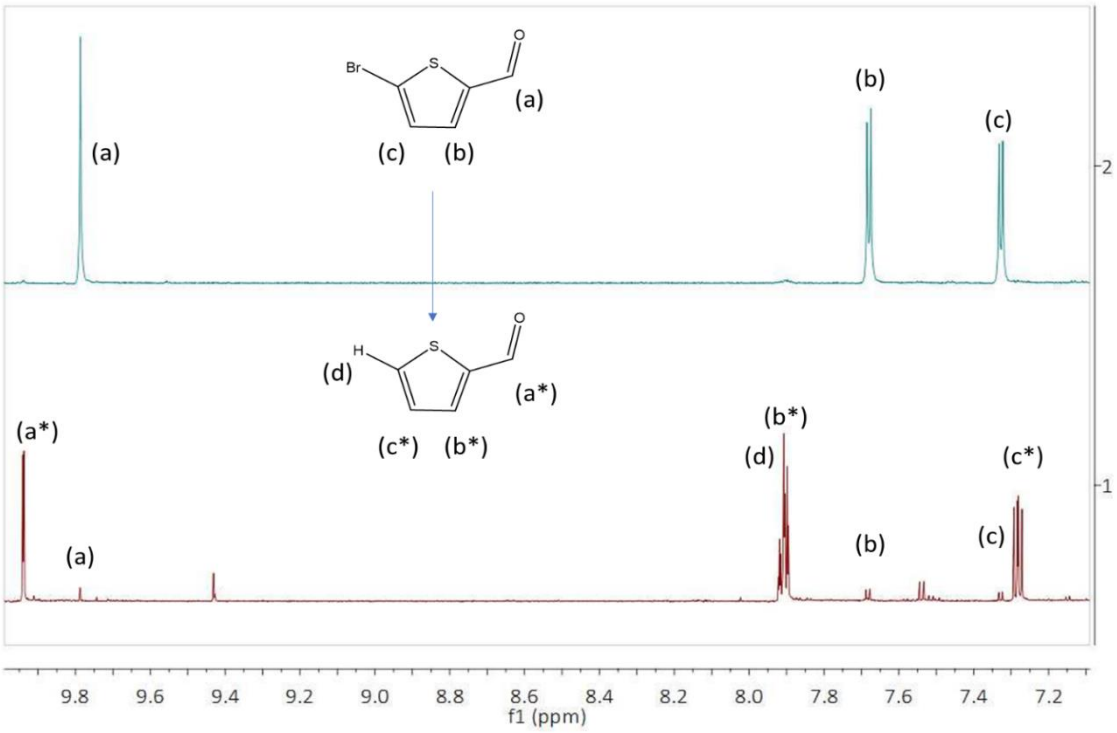

Figure 2.14. The ^{1}H NMR spectra before and after irradiation of compound (3) and DIPEA deuterated acetonitrile (CD_3CN).

Importantly, since the NMR signals of the debromination product and substrate for compound 8 are partially overlapping (Annex 2.3; Figure 2.24), the conversion rate and the reaction selectivity were roughly calculated based on GC-MS analysis, according to the equations:

$$Conversion = (1 - \frac{A_{S_{24h}}}{\sum A_R}) * 100\% \quad (2.7)$$

$$Selectivity = \frac{A_{MD}}{(\sum A_R - A_{S_{24h}})} * 100\% \quad (2.8)$$

where $A_{S_{24h}}$- is the area of signal at 24.263 min, assigned to substrate after 24 h of irradiation; $\sum A_R$- is the sum of all signals appeared on the chromatogram; A_{MD} - is the area of signal at 22.627 min, assigned to the mono-debromination; A_{DD}- is the area of signal at 20.564 min, assigned to the double-debromination; A_{SP} is the area of signal at 26.998 min, assigned to the unidentified side product. The representative chromatogram is shown in Figure 2.15.

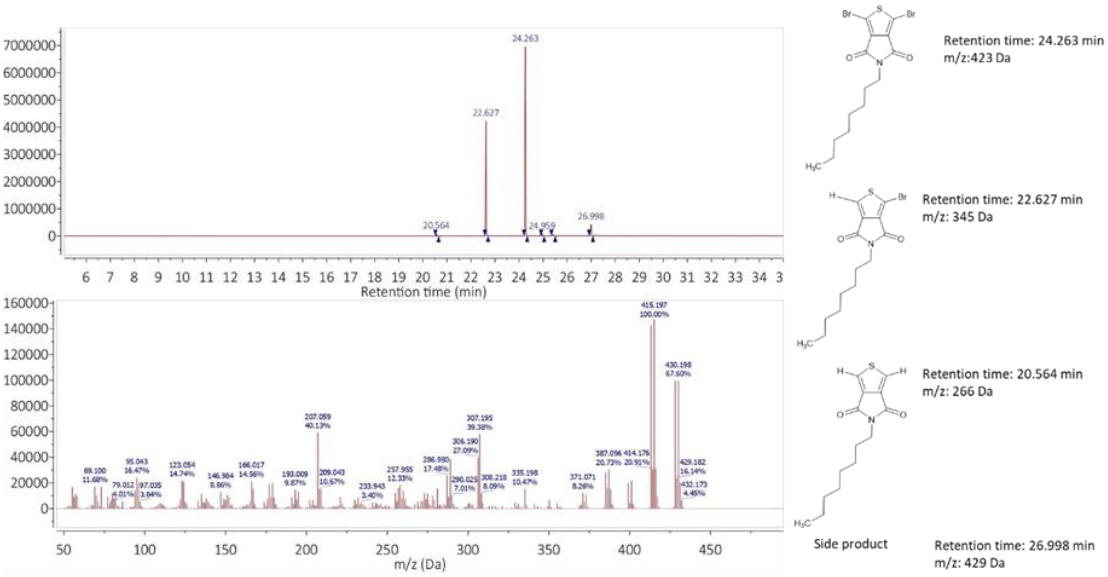

Figure 2.15. The GC-MS chromatogram of *1,3-dibromo-5-octyl-4H-thieno[3,4-c]pyrrole-4,6(5H)-dione* (compound 8) and DIPEA after 24h irradiation.

These complementary studies show that, the brominated thiophenes compound (3) and compound (8) reach around **93%** and **41%** of the conversion rate, affording **74%** and **88%** of selectivity to debrominated product, respectively. In both cases, the formation of by-side product is confirmed by the ^{1}H NMR analysis, in which observed chemical shift of DIPEA (after irradiation) may indicate an interaction between amine and thiophene

compound (Annex 2.3; Figure 2.25). Nevertheless, due to complex ^{1}H NMR spectra of crude mixture in aliphatic region and low integral relative to amine derivatives, structure of side product is difficult to predict. Furthermore, in the case of the debromination reaction of compound (3), only formation of the debrominated product is detected by GC-MS analysis, which additionally impedes the side product identification. Even though, any of the performed analysis does not give a clear answer that could lead to precise identification, obtained data allow to foresee a possible reaction pathway, which may result in the side products presented below. The formation of amino-thiophene derivatives and *1-bromo-3-(ethyl(isopropyl)amino)-5-octyl-4H-thieno[3,4-c]pyrrole-4,6(5H)-dione* is proposed (Figure 2.16). As reported by Kirsch [17], weakly activated heteroaromatic ring systems of *5-bromothiophene-2-carboxaldehyde* might undergo aromatic nucleophilic substitution in the presence of amine and results in amination reaction.

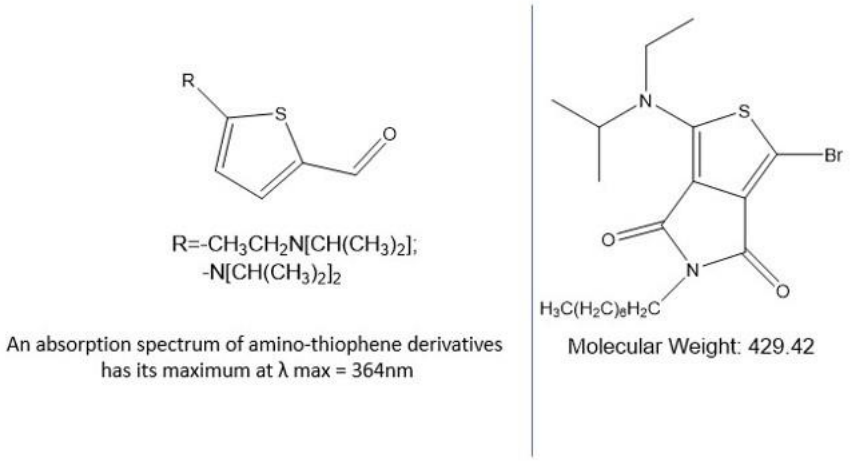

Figure 2.16. Possible side products formed in the presence of DIPEA during the debromination reaction of compound (3) (estimated based on the UV-Vis absorption spectra [17]) and compound (8) (estimated based on the GC-MS analysis).

2.3.3 Influence of amine

To clarify the role of DIPEA in the formation of the final product, the debromination reaction of compound (3) was run in the presence of other bases like tetramethylethylenediamine (TEMED), triethylamine (Et_3N) and quincilidine. Changes in the absorption spectra, upon the addition of selected amines, are not so remarkable as in the presence of the DIPEA, which indicates that the EDA complex formation strongly depend on the individual interaction between the amine and reagent.

Additionally, further irradiation of the compound (3), results in non-debromination reaction and non-side product formation in the presence of TEMED and Et_3N (Annex 2.4). Whereas, the similar changes in the absorption spectra (*i.e.* formation of the new absorption bands at ʎ=370 nm), are observed in the presence of quincilidine (Annex 2.4). In this case, the chemical shift of the ^1H NMR signals, relative to the thiophene core, suggests a substitution in position 5 by any other atom than hydrogen (Figure 2.17). Hence, presented data indicate that the performed reaction results in the higher formation rate of **side-product** than debrominated one. Furthermore, since the basicity of DIPEA (pKa=10.75) and quincilidine (pKa=11.00) is comparable, one may suspect that the side product formation is promoted by more nucleophilic bases like quincilidine, where a non-nucleophilic bases, like sterically hindered DIPEA, promote the formation of the final debrominated product.

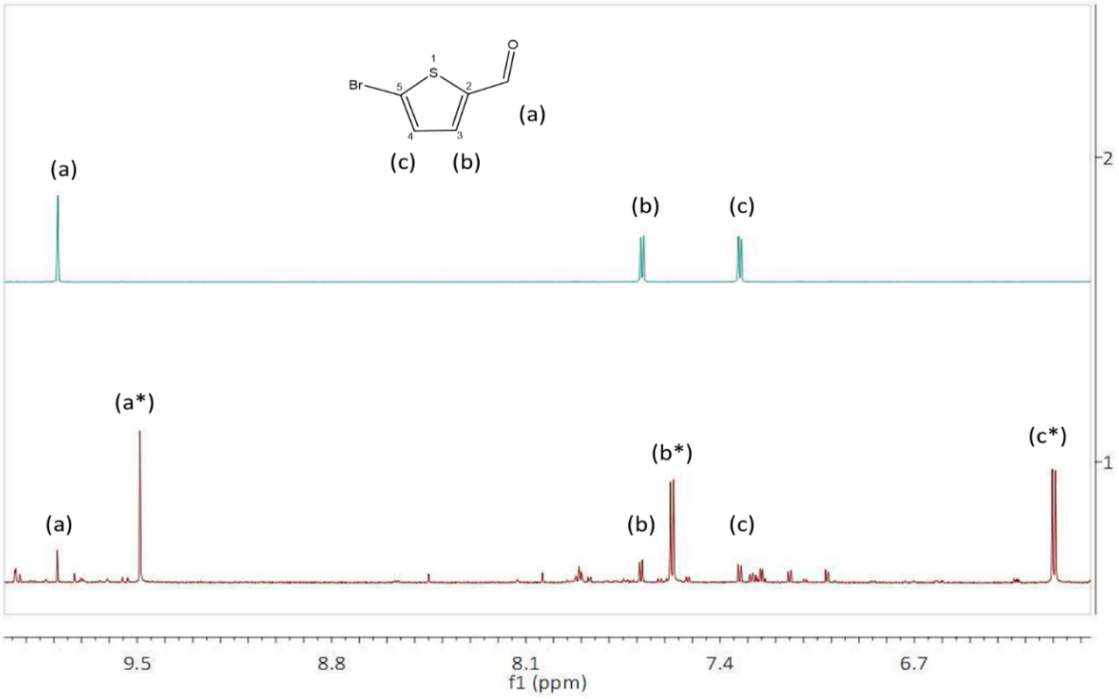

Figure 2.17. The ^1H NMR spectra before (2) and after 24h irradiation (1) of compound (3) and quincilidine in deuterated acetonitrile (CD_3CN).

2.3.4 Influence of the photocatalyst in the EDA photoreaction

In order to evaluate the effect of the photocatalyst, on the selectivity and conversion rate of the photoreactions (which proceed *via* EDA complex formation), the debromination reaction of **compound (3) and (8)** was performed in presence of **T_3BTCH_3**.

The results collected in Table 2.3, indicate that the addition of the T_3BTCH_3 does not have a significant influence on the final conversion rate. However, in some cases (*i.e.* compound 3) presence of the photocatalyst might result in the higher selectivity towards the desired debromination product.

Table 2.3 Influence of photocatalyst on debromination reaction.

Compound	without T_3BTCH_3		with T_3BTCH_3	
	Selectivity [%]	Conversion [%]	Selectivity [%]	Conversion [%]
(3) *5-bromothiophene-2-carboxyaldehyde**	**74**	93	**88**	89
(8) *1,3-dibromo-5-octyl-4H-thieno[3,4-c]pyrrole-4,6(5H)-dione***	**88**	41	**82**	41

Conversion rate and selectivity to mono-debrominated product estimated, in rough approximation, *based on ^{1}H NMR analysis,** based on GC-MS analysis, reaction carried out 24h (λ_{em}=460nm) in the presence of DIPEA (Annex 2.5).

2.3.5 Photocatalytic reaction pathway of debromination reaction

The photocatalytic reaction pathway for debromination reaction of **compound (7)** (Figure 2.18) is examined in more details, since is taking place only in the presence of the photocatalyst and light (preliminary results described in section 2.3).

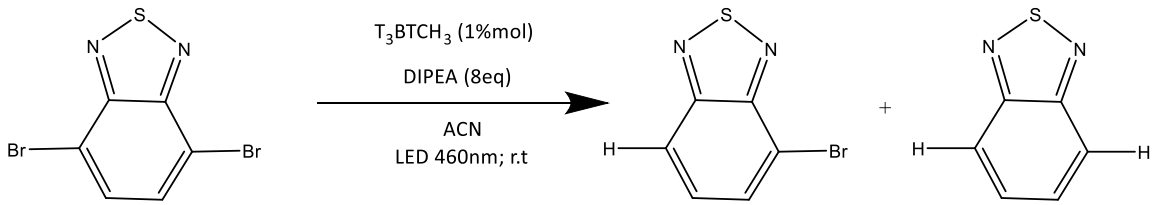

Figure. 2.18. General scheme of the debromination reaction of compound (7).

Previously performed fluorescence quenching measurements indicate that in the present system an efficient electron transfer might occurs by the reduction of halogen **compound (7)** and the oxidation of **DIPEA**. To understand, which one of these processes is favoured, the fluorescence quenching rates were estimated. The Stern-Volmer analysis involved in that studies, proves that the fluorescence quenching rates for *4,7-*

dibromobenzo[c][1,2,5]thiadiazole (k=2.3x10^7 M^{-1}s^{-1}) is considerably lower than the one determined for DIPEA (k=3.0x10^8 M^{-1}s^{-1}) (Table 2.2).

Consequently, one would assume that the photocatalytic dehalogenation occurs through a photooxidative mechanism (Figure 2.19A), where the oxidation of DIPEA can form reduced photocatalytic species ($T_3BTCH_3^{\bullet-}$). In such system, $T_3BTCH_3^{\bullet-}$ radical anions might further interact with the bromide compound giving thiadiazol radicals ($R^{\bullet}$). Once formed, $R^{\bullet}$ can successively lead to the final debromination product *via* hydrogen-atom transfer (HAT) from amine. Nevertheless, the formation of side product might be observed since oxidized amine ($DIPEA^{\bullet+}$) might undergo various reaction pathways (Figure 2.19B).

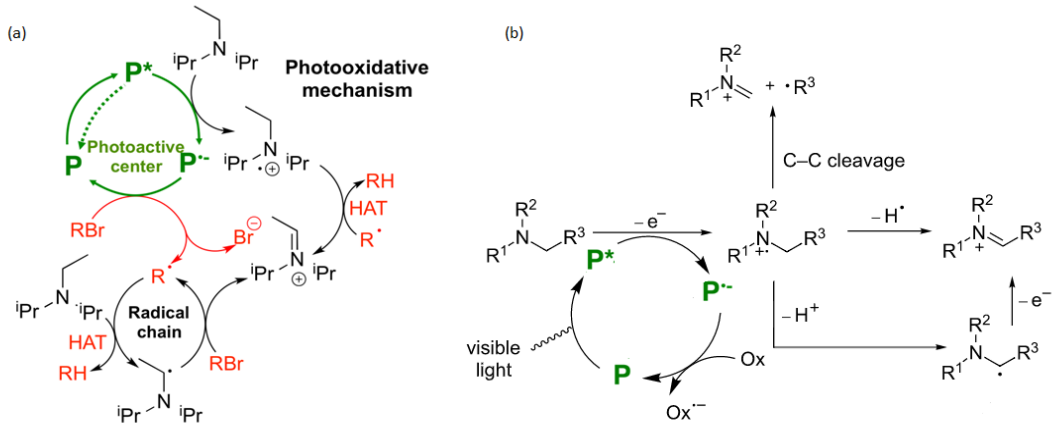

Figure 2.19. (A) Possible mechanism of dehalogenation reaction in the presence of DIPEA as a sacrificial agent [18] (B) Amine radical cations' mode of reactivity [19]. Reproduced with permission [18,19].

Performed UV-Vis and GC-MS analysis show that debromination reaction, affording **51%** conversion with **91%** yield towards **mono-debrominated product** (after 24h irradiation). The formation of the side product is confirmed by ^{1}H NMR and GC-MS analysis. However, its identification is difficult to predict in detail due to its low concentration (Annex 2.6).

2.4 Experimental part III: Coupling reaction

If thiadiazole radicals formed during the dehalogenation might further undergo coupling reaction, presented photocatalytic system (based on **T_3BTCH_3**) might be expanded

towards the direct C-C bond formation. In order to prove this possibility, several coupling reactions of *4,7-dibromobenzo[c][1,2,5]thiadiazole* (compound 7) and ***2-methylthiophene*** were carried out.

2.4.1 Photocatalytic reaction system for C-C bond formation

Initially, the stability of the photocatalytic system upon irradiation, in the presence of the coupling agent (***2-methylthiophene***) was monitored by UV-Vis spectroscopy (Figure 2.20). The absorption spectra of the reaction mixture after 6h irradiation, shows a new band at λ=410nm, most likely relative to the coupling product. Whereas, non-remarkable changes of the band assigned to T_3BTCH_3 (at λ=460nm) prove the stability of the photocatalyst upon selected reaction conditions. Furthermore, according to fluorescence quenching measurements, the addition of *2-methylthiophene* does not provide any changes in the fluorescence of T_3BTCH_3, supporting the previously discussed photooxidative mechanism, in which reduced photocatalytic species provides the thiadiazole radicals (Figure 2.19A). Nevertheless, since the thiadiazole radicals can react simultaneously with *2-methylthiophene* or with a proton abstracted from DIPEA, the coupling and debromination reactions might be in competition.

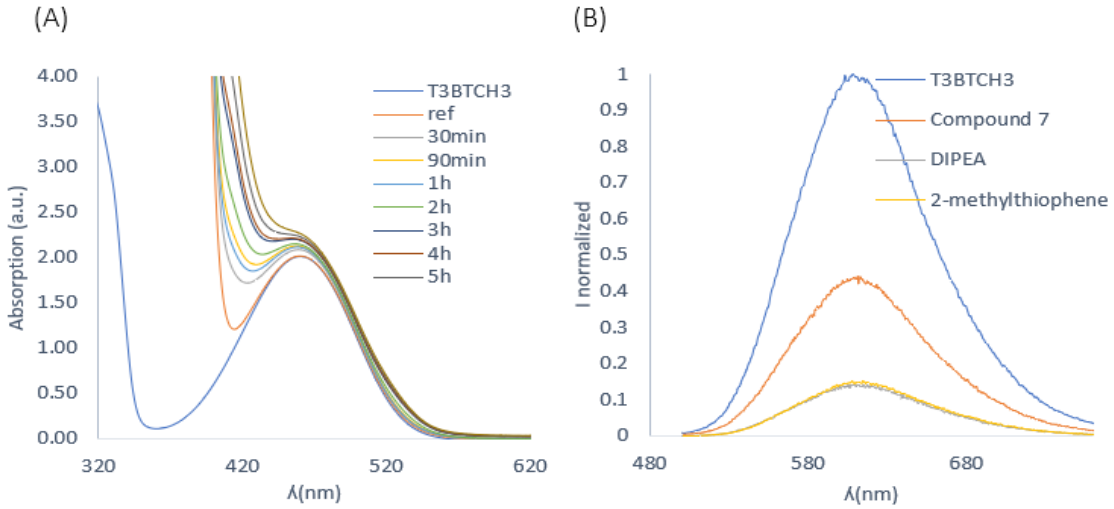

Figure 2.20. (A) Changes in the absorption spectra upon the irradiation of the coupling reaction between *2-metyhlthiophene* and *4,7-dibromobenzo[c][1,2,5]thiadiazole* in the presence of T_3BTCH_3. (B) Changes in the emission spectra of T_3BTCH_3 upon the addition of *4,7-dibromobenzo[c][1,2,5]thiadiazole, diisopropylethylamine, 2-methylthiophene,* respectively.

2.4.2 Optimization study

The first attempt of coupling reaction, in the presence of 2 equivalents of coupling agent and 8 equivalents of amine, results only in the formation of the mono-debrominated product. Hence, to increase the selectivity towards the C-C bond formation, a different ratio of the reaction reagent was studied (Table 2.4). Surprisingly, an increased amount of the coupling agent (20-fold excess of 2-methylthiophene) does not increase significantly the selectivity to the coupling product, indicating that the hydrogen abstraction process is still the dominant reaction. Indeed, decreasing the amount of the amine (four times less than standard one) provided a remarkable lower conversion rate and higher selectivity towards the coupling product. Upon this reaction conditions, the excited state of photocatalyst is quenched in the great majority by *4,7-dibromobenzo[c][1,2,5]thiadiazole* (60%) and in the minority by amine (roughly 45%), which can influence the photocatalytic reaction pathway. Looking for more selective conditions, DIPEA was replaced by other amines as triphenylamine and 2,6-lutidine, which cannot act as hydrogen donor. Triphenylamine was selected as potential sacrificial agent, which like DIPEA provides direct quenching of T_3BTCH_3. Regrettably, in that case, no coupling and no debromination reaction is observed, which might indicate that presence of the proton is required to avoid further recombination of thiadiazol and halogen radicals. Furthermore, no debromination reaction is observed also in the presence of 2,6-lutidine, which in contrast to other amines cannot directly quench the excited state of photocatalyst. The last experiment indicates that the amine must act as the hydrogen donor and the sacrificial agent simultaneously to provide at least debromination reaction. This hypothesis was further confirmed by the control experiment (performed without the addition of amine), which results in no reactions.

Table 2.4. Influence of different ratio of reaction reagent on the coupling reaction between *2-metyhlthiophene* and *4,7-dibromobenzo[c][1,2,5]thiadiazole*.*

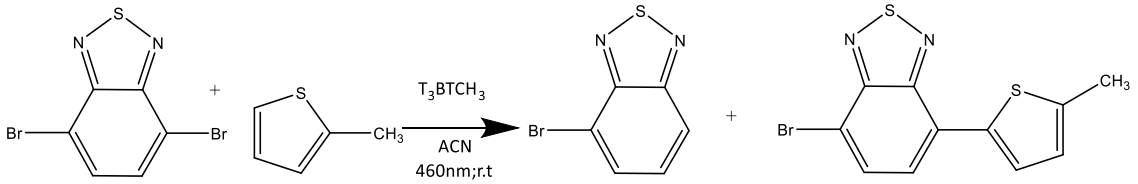

4,7-dibromobenzo[c][1,2,5]thiadiazole	*2-methyl thiophene*	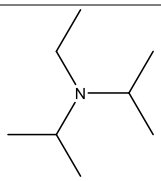	Conversion	Selectivity to mono debromination	Selectivity to mono coupling
1eq	2eq	8eq	28%	99%	-
1eq	12eq	8eq	65%	64%	5%
1eq	20eq	8eq	16%	70%	8%
1eq	20eq	2eq	8%	28%	5%

4,7-dibromobenzo[c][1,2,5]thiadiazole	*2-methyl thiophene*	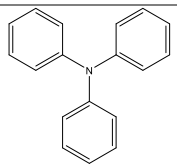	Conversion	Selectivity to mono-debromination	Selectivity to mono-coupling
1eq	12eq		2%	99%	-

4,7-dibromobenzo[c][1,2,5]thiadiazole	*2-methyl thiophene*	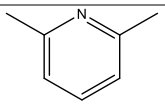	Conversion	Selectivity to mono-debromination	Selectivity to mono-coupling
1eq	12eq	8eq	0%	-	-

*General scheme of the coupling reaction between *2-metyhlthiophene* and *4,7-dibromobenzo[c][1,2,5]thiadiazole.* Conversion rate and selectivity to mono-debrominated product estimated, in rough approximation, based on GC-MS analysis, reaction carried out 24h (λ_{em}=460nm). Selected GC-MS chromatogram indicating coupling product formation is shown in Annex 2.7.

2.5 Conclusion

The extensive studies performed on thiophene derivatives allow to select T_3BTCH_3 as promising metal-free photocatalyst for organic synthesis. The T_3BTCH_3 was successfully applied toward debromination reaction of *4,7-dibromobenzo[c][1,2,5]thiadiazole* in the presence of DIPEA as a sacrificial agent. In this case, the selection of amine that acts as hydrogen atom donor and sacrificial agent at the same time is a crucial parameter, which determines the final conversion rate. Nevertheless, performed attempts towards coupling reaction between *4,7-dibromobenzo[c]-[1,2,5]thiadiazole* and *2-methylthiophene* in the presence of DIPEA, indicate that the hydrogen abstraction process is the dominant reaction, which blocks further C-C bond formation. In order to improve the conversion rate towards the coupling reaction, the optimization of the experimental conditions or the presence of more active coupling agent is required. In this light, the potential application of the thiadiazole radicals will be further discussed toward polymerization reaction.

In parallel, the comprehensive studies carried out on the reagents disclosed that proper selection of the individual substrates might provide a light-mediated non-photocatalytic reaction pathway. The interaction between selected amine (DIPEA) and halogen compounds, as compound (3) and compound (8), results in the formation of electron donor-acceptor complex that absorbs directly in the visible region, initializing the photoinduced electron transfer process. The addition of T_3BTCH_3 is not required and have any significant influence on the final conversion rate and selectivity towards debromination product. Moreover, in the present reaction system, the amine is not working as a sacrificial agent but as a base. The nucleophilicity of base determines reaction pathway and the final product formation. The formation of debrominated product is favored in the presence of non-nucleophilic amine. As demonstrated, understanding the roles of amine gives the possibility to form system, in which different products are formed selectively from the same starting substrate.

Reference:

[1] N.A. Romero, D.A. Nicewicz, *ACS Catal*., 2018, 86, 4735.

[2] S. Sharma, A. Sharma, *Org. Biomol. Chem*., 2019, 17, 4384.

[3] A. Alvarez-Martina, S. Trashin, M. Cuykx, A. Covaci, K. De Wael, K. Janssens, *Dyes Pigments*, 2017, 145, 376.

[4] Y.H Chiu, T.F.M. Chang, C.Y. Chen, M. Sone, Y.J. Hsu, *Catalyst*, 2019, 9, 430.

[5] G. Barbarella, M. Zangoli, F. Di Maria., *Adv. Heterocycl. Chem*, 2017, 123, 105.

[6] C.D. Mc Tiernan, S.P. Pitre, J.C. Scaiano, *ACS Catal*., 2014, 4, 4034.

[7] S.P. Pitre, C.D. Mc Tiernan, J.C. Scaiano, *Acc. Chem. Res*., 2016, 49, 1320.

[8] L. Wang, W. Huang, R. Li, D. Gehrig, P.W.M. Blom, K. Landfester, K.A.I. Zhang, *Angew. Chem. Int. Ed*., 2016, 55, 9783.

[9] L. Wang, I. Rörich, C. Ramanan, P.W.M. Blom, W. Huang, R. Li, K.A.I. Zhang, *Catal. Sci. Technol*., 2018, 8, 3539.

[10] L. Wang, W. Huang, R. Li, D. Gehrig, P.W.M. Blom, K. Landfester, K.A.I. Zhang, *Angew. Chem. Int. Ed.,* 2016, *55*, 9783.

[11] S. Zhu, D. Wang, *Adv. Energy Mater.,* 2017, 7, 1700841.

[12] K. Zeitler, *Angew. Chem. Int. Ed.*, 2009, 48, 9785.

[13] J.J. Devery, J.D. Nguyen, Ch. Dai, C.R.J. Stephenson, *ACS Catal.,* 2016, *6* (9), 5962.

[14] D. Ravelli, D. Dondi, M. Fagnonia, A. Albini*, Chem. Soc. Rev.,* 2009, 38, 1999.

[15] G. Cavallo, P. Metrangolo, R. Milani, T. Pilati, A. Priimagi, G. Resnati, G. Terraneo, *Chem Rev.,* 2016, 116 (4), 2478.

[16] Y. Liu, XL. Chen, K. Sun, XY. Li, F.L. Zeng, X.C. Liu, L.B. Qu, YF. Zhao, B. Yu, *Org. Lett.,* 2019, 21 (11), 4019.

[17] D. Prima, G. Kirsch, J.F. Nicoud, *Synlett*., 1998, 383.

[18] A. Sciutto, A. Fermi, A. Folli, T. Battisti, J.M. Beames, D.M. Murphy, D. Bonifazi, *Chem. Eur. J.*, 2018, 24 (17), 4382.

[19] J. Hu, J. Wang, T.H. Nguyen, N. Zheng*, Beilstein J. Org. Chem*., 2013, 9, 1977.

ANNEX 2

Annex 2.1 Catalyst selection

Figure 2.21. Absorption (A) and emission (B) spectra of photoactive thiophene derivatives.

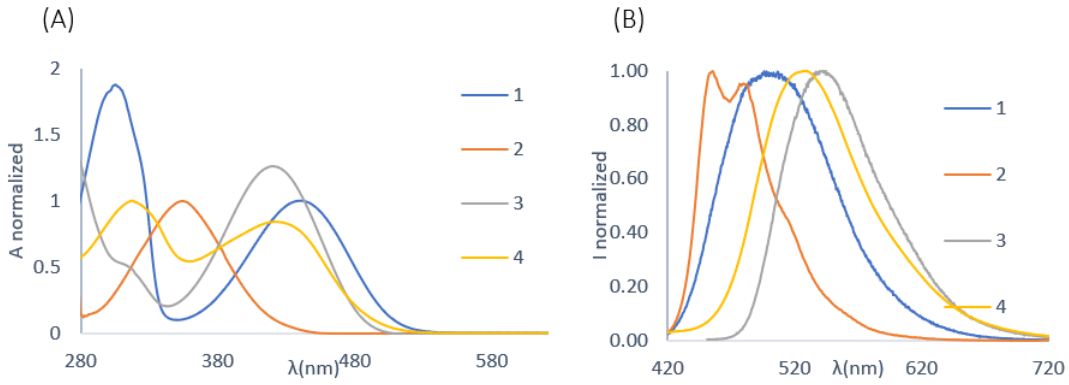

	Name of compound
C1	4,7-bis(5-methylthiophen-2-yl)benzo[c][1,2,5]thiadiazole
C2	5,5'''-dimethyl-2,2':5',2'':5'',2'''-quaterthiophene
C3	2-(5-(hydroxymethyl)thiophen-2-yl)-3,5-dimethyl-6-phenyldithieno[3,2-b:2',3'-d]thiophene 4,4-dioxide
C4	2,3-di([2,2'-bithiophen]-5-yl)benzo[b]thiophene 1,1-dioxide

Figure 2.22. Absorption spectra of: (A) (**compound C2**) *5,5'''-dimethyl-2,2':5',2'':5'',2'''-quaterthiophene* upon irradiation in acetonitrile solution; (B) (**compound C3**) *2-(5-(hydroxymethyl)thiophen-2-yl)-3,5-dimethyl-6-phenyldithieno[3,2-b:2',3'-d]thiophene 4,4-dioxide* upon irradiation in the presence of 2-bromothiopene and N,N-Diisopropylethylamine (standard reaction conditions). Molecules are not stable.

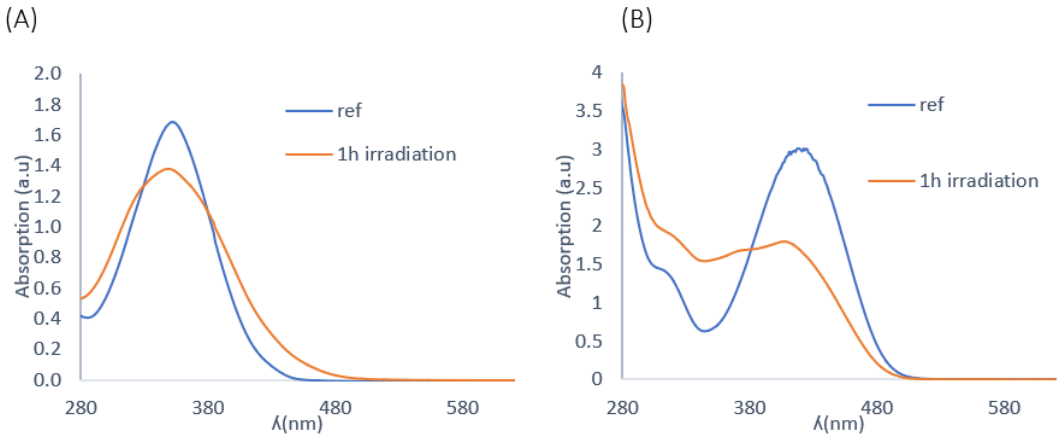

Annex 2.2 Halogen compounds

Figure 2.23. The emission spectra of halogen compounds upon the addition of 8 equivalents of DIPEA register in (A) acetonitrile (B) toluene solution.

(A) (B)

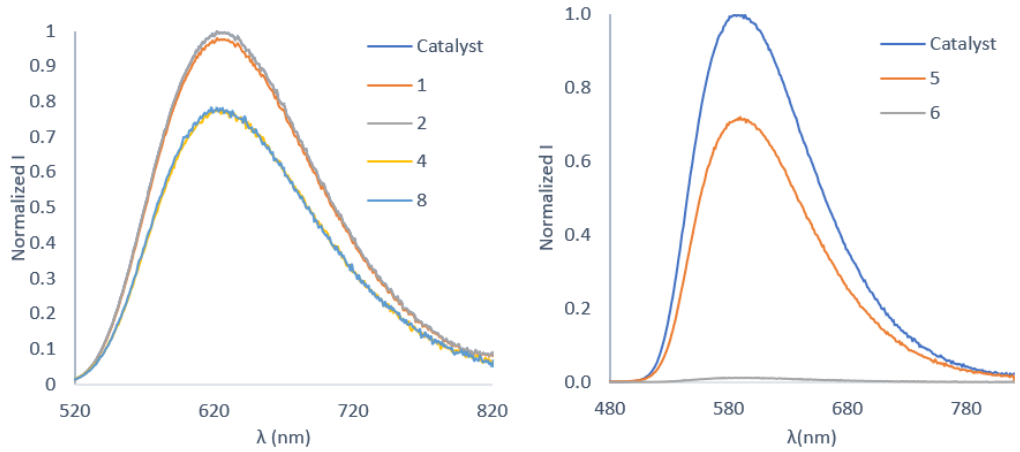

Entry	Name of compound
1	2-bromothiophene
2	2-bromo-5-methylthiophene
4	5-bromothiophene-2-carobxylic acid
5	5,5'-dibromo-2,2'-bithiophene
6	5,5''-dibromo-2,2':5.5'-terthiophene
8	1,3-dibromo-5-octyl-4H-thieno[3,4-c]pyrrole-4,6(5H)-dione

Annex 2.3 Side product formation

Figure 2.24. The ^{1}H NMR spectra before (1) and after (2) irradiation of **compound (8)** and **DIPEA**. Spectra recorded in deuterated acetonitrile (CD_3CN).

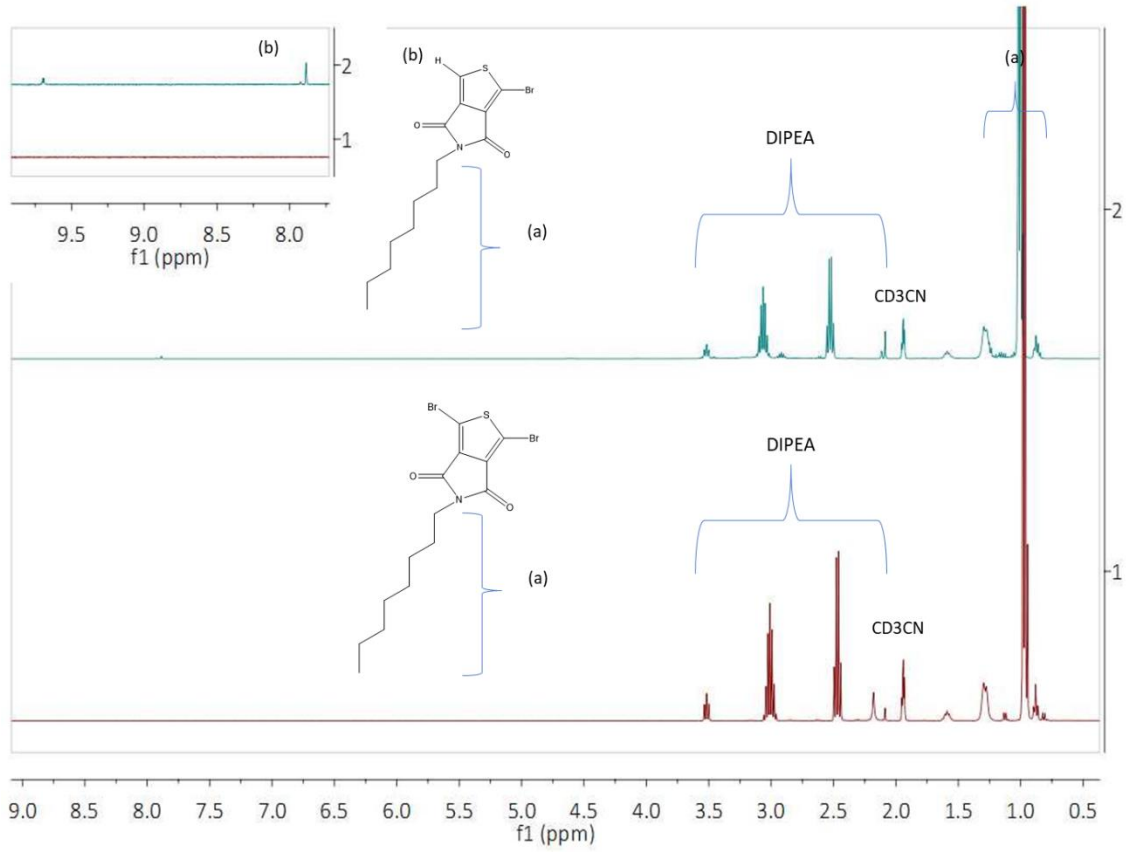

Figure 2.25. The ^{1}H NMR spectra before (1) and after (2) irradiation of **compound (3)** and **DIPEA**. Spectra recorded in deuterated acetonitrile (CD_3CN) (s-signal related to side product formation).

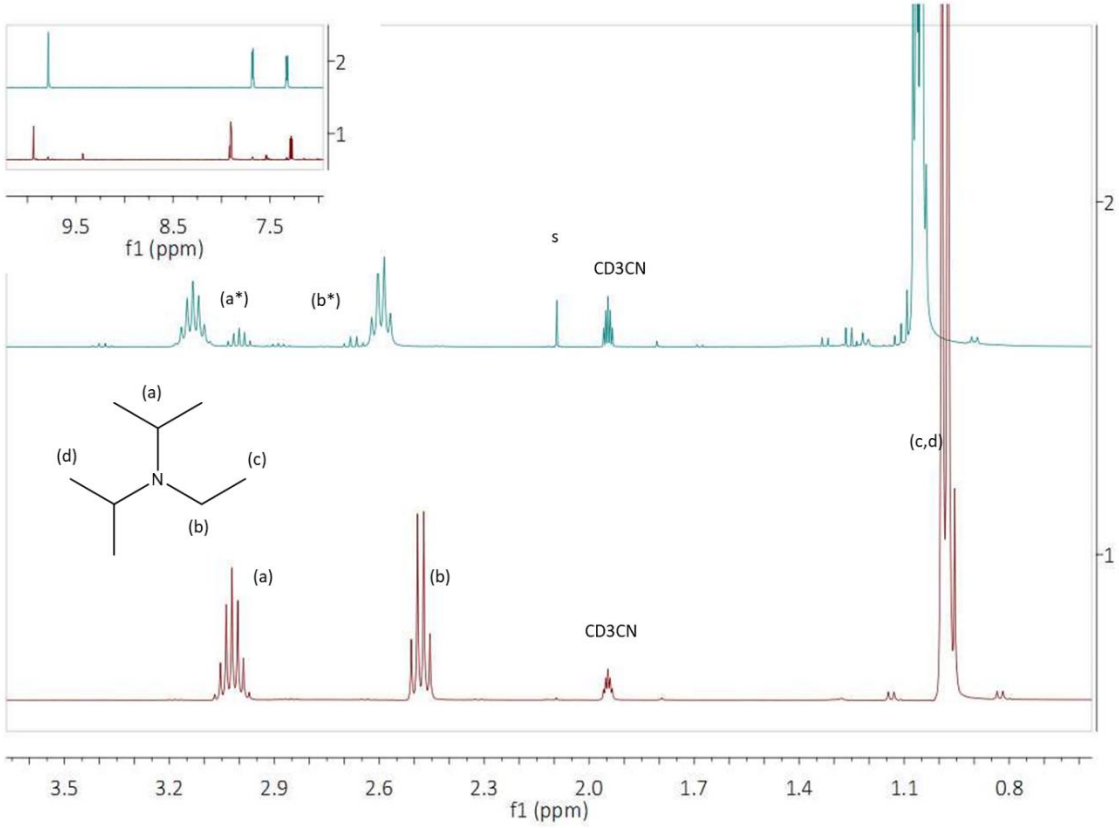

Annex 2.4 Influence of amine

Figure 2.26. The absorption spectra recorded during irradiation of compound (3) in the presence of (A) **tetramethylethylenediamine** (TEMED), (B) **triethylamine** (Et_3N) (C) **quincilidine** and (D) **DIPEA**.

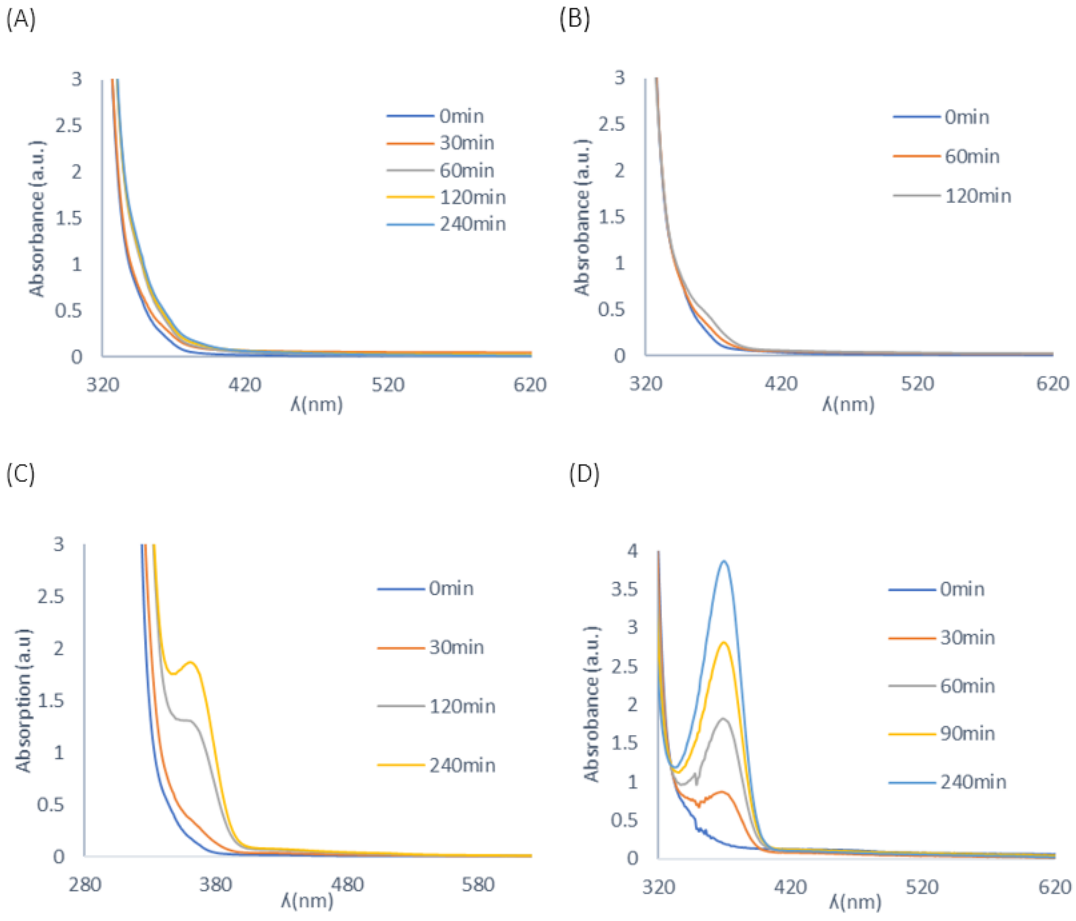

Annex 2.5 Influence of photocatalyst in the EDA photoreaction

Figure 2.27. The representative ^{1}H NMR spectra, before (1) and after (2) irradiation of **compound (3)** and **DIPEA** in the presence of photocatalyst (s-signal related to side product). Spectra recorded in deuterated acetonitrile (CD_3CN).

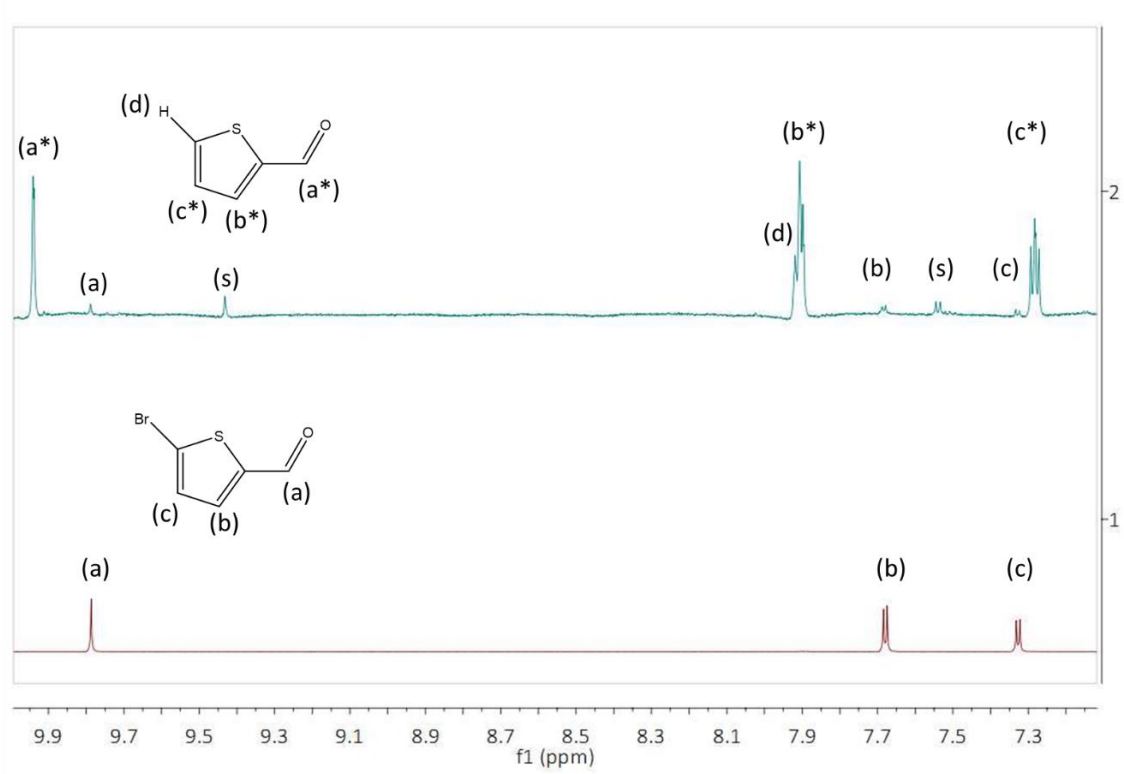

Figure 2.28. The GC-MS chromatogram of **compound (8)** and **DIPEA** before (1) and after (2) irradiation in the presence of photocatalyst.

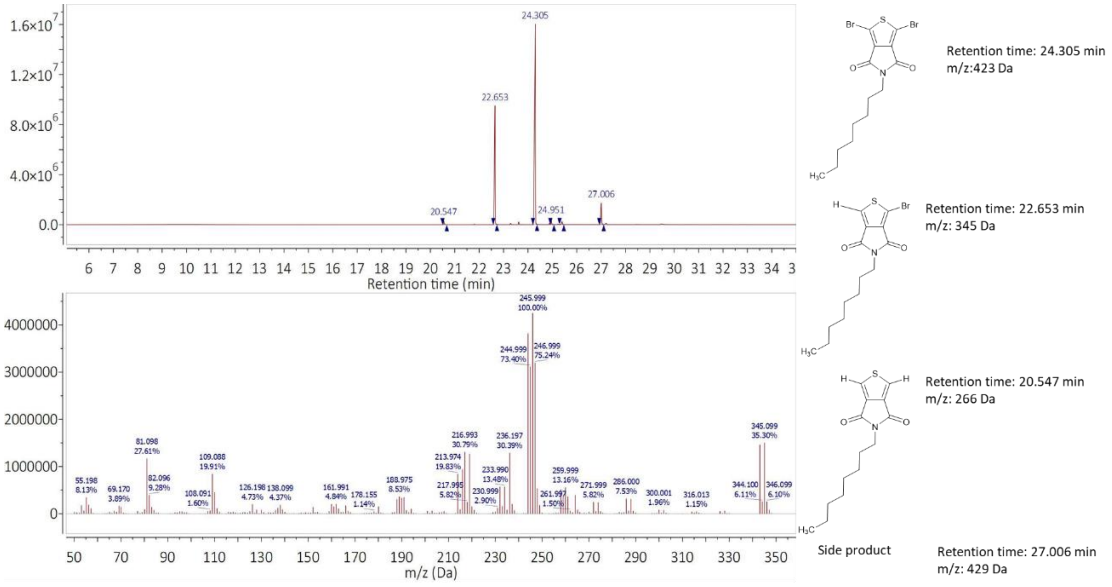

Annex 2.6 Photocatalytic reaction pathway of debromination reaction

Figure 2.29. The ^{1}H NMR spectra before (1) and after (2) irradiation of **compound (7)** and **DIPEA** in the presence of photocatalyst. Spectra recorded in deuterated acetonitrile (CD_3CN).

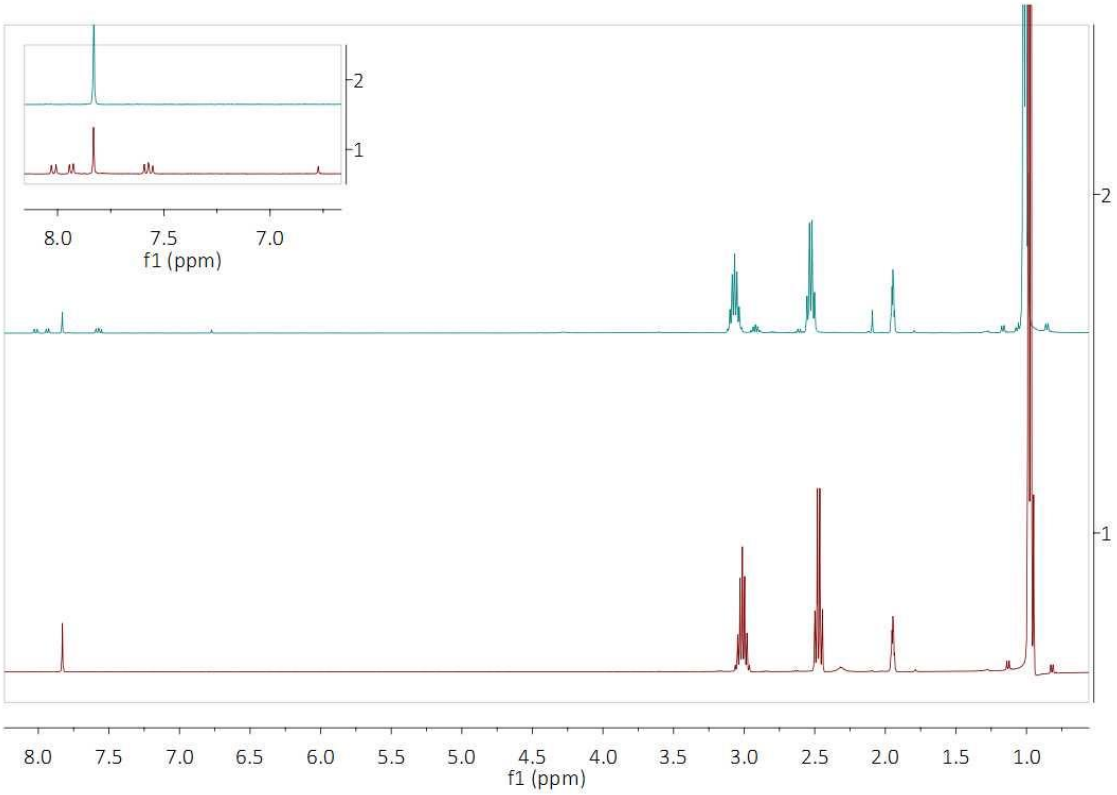

Figure 2.30. The GC-MS chromatogram of **compound (7)** and **DIPEA** in the presence of photocatalyst after 24h irradiation.

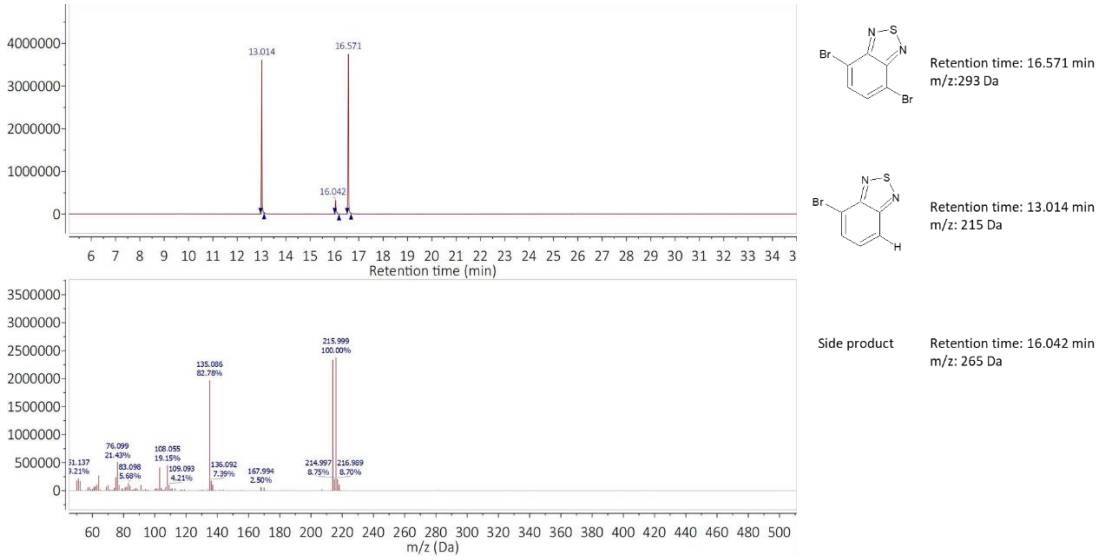

Annex 2.7 Coupling reaction

Figure. 2.31 The representative GC-MS chromatogram after 24h irradiation of coupling reaction between **2-methylthiophene** (20 equivalents) and ***4,7-dibromobenzo[c]-[1,2,5]thiadiazole*** (1 equivalent) in the presence of DIPEA (8 equivalents).

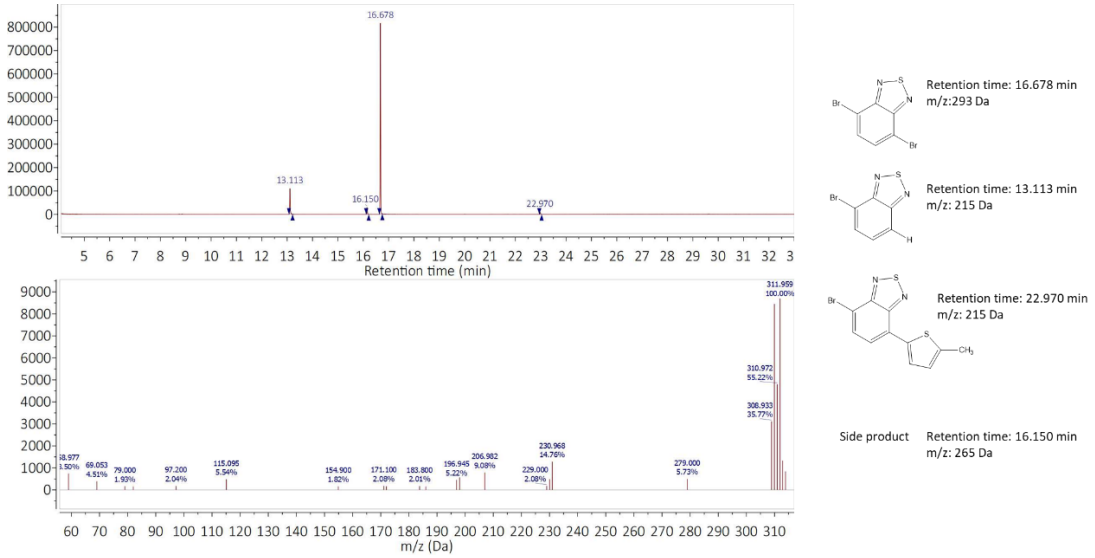

CHAPTER 3: PHOTOPOLYMERIZATION

3. Theoretical part

3.1.1 Photochemistry in the polymer synthesis

Photochemistry might be employed to initiate a chain-growth polymerization (Figure 3.1), *in which the growth of a polymer chain proceeds exclusively by reaction between monomer and active site on the polymer chain with regeneration of the active site at the end of each growth step* (IUPAC definition). The chain-growth polymerization consists of initiation and propagation reaction and may also include termination and chain transfer [1]. Unlike to conventional thermal polymerization, in which the initiation step requires high temperature, photopolymerization process is triggered by the light, where created upon irradiation initiating species may drive radical, cation, or anion polymerization [2].

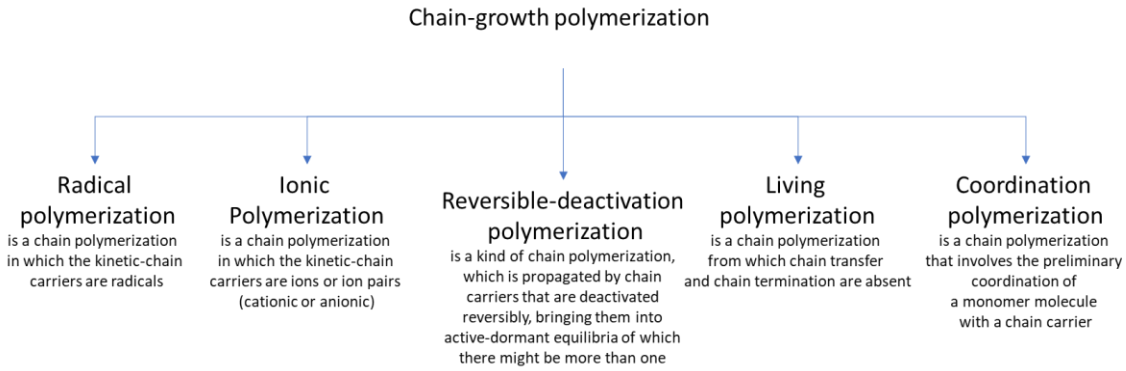

Figure 3.1. Classes of chain-growth polymerization.

3.1.2 Photoinitiated polymerization reaction

In general, photopolymerization reaction is induced by irradiation of a photointiator (PI). Hence, the initiation mechanism of polymerization process depends on the photoinitiator and is provided by its homolytic bond cleavage (I Type Photoinitiator) or by its interaction with co-initiator (II Type Photoinitiator). The interaction between the photointiator and co-initiator (DH) might occur through different pathways including electron or hydrogen abstraction, providing initiating active sites ($D^{\bullet}$) (Figure 3.2) [2,3].

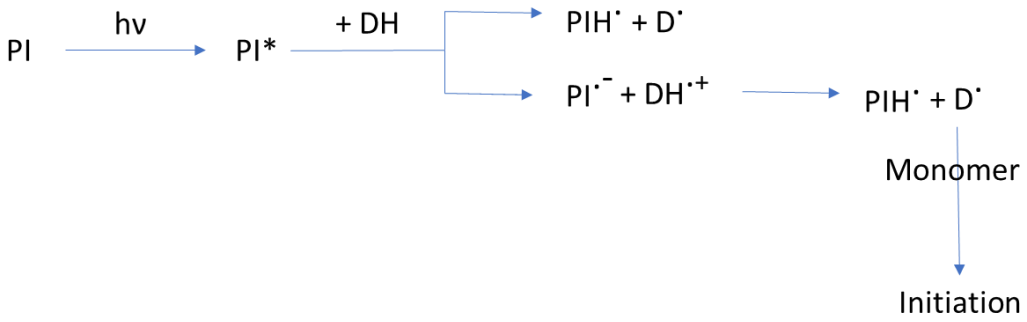

Figure 3.2. Mechanism of II type photoinitiation reaction. Reproduced from [3] with permission.

Selection of the photoinitiator and co-initiator is crucial to provide a successful photopolymerization reaction, since in this two-component initiator system, the kinetic of photopolymerization reaction is rather limited [2]. Moderate reactivity is caused by the uncontrolled radical reactions (like bimolecular reactions, radical recombination reaction, or termination reaction) between monomer, active species ($D^{\bullet}$) and inactive species ($PIH^{\bullet}$). To avoid an untimely termination of the growing chain, regeneration of the inactive radicals ($PIH^{\bullet}$) into reactive species (PI) is required. Regeneration of the photoinitiator is mainly achieved by the addition of a third component (A), which consumes the inactive radicals ($PIH^{\bullet}$) (Figure 3.3).

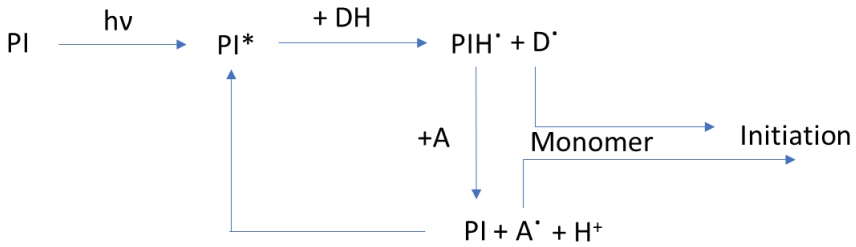

Figure 3.3. The multi-components photoinduced reaction system. Reproduced from [3] with permission.

A remarkable improvement on the reaction control in three-component initiator system is achieved when the **photoinitiator** is restored during the process and consequently **behaves as photocatalyst** [2,3]. Therefore, in the following subsections, the photoinitiator will be called photocatalyst and the co-initiator will be called initiator.

3.1.3 Photoredox catalysis for polymer synthesis

Recently, the utilization of photocatalytic system is mainly limited towards photoinitiated free radical and ionic polymerization or controlled radical photopolymerization (CPR) [3]. Nevertheless, photoredox catalysis has become increasingly important for polymer science, in which photocatalyst can be successfully implemented not only in the polymerization process but also in a post-functionalization of polymer materials [4]. This implementation may significantly change the polymer chemistry providing facile synthesis of polymers with precisely controlled molecular weight (molecular weight distribution), different functionalities, well-defined architectures, and therefore with desirable physicochemical properties [5,6,7].

3.1.4 Photo-controlled polymerization

To own control over polymer composition and associated features, challenge of random polymerization must be addressed. The traditional photoinitiated free radical polymerization is controlled only at the initiation step, whereas all subsequent growth steps (propagation and termination) responsible for polymer properties are uncontrolled. The radicals created in the system are not immediately and reversibly consumed and can continuously propagate until they incidentally terminate. Hence, the growth of an individual polymer chain must be balance by initial monomer/initiator ratio, as with traditional radical polymerization [8].

Controlled photopolymerization might be achieved by the reversible deactivation strategy, where the addition of **radical trapping agent** allows to keep low concentration of propagating radicals and thus prevent random termination. The radical trapping agent (*e.g.* **halogen atom** (X)) is necessary to deactivate propagating radicals ($R^{\bullet}$) and provide dormant non-propagating species (R-X), which are reversibly activated (Figure 3.4). Since, most of the polymer chains are in the dormant state and radicals remain at low concentration, it is possible to initiate all chains at approximately same time and achieve uniform individual chains growth [9]. Therefore, in the controlled radical polymerization (CPR), the rate of initiation (k_i) should be faster than the rate of propagation (k_p) reaction.

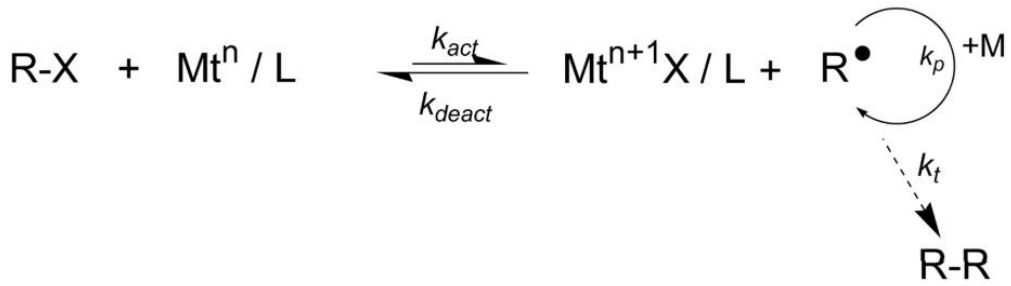

Figure 3.4. Mechanism of the reversible deactivation on the example of ATPR polymerization (X-halogen atom, Mt^nL- catalyst, M-monomer, $R^{\bullet}$-propagating radical, R-R undesired termination).

The reversible deactivation strategy might be accomplished in many ways: by the atom transfer polymerization (ATPR), reversible fragmentation chain transfer (RAFT) or organometallic radical mediated polymerization (OMRP)) [3,9,10]. Nevertheless, the balance between deactivation of radical chains and reactivation of the dormant species remains the main issue of CPR process [3].

The equilibrium between the reversible activation and deactivation reaction is the clue to achieve a control on the polymer chain growth. For this reason, the deactivation reaction rate (k_{deact}) should be faster than the activation rate (k_{act}). Consequently, the concentration of dormant species must be sufficiently higher than the concentration of propagating radical and sufficiently lower to prevent slowing down or halting the reaction [11,12].

The efficient reactivation of dormant species might be easily achieved in the photoactive reaction system, where the absorption of photon by the catalyst or reagent triggers the dormant species. This approach provides to photo-controlled polymerization, in which the growth of individual polymer chains is switchable between “on” and “off” states [8,9].

3.2 Experimental part

Radical intermediates (like radical and radical ions) play a key role in many chemical transformations. Especially, in organic and polymer synthesis where the radical chain reaction mechanism is involved [13]. On this account, the photogenerated radicals, formed

during debromination reaction of ***4,7-dibromo-2,1,3-benzothiadiazole*** (compound 7), were apply in polymerization transformation, to extend application of the previously presented photocatalytic system based on **T_3BTCH_3 photocatalyst**.

3.2.1 Selection of the reagent

As previously discussed in Chapter 2.3.6, debromination reaction of **compound (7)** might take place by the photoreductive or by the photooxidative mechanism, since in the photocatalytic system based on **T_3BTCH_3**, an efficient electron transfer occurs by the reduction of halogen **compound (7)** and the oxidation of **DIPEA** (sacrificial agent). Therefore, in both these cases, the photocatalytic species (oxidized or reduced depends on the mechanism) might react with *4,7-dibromo-2,1,3-benzothiadiazole* **(compound 7)**, providing the **thiadiazole radicals**. The thiadiazole radicals might further interact with the selected monomer and trigger desired polymerization reaction. Therefore, **compound 7** might act as **initiator** of polymerization reaction. However, as previously mentioned in Chapter 2.4.2, the selection of reagents is crucial to redirect dominant debromination reaction with respect to other. Looking for a suitable reaction partner for the polymerization reaction, methacrylate monomers were proposed. Presented monomers (Table 3.1) belong to class of highly reactive compounds, which can easily stabilize the propagating radicals [14].

Table. 3.1. Selected monomer.

Monomer name	Abbreviation	Chemical structure
Methyl methacrylate	MMA	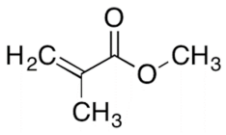
Lauryl methacrylate	LMA	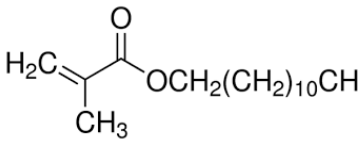

As a reminder, the presence of DIPEA in the photocatalytic system, promotes the photooxidative mechanism, in which the oxidation process of amine leading to the formation of amine radical cation. Consequently, the amine radical might provide a cascade of uncontrolled radicals reactions, including the recombination processes, which might slow down or inhibit desired polymerization reaction. Additionally, the uncontrolled radical reactions might further result in the generation of side products. For that reason, the use of amine in the present photocatalytic system has been questioned. To understand if the addition of DIPEA promotes or blocks polymerization reaction, the first experiment was carried out with and without the amine, in the presence of T_3BTCH_3 (as photocatalyst) and compound 7 (as initiator). The reaction progress was monitored using UV-Vis spectroscopy, where an increasing of the absorption background indicates a polymer formation, because unlike to the selected monomer, the polymer is not well soluble in acetonitrile. Hence, the formation of polymer results in clouding of the reaction mixture, which simultaneously increases of the absorption background. As shown in Figure 3.5, the faster growth of the absorption is observed without the presence of amine, which suggests that addition of DIPEA might block the polymerization process. Thereby, DIPEA was not further applied to carry out polymerization reaction.

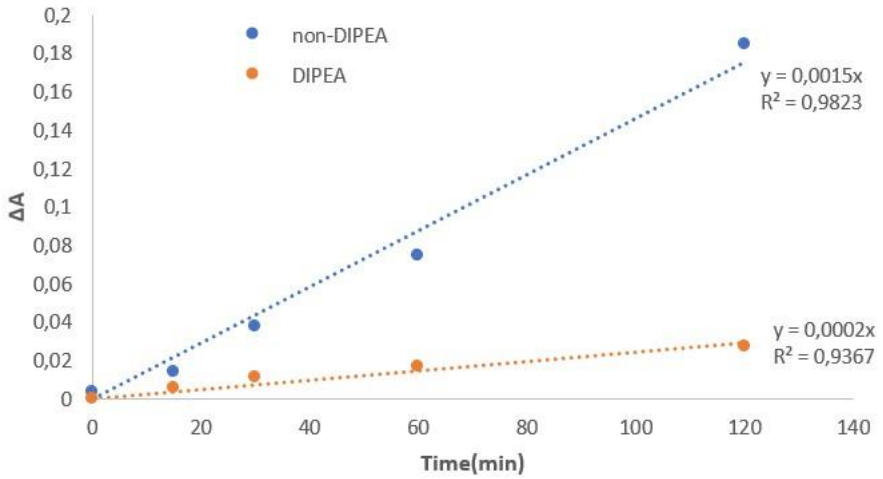

Figure 3.5. The changes in the absorption spectra given at λ=620nm during polymerization reaction of lauryl methacrylate ($1x10^{-3}$moles) in the presence of 4,7-dibromobenzo[c][1,2,5] thiadiazole ($5x10^{-5}$moles) as initiator; T_3BTCH_3 as photocatalyst ($5x10^{-7}$moles) and DIPEA ($1x10^{-4}$moles) in acetonitrile solution (3mL).

3.2.2 Mechanistic studies

To confirm the previously proposed reaction pathway, in which T_3BTCH_3 acts as the photocatalyst and compound (7) acts as the radical initiator, the spectroscopic studies were performed. Initially, the absorption and emission spectra of reaction mixtures were recorded upon the addition of selected monomers. In all cases, non-remarkable changes of the absorption and emission indicate that all the monomers do not quench an excited state of T_3BTCH_3. Consequently, in the present reaction system, an efficient electron transfer takes place only between photocatalyst and initiator. An exemplar absorption and emission spectra upon addition of lauryl methacrylate are shown in Figure 3.6.

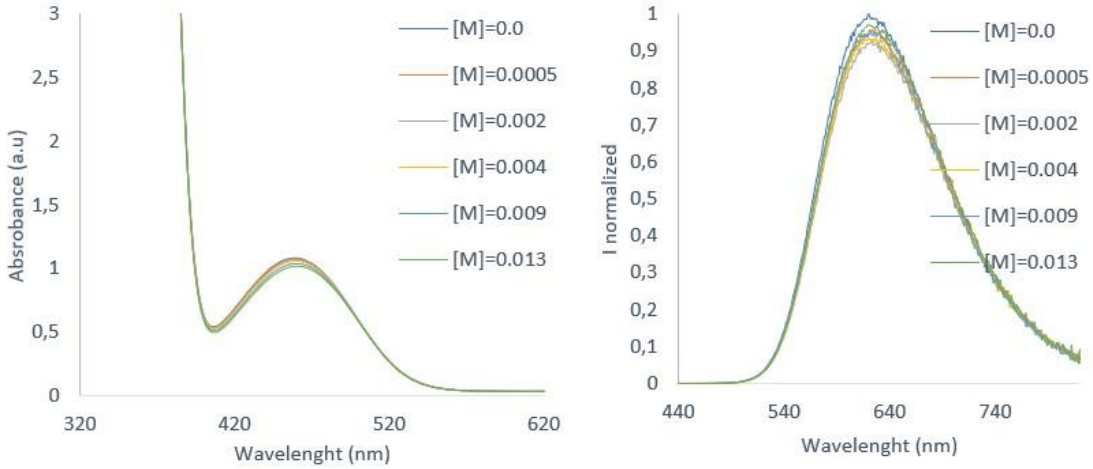

Figure 3.6. Absorption and emission spectra of reaction mixture (*i.e.* T_3BTCH_3 ($1.6x10^{-4}$M) and compound (7) ($1.6x10^{-2}$M) registered upon the addition of lauryl methacrylate, in acetonitrile solution.

To further support the photocatalytic mechanism of polymerization reaction, a range of experimental conditions were examined. The polymerization was performed without the presence of photocatalyst, without the presence of initiator and in the absence of light. In all the cases no reaction, after 16h of irradiation, is observed. This corroborates that an efficient polymerization undergoes *via* photocatalytic reaction pathway.

As shown in Figure 3.7, the presence of photocatalyst in its excited state (Cat*) is required to reduce the halogen compound (Pn-Br), which upon the addition of monomer (R) initialize the chain propagation. The propagating radical ($P_n^{\bullet}$) after a single or several monomer additions is deactivated and forms a dormant polymer chain with a bromo end group (R-P_n-Br). To deactivate chain propagation and to close photocatalytic cycle, formed radical cation ($Cat^{+\bullet}$) must be able to oxidize the propagating radical ($Pn^{\bullet}$). If is the case, present polymerization process is an analogous manner to **traditional atom transfer radical polymerization (ATPR)** [15,16].

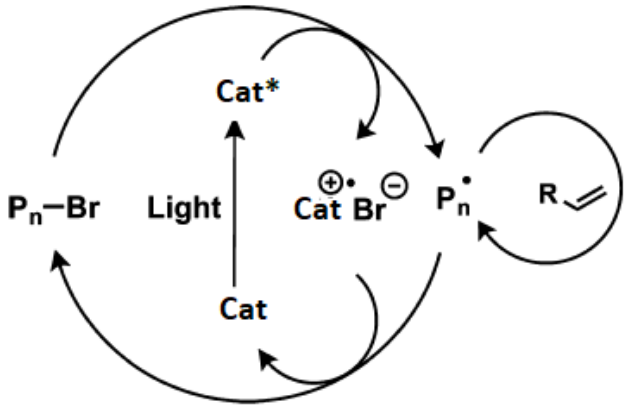

Figure 3.7. Proposed mechanism of photomediated radical polymerization (Cat-photocatalyst, Cat*- excited state of photocatalyst, $Cat^{+\bullet}$- highly oxidizing radical cation, P_n-polymer chain (n=0,1,2…,)). Reprinted with permission from [17]. Copyright (2014) American Chemical Society [17].

In traditional ATPR method, repeatedly reattachment the Br chain-end group onto the polymer, allows to use isolated polymers to reinitiate polymerization process [16]. To confirm presence of initiator in polymer structure, the UV-Vis spectroscopy was applied. Recorded absorption spectra of isolated polymethyl methacrylate indicate the presence of initiator inside the polymer chain (Figure 3.8).

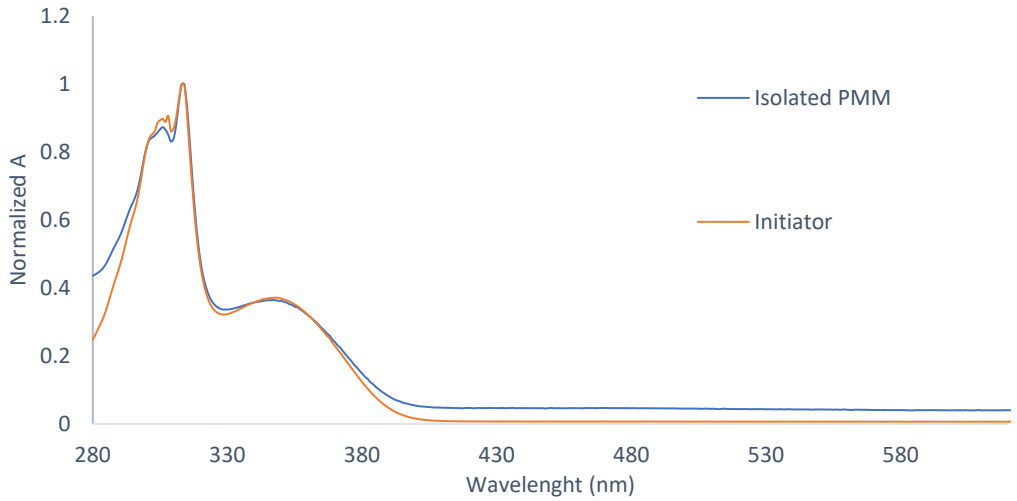

Figure 3.8. Normalized absorption spectra of initiator and isolated polymer of methyl methacrylate (reaction conditions are described in Table 3.3; Entry 2) in tetrahydrofuran (THF).

3.2.3 Influence of the light

Since in **the photo-controlled** ATPR polymerization, propagation of the polymer chain should occur only in the presence of excited state of photocatalyst, no polymerization reaction should be observed without the presence of light. To prove this hypothesis, the polymerization reaction was carried out switching on and off the light. As first, the reaction mixture was exposed to irradiation for 15 minutes and then the same sample was stored in the dark for the next 15 min. Before and after each "on"-"off" cycle, the absorption spectra were registered (Figure 3.9). As demonstrated, a significant growth of the absorption background (indicates the polymer formation) is observed only when reaction mixture is exposed on the light. No remarkable changes are observed during the dark period. These results clearly show that the polymerization reaction strictly depends on the light and is stopped almost immediately in the dark period. Hence, presented approach might lead to successful strategies for photo-controlled polymerization process, where the reversible activation and deactivation of reaction is switchable between ''on'' and ''off'' state.

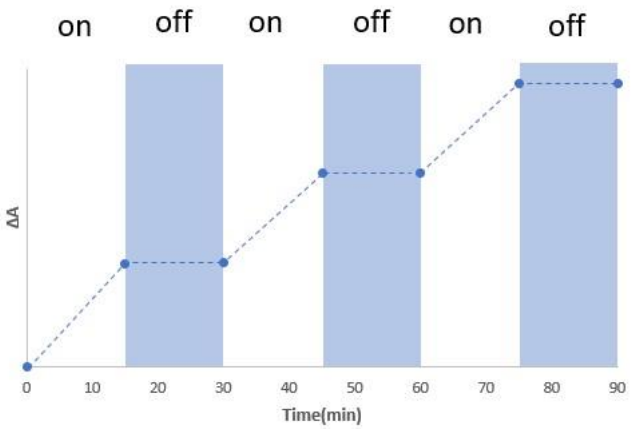

Figure 3.9. The changes in the absorption spectra given at λ=620nm during polymerization reaction of lauryl methacrylate ($1x10^{-3}$moles) in the presence of 4,7-dibromobenzo[c][1,2,5]-thiadiazole ($5x10^{-5}$ moles) as initiator and T_3BTCH_3 as photocatalyst ($5x10^{-7}$moles) in acetonitrile solution (3mL). Increasing absorption background upon irradiation (on) corresponding to polymer formation (not changes observed after the light was switched off).

Importantly, prolonged irradiation of the reaction mixture does not lead to photocatalyst degradation. However, polymerization reaction must be performed under inert conditions, since the present of the oxygen in the reaction system causes secondary reaction and catalyst decomposition (Annex 3.1).

3.2.4 Molecular weight and polydispersity

Initially, polymerization reaction of lauryl methacrylate ($1x10^{-3}$moles) was carried out in the presence of 4,7-dibromobenzo[c][1,2,5]-thiadiazole ($5x10^{-5}$moles) as initiator and T_3BTCH_3 as photocatalyst ($5x10^{-7}$moles) in acetonitrile solution (3mL). The concentration of reagents was selected according to previously described procedure for coupling reaction (Chapter 2.4). Upon this reaction conditions, concentration of the initiator is sufficient to quench approximately 54% of excited state of photocatalyst (Chapter 2.2.3; Figure 2.7). The conversion rate of polymerization reaction was estimated by ^{1}H NMR spectroscopy and afforded **67%** after 16h of irradiation (Figure 3.10). The polymer molecular weight distribution was calculated based on the gel permeation

chromatography (GPC) technique and is presented in the Table 3.2. The polymerization and isolation procedures and further characterization of polymer are described in Annex 3.2/3.3.

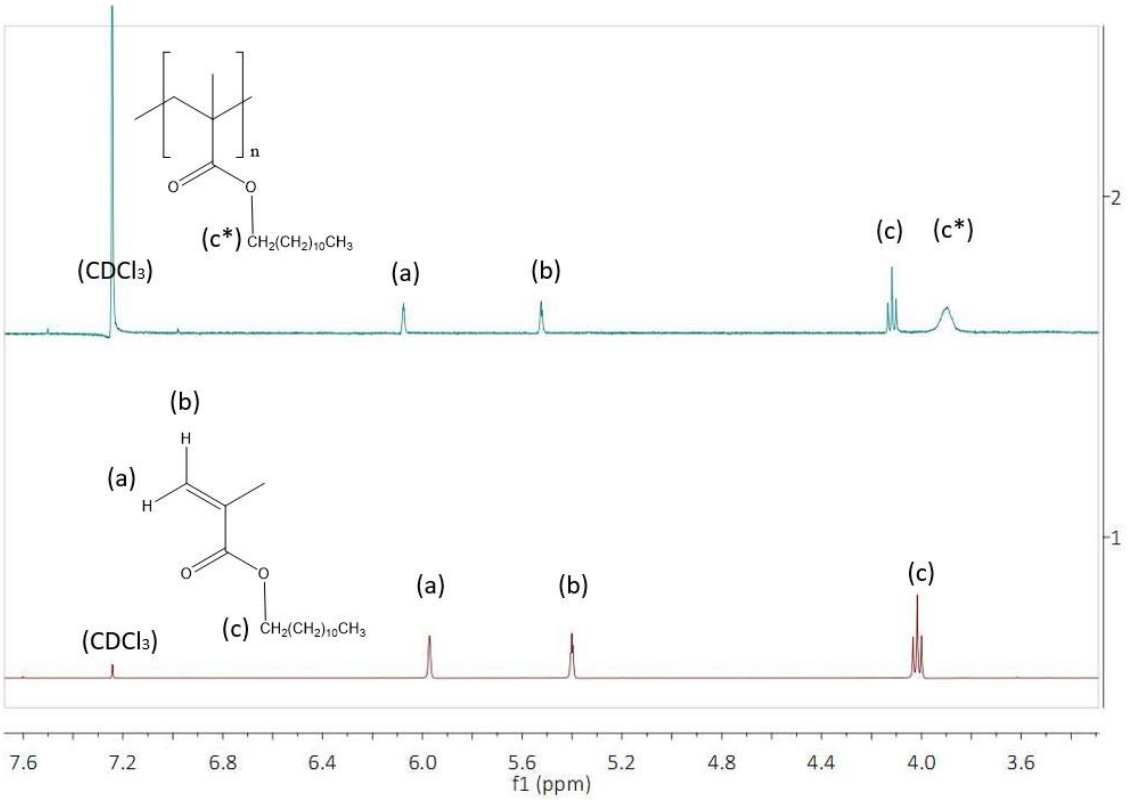

Figure 3.10. The ^{1}H NMR spectra of lauryl methacrylate (1) and post reaction mixture (2) in deuterated chloroform ($CDCl_3$).

The polymer consists of monomers (constitutional units) chemically bonded into long chains. Therefore, the molecular weight of the polymer is described as average molecular weight calculated from the molecular weights of all the chains, and is characterized by the number-average molar mass (or molecular weight) (Mn):

$$M_n = \frac{\sum_i N_i M_i}{\sum_i N_i} \tag{3.1}$$

and the mass-average molar mass (or molecular weight) (Mw):

$$M_w = \frac{\sum_i N_i M_i^2}{\sum_i N_i M_i} \tag{3.2}$$

where $\boldsymbol{N_i}$ is the number of chains of molecular mass $\boldsymbol{M_i}$.

Ratio between (Mw) and (Mn) is defined as the polydispersity index (D), which indicates the molecular weight distribution of polymer chains. The monodisperse polymers, in which all the chain are equal, correspond to D equal to 1. In general, the polydispersity index for

the radical polymerization is in the range 1.5-2.0, whereas for well-controlled polymerization process is between 1.0-1.5 [15-18].

As shown in Table 3.2; Entry 1, upon the initial reaction condition relatively high dispersity (D=1.95) is reached. Polymerization reaction allows to gain a little bit better control over the molecular weight distribution when the half of the initiator (with constant amount of monomer) is applied.

Table 3.2. Molecular weight and polydispersity of lauryl methacrylate*.

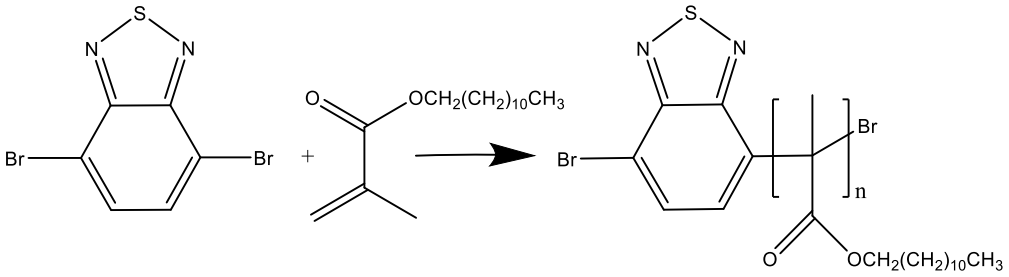

Entry	Initiator Equivalents	Monomer Equivalents	Time [h]	Mn [g/mol]	D(Mw/Mn)
1	1	20	16	94264	1.95
2	0.5	20	16	11063	1.45

*General scheme of the polymerization reaction of lauryl methacrylate. Reaction conditions: T_3BTCH_3 ($1.6x10^{-4}$M); *4,7-dibromo-2,1,3-benzothiadiazole* (1 equivalent = $1.6x10^{-5}$moles), MMA (according to the table); solvent ACN (1mL); room temperature, irradiation source: 460nm LED lamp. GCP chromatogram is shown in Annex 3.3.

To find the best reaction conditions, in which polymers with a high number average molecular weight (Mn) and low dispersity (D) are obtained, several polymerization reactions of methyl methacrylate, with various initiator-monomer ratio, were carried out (Table 3.3, Entry 1-4). The concentration of reagents (*i.e.* amount of initiator and monomer) was increased to facilitate isolation of the product. Whereas, the concentration of photocatalyst remains constant. In all cases, polymerization reaction leads to full conversion of methyl methacrylate (no signal from monomer in the post reaction mixture is observed) after 16h of irradiation. Spectra of isolated polymer is present in Annex 3.4.

Table 3.3. Influence of monomer-initiator ratio on the polymerization reaction of methyl methacrylate*.

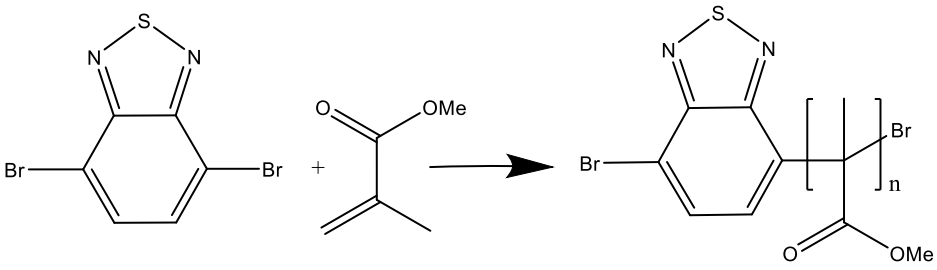

Entry	Initiator equivalent	Monomer equivalent	Time	Mn	D (Mw/Mn)
1	1	100	16h	135800	2.21
2	1	200	16h	236700	1.85
3	0.2	100	16h	224700	1.88
4	2	100	16h	174800	2.41

*General scheme of the polymerization reaction of methyl methacrylate. Reaction conditions: T_3BTCH_3 ($1.6x10^{-4}$M); *4,7-dibromo-2,1,3-benzothiadiazole* (1 equivalent= $4.6x10^{-5}$moles), MMA (according to the table); solvent ACN (1mL); room temperature, irradiation source: 460nm LED lamp.

Presented data indicate that the molecular weight (Mn) might be adjusted by the monomer to initiator ratio (Table 3.3, Entry 1-2) and increases with increased amount of monomer. However, upon selected reaction conditions (constant concentration of initiator) polymer dispersity remains quite high. High polydispersity might be reduced by decreasing amount of initiator and by selection of suitable ratio between initiator and photocatalyst. This is clearly seen on the previous example (Table 3.2, Entry 2), where lower concentration of initiator (3 x times lower concentration) results in lower quenching of photocatalyst and hence provides lower number of propagating radicals. Since polydispersity strictly depends on the equilibrium between dormant species and active radicals, too high concentration of propagation radicals (Table 3.3, Entry 4) leads to a wide distribution of the polymer chains. Furthermore, in the ATPR system formation of polymers with low dispersion (D<1.3) and high molecular weight (Mn> 100 000) is challenging to obtain, due to kinetics of the process [18]. In general, polydispersity increases rapidly beyond 1.2 when the number-average molecular weight (Mn) exceeds 100 000 [19]. Hence, selection of suitable reaction

conditions depends on the target *i.e.* desired polymer properties. Comparison between the molecular weight distribution for all performed reaction conditions are presented in the Annex 3.5.

3.3 Conclusion

Photocatalytic system based on T_3BTCH_3 was successfully applied for the radical polymerization reaction of methacrylate compound with two different functional groups (-lauryl, and -methyl). As demonstrated, polymerization reaction can be controlled through external light stimulation (switch off-off state) and occurs in analogy to traditional atom transfer radical polymerization (ATPR), in which incorporation of initiator structure into polymer chain is observed. Furthermore, unlike to standard controlled radical polymerization method, presented photocatalytic system allows to synthesise polymers with very high number-average molar mass (Mn). However, since the high number-average molar mass results in their low dispersity, selection of suitable reaction conditions (like [monomer]:[initiator], [initiator]:[photocatalyst] ratio) is crucial to gain better control over the molecular weight distribution.

The prolonged stability of selected photocatalyst upon irradiation gives the possibility to replace an expensive and toxic metal catalyst (commonly use in ATPR method [15-17]) and develop a more sustainable way to produce a wide range of functional polymer materials. For instance, incorporation of thiophene-based organic dyes into polymer structure might provide a new class of semiconductor polymers for electronic application.

Reference

[1] I. Mita, R.F.T. Stepto, U.W. Suter, *Pure &App. Chem*., 1994, 66 (12), 2483.

[2] S. Dadashi-Silab, S. Doran, Y. Yagci, *Chem. Rev*., 2016, 116, 10212.

[3] N. Zivic, M. Bouzrati-Zerelli, A. Kermagoret, F. Dumur, J.P. Fouassier, D. Gigmes, J.Lalevèe, *ChemCatChem*, 2016, 8, 1617.

[4] N. Corrigan, S. Shanmugam, J. Xu, C. Boyer, *Chem. Soc. Rev*., 2016, 45, 6165.

[5] N.V. Tsarevsky, K. Matyjaszewski, *Chem. Rev*., 2007, 107, 2270.

[6] M. Ouchi, T. Terashima, M. Sawamoto, *Chem. Rev.,* 2009, 109, 4963.

[7] A. Anastasaki, V. Nikolaou, G. Nurumbetov, P. Wilson, K. Kempe, J.F. Quinn, T.P. Davis, M.R. Whittaker, D.M. Haddleton, *Chem. Rev.,* 2016, 116, 835.

[8] M. Chen, M. Zhong, J.A. Johnson, *Chem. Rev*., 2016, 116, 10167.

[9] K. Matyszewski, *ACS Symposium Series*, 2000, 768, 2.

[10] G. Zhang, I. Young Song, K. Han Ahn, T. Park, W. Choi, *Macromolecules*, 2011, 44, 7594.

[11] A.D. Jenkins, R.G. Jones, G. Moad, *Pure Appl. Chem*., 2009, 82 (2), 483.

[12] K. Matyjaszewski, J. Xia, *Chem. Rev*., 2001, 101 (9): 2921.

[13] M.A. Cismesia, T.P. Yoon, *Chem. Sci.,* 2015, 6, 5426.

[14] T.E. Patten, K. Matyjaszewski, *Adv. Mater*., 1998, 10, 901.

[15] B.P. Fors, C.J. Hawker, *Angew. Chem. Int. Ed.*, 2012, 51, 8850.

[16] J.C. Theriot, C.H. Lim, H. Yang, M.D. Ryan, C.B. Musgrave, G.M. Miyake, *Science*, 2016, 352 (6289), 1082.

[17] N.J. Treat, H. Sprafke, J.W. Kramer, P.G. Clark, B.E. Barton, J. Read de Alaniz, B.P. Fors, C.J. Hawker, *J. Am. Chem. Soc*., 2014, 136, 16096.

[18] P. Kwiatkowski, J. Jurczak, J. Pietrasik, W. Jakubowski, L. Mueller, K. Matyjaszewski, *Macromolecules,* 2008, 41, 1067.

[19] L. Xue, U.S. Agarwal, P.J. Lemstra, *Macromolecules*, 2002, 35, 8650.

ANNEX 3

Annex 3.1 Stability of the photocatalytic system

Figure 3.11. Absorption spectra of lauryl methacrylate ($1x10^{-3}$moles) in the presence of 4,7-dibromobenzo[c][1,2,5] thiadiazole ($5x10^{-2}$moles) as initiator and T_3BTCH_3 as photocatalyst ($5x10^{-7}$moles) in acetonitrile solution (3mL), after 7 h irradiation (A) under inert atmosphere (B) in the presence of oxygen.

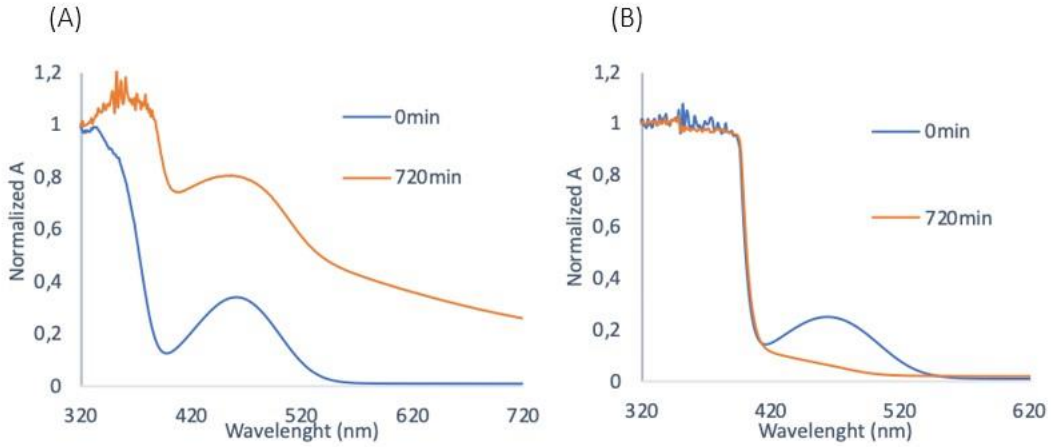

Annex 3.2 Polymerization reaction procedures

1) Reaction mixture

A 20mL vial was charged with previously prepared solution of the photocatalyst in acetonitrile and then with selected amount of initiator and monomer (depending on the reaction conditions). The reaction mixture was purged with argon (15 min degassed) and illuminated under inert atmosphere, using 460nm LED light.

2) Isolation procedure

The post-reaction mixture was pouring into a 50-fold excess of cold CH_3OH, causing the polymer to precipitate. After 20 minutes of centrifugation, the precipitate was collected *via* vacuum filtration and dried under reduced pressure.

Figure 3.12 Isolated polymer in a 50-fold excess of methanol.

Annex 3.3 Characterization

1) The gel permeation chromatography (GPC) analysis

Isolated polymers (approximately 3mg) were re-dissolved in (1mL) tetrahydrofuran (THF) and filtered before injection. A molecular weight calibration curve was obtained with polystyrene (PS) standards. Presented chromatogram shows the molecular weight distribution of the lauryl methacrylate synthesized upon the reaction conditions described in Table 3.2 (Chapter 3).

Figure 3.13. Presented chromatogram shows the molecular weight distribution of the lauryl methacrylate synthesized upon the reaction conditions described in Table 3.2 (Chapter 3).

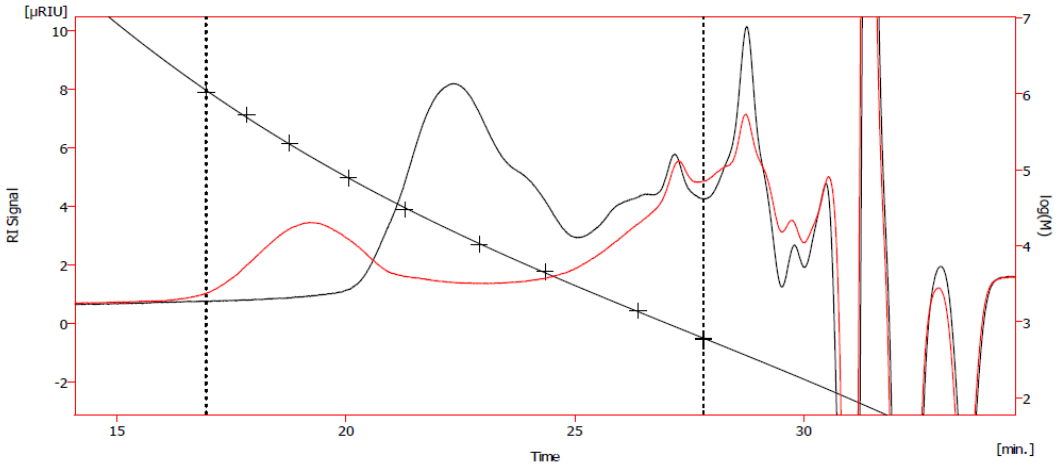

*Equation: Y = - 0,00051*X^3 + 0,04196*X^2 - 1,40123*X + 20,18628*
Correlation Factor: 0,9998134

	Max. RT	Flow Rate Correction	PD	Mp	Mn	Mw
1	22,36	0,999901	1,4508	14819	11063	16050
2	33,58	0,999901	1,0168	19	18	19

	Max. RT	Flow Rate Correction	PD	Mp	Mn	Mw
1	19,21	0,998511	1,9541	142284	94264	184202
2	33,53	0,998511	1,0171	19	18	19

2) ^{1}H NMR analysis

To analyse the progress of a polymerization at a given time point, a 50uL aliquot of the reaction media was removed *via* syringe and injected into a vial containing 0.75 mL $CDCl_3$. Monomer conversion was roughly estimated by ^{1}H NMR analysis by comparison of the integrations as follow:

$$Conversion = \frac{I_{c^*}}{(I_c + I_{c^*})} * 100\% \quad (3.3)$$

I_c - is an integration of the lauryl ester monomer peak at 4.12 ppm; is I_{c^*} - is an integration corresponding to lauryl ester polymer peak at 3.90 ppm.

Figure 3.14. Representative ^{1}H NMR spectra of crude reaction mixture after polymerization of the lauryl methacrylate (Table 3.2; Entry 1) in deuterated chloroform ($CDCl_3$).

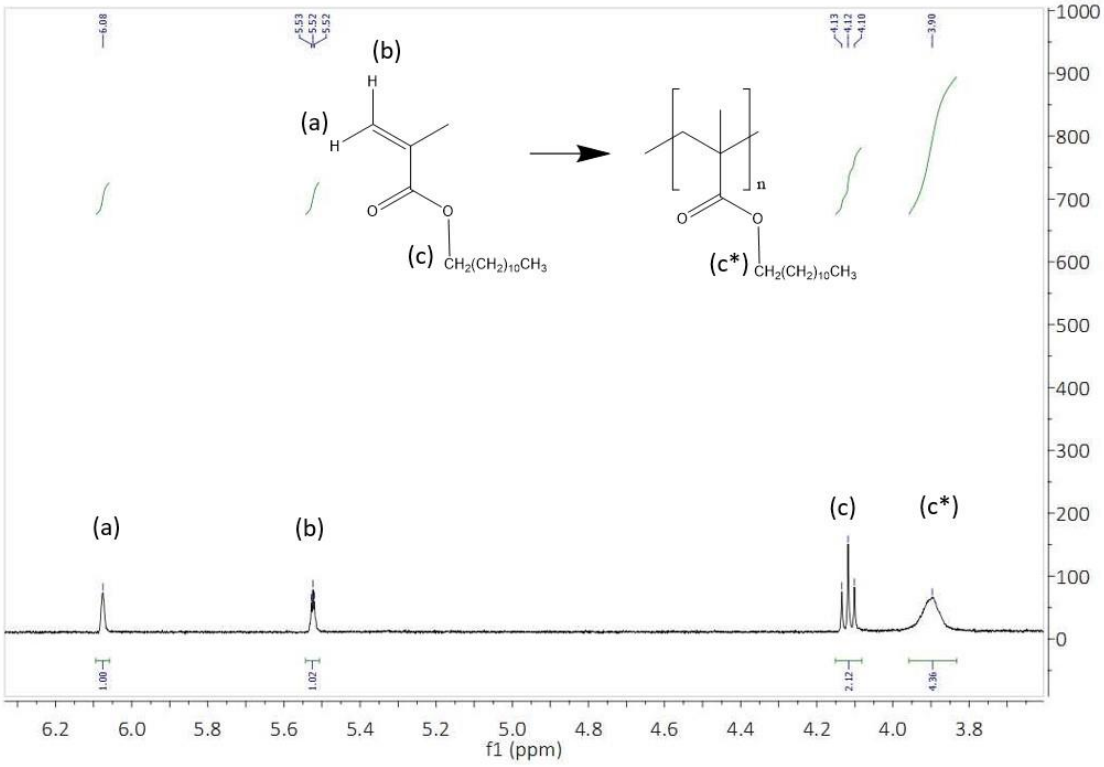

Annex 3.4 ^{1}H NMR spectra of isolated polymer

Figure 3.15. Representative spectra of poly(methyl methacrylate) in deuterated chloroform ($CDCl_3$).

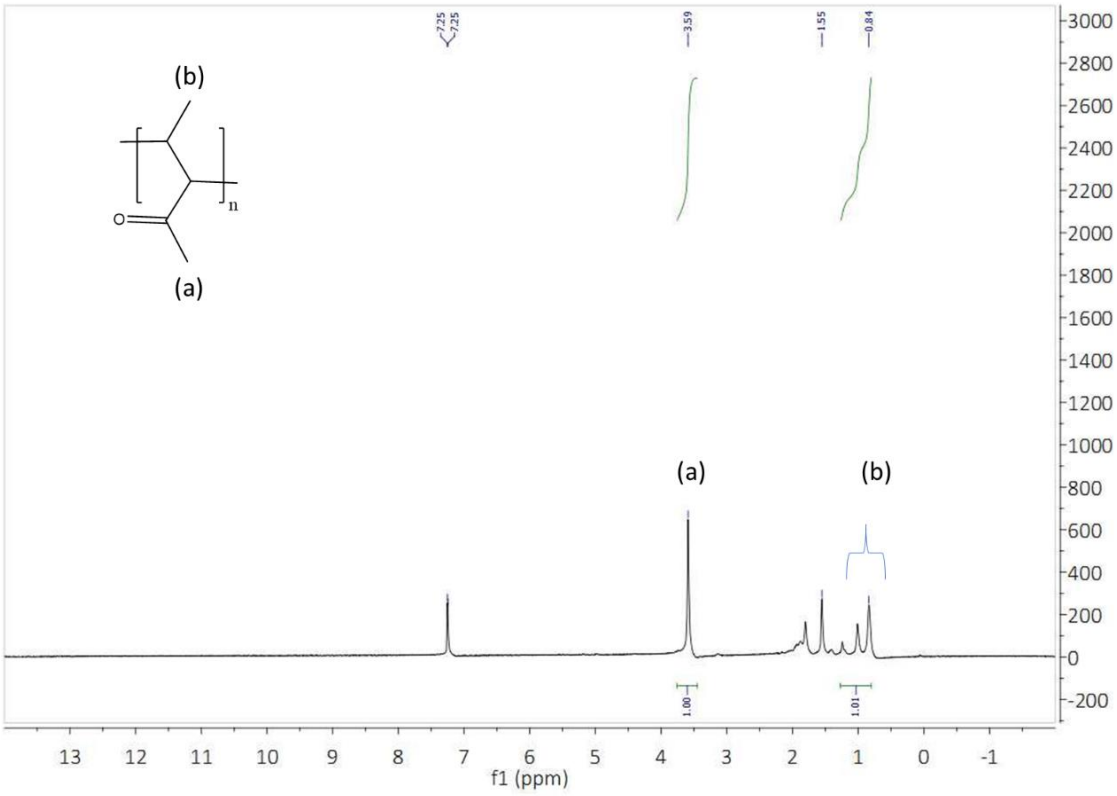

Annex 3.5 The molecular weight distribution of isolated polymer

Figure 3. 16. The GPC chromatogram for isolated poly(methyl methacrylate).

Entry	Initiator equivalent	Monomer equivalent	Time	Mn	D (Mw/Mn)
1	1	100	16h	135800	2.21
2	1	200	16h	236700	1.85
3	0.2	100	16h	224700	1.88
4	2	100	16h	174800	2.41

Reaction conditions: T_3BTCH_3 ($1.6x10^{-4}$M); *4,7-dibromo-2,1,3-benzothiadiazole* (1 equivalent= $4.6x10^{-5}$moles), MMA (according to the table); solvent ACN (1mL); room temperature, irradiation source: 460nm LED lamp.

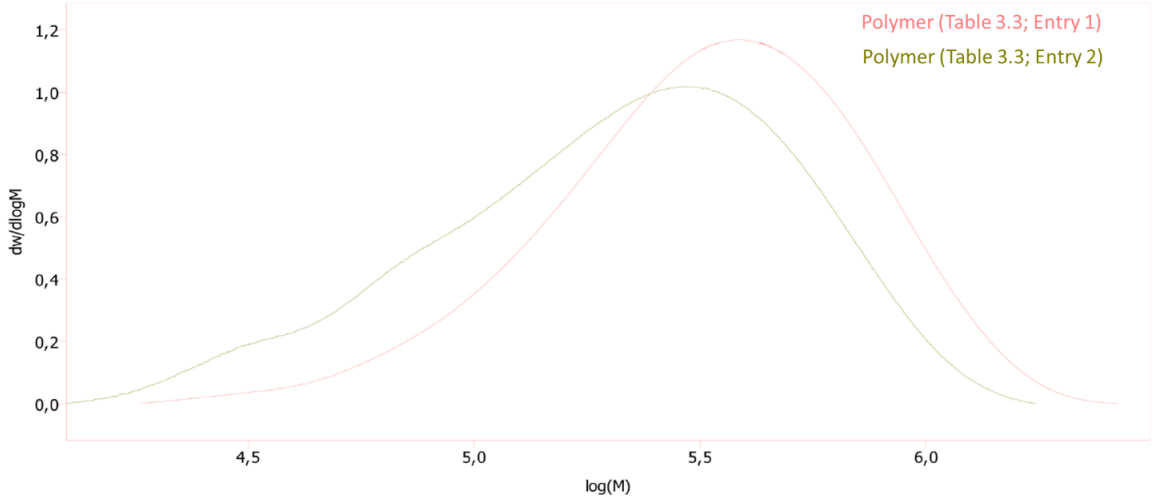

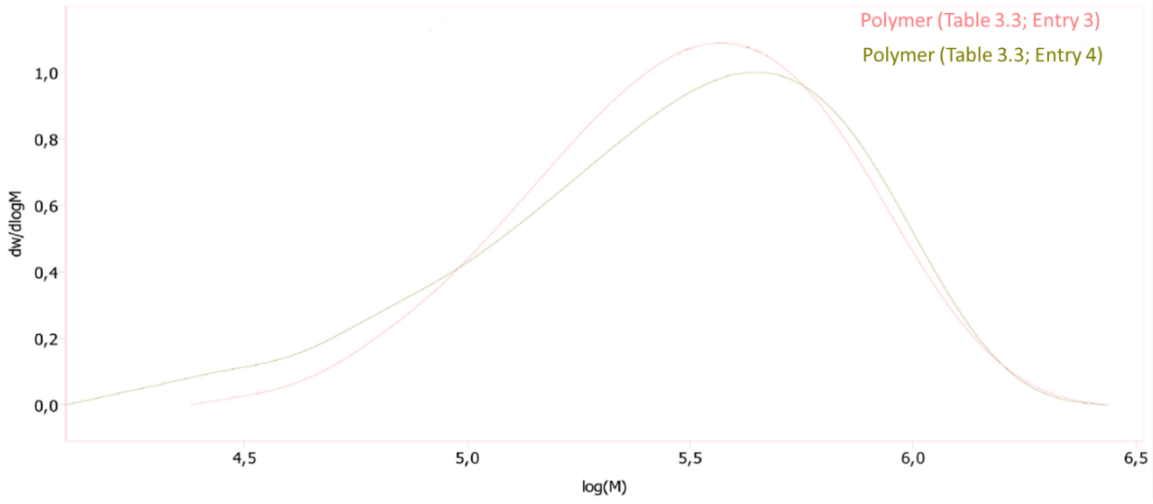

CHAPTER IV: FLOW PHOTOCHEMISTRY

4.1 Theoretical part

4.1.1 Basic concepts of flow photochemistry

The continuous flow chemistry has a pivotal importance to overcome the classical limitations of photochemical transformation performed in batch reactors. The main obstacle of the photochemical batch process is limited photon-transport phenomena. The attenuation effect of photon transfer in the batch rector is caused by the decreasing intensity of light passing through the reaction medium (Figure 4.1) [1]. As dictated by the Bouguer-Lambert-Beer law, the transmission of light decreases logarithmically with respect to optical path length. Consequently, in the applied large-scale batch reactors, a homogeneous radiation distribution is not possible to obtain. This non-uniform irradiation often results in a prolonged reaction time, which might cause the over-irradiation of reaction mixture and hence provides the side product formation [2]. Consequently, to avoid inhomogeneous radiation distribution, the dimension of the photoreactor should be reduced to the minimum.

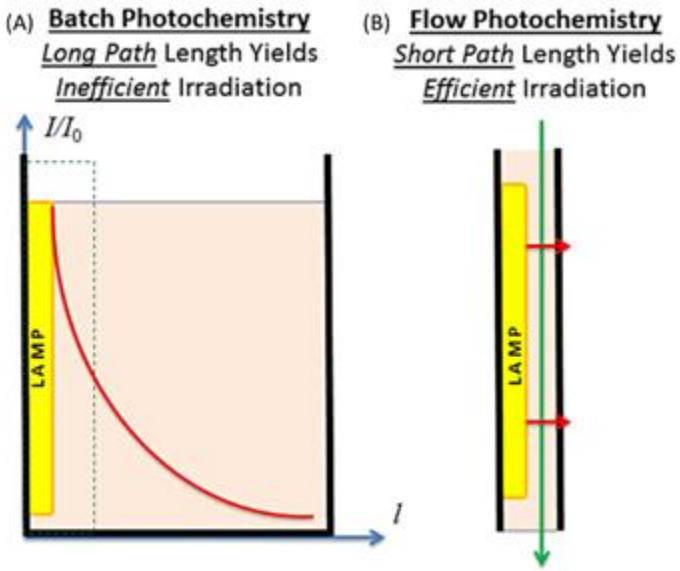

Figure 4.1. Light penetration in the photochemical (A) batch and (B) flow reactor. Reprinted with permission [1].

Unlike to batch reactors, the internal section of flow reactors is typically in the meso- (≥1mm) or micro- (≤1mm) scale. Thus, their small dimension provides high surface-to-volume ratio and allows to achieve a uniform irradiation of the reaction system. In this case, most of the light is efficiently absorbed by the reagents, which significant decreases the reaction time and allows to avoid over-irradiation. Furthermore, the high surface-to-volume ratio in microfluidic reactors leads to an efficient heat dissipation. It is especially important in photochemical transformations to control the reaction temperature, which might increase during the irradiation and result in local overheating of the reaction mixture [3,4].

The size and geometry of the reactor are crucial parameters to control the mixing phenomena, which is directly related to mass transfer. Since the mass transfer contributes to the overall reaction rate and might compete with the reaction kinetics, the characteristic mixing time of reagents must be optimised. In microfluidic reactors, where the laminar flow is dictated by the channel geometry, the mixing of reagents is driven by the molecular diffusion (D) [5]. The mixing reaction time (t_m) increases to the square of the diffusion path length (L), according to the Einstein-Smoluchovski equation.

$$t_m = \frac{L^2}{D} \tag{4.1}$$

Consequently, the microfluidic reactors can be designed to reinforce or diminish the mixing process. To eliminate the effect of mixing, the ratio of the characteristic mixing time (t_m) to the characteristic reaction time (t_r), defined as the second Damköhler number (DaII), should be less than 1. If this is the case, the chemical transformation is limited only by the reaction rate [5].

$$Dall = \frac{t_m}{t_r} \tag{4.2}$$

To reach a full conversion, the characteristic reaction time (t_r) should be lower than the residence time (t_p). Residence time is the average time of reagents inside the reactor and is expressed by the first Damköhler number (DaI). In the microfluidic reactor, the residence time might by easily controlled by the flow rate or the length of the channel.

$$Dal = \frac{t_p}{t_r} >> 1 \quad (4.3)$$

In general, the selection of suitable photoreactors and reaction conditions (*i.e.* flow rate), strictly depends on the performed chemical transformations, in which the knowledge of mass-transport phenomena and reaction kinetics might help to design an efficient reaction system. The possibility to control photon-, mass- and heat- transfer inside the microfluidic reactor results in the high reproducibility of the reaction conditions and thus in a better optimization of photochemical transformation. Furthermore, in contrast to batch reactors, the applied flow technology can be scaled up using parallel system of multi-reactors (numbering-up) [6] or by longer operation times (recycling) which significantly increases the productivity of photochemical process [7].

Transfer of the photochemical reactions from batch to flow results in a substantial acceleration of photocatalytic reaction, reducing reaction time from hours to seconds and providing higher selectivity towards the desired final product. Therefore, the continuous-flow chemistry has gained an increasing amount of interest in the past decade [4,8]. Especially, in the organic chemical synthesis in which the microfluidic technology provides the safe handling of hazardous intermediates [8]. Not surprisingly, numerous examples demonstrate the flow visible-light photoredox catalysis as a green and sustainable strategy for chemical [8,9] and polymer [4,10,11] synthesis.

4.1.2 Continuous-flow technology for photocatalytic application

The continuous-flow technology allows to address the problems of photocatalytic processes related to their industrial implementation. The scalability and the economic viability of photocatalytic process depend mainly on (i) the cost of the photocatalyst and (ii) the cost of recuperation and recycling of catalyst [4,12]. In the flow photoreactors, this issue can be accomplished in many ways according to the nature of the photocatalytic process.

In the heterogenous flow catalysis, the catalyst is often placed in packed bed fixed reactor, where the reaction mixture is flown through it [13]. The photocatalyst remains in a specific part of the reactor during processing of the reaction mixture. Thus, the reaction

product and catalyst are easily separated. This approach provides a high catalyst loading and simply fabrication of microfluidic devices, in which the channel is filled with the supported particles of catalyst (Figure 4.2A). However, due to the high resistance of the system, uncontrolled fluid dynamics and pressure drops along the channel are observed [14].

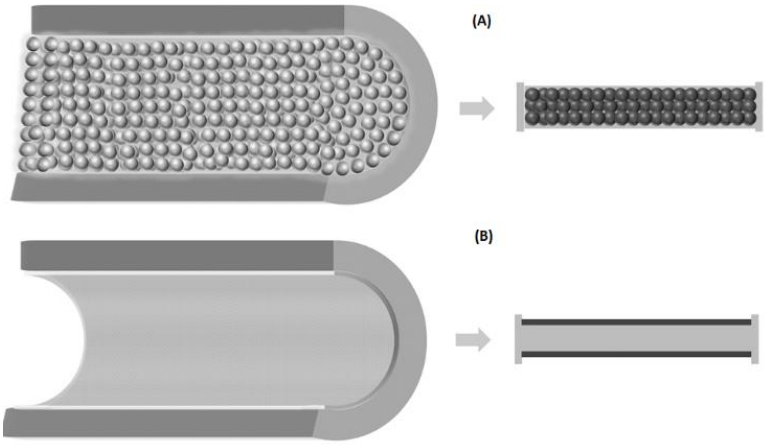

Figure 4.2. The applied flow reactors for heterogenous photocatalysis (A) packed-bed and (B) wall-coated microreactors. Reprinted with permission [14].

An alternative approach is wall-coating strategy, where the photocatalyst is immobilized on the internal walls of the microchannel (Figure 4.2B). The immobilized internal surface of the microfluidic device minimalizes the mass transfer resistance and ensures the smooth flow of reagents [14]. In this case, the monolayer or the thin film layer of photocatalyst is required to avoid clogging of the microreactor and provides efficient light penetration. Nevertheless, the uniform immobilization of photocatalyst might be impeded due to limited access to the internal area of the channel and inert surface of materials used for the microchannel fabrication. Since the microfluidic reactor can be constructed from a wide range of materials [15], the deposition of the photocatalyst might require complex technique, including physico-chemical processes such as surface activation, physical adsorption or covalent modifications [16-19]. In spite of this, the wall-coated microreactors find a broad application in many catalytic transformations. Especially in multiphase processes, where the high interfacial area between catalyst and two or more immiscible phases is crucial to accelerate the mass transfer and thus to intensify multiphase reactions [20].

The continuous flow technology is also applied in the homogeneous catalytic reaction system, where the catalyst and reagents are soluble in the same phase. So far, the microreactors for homogenous photocatalytic applications, are designed to enhance mixing process between the catalyst and reagents or to provide a multi-step sequence of homocatalytic processes (Figure 4.3) [5,22]. This strategy drives the safe handling of highly thermally, unstable or dangerous intermediates and allows to avoid their further isolation [22]. Nevertheless, the presented approaches still require a final catalyst and product separation.

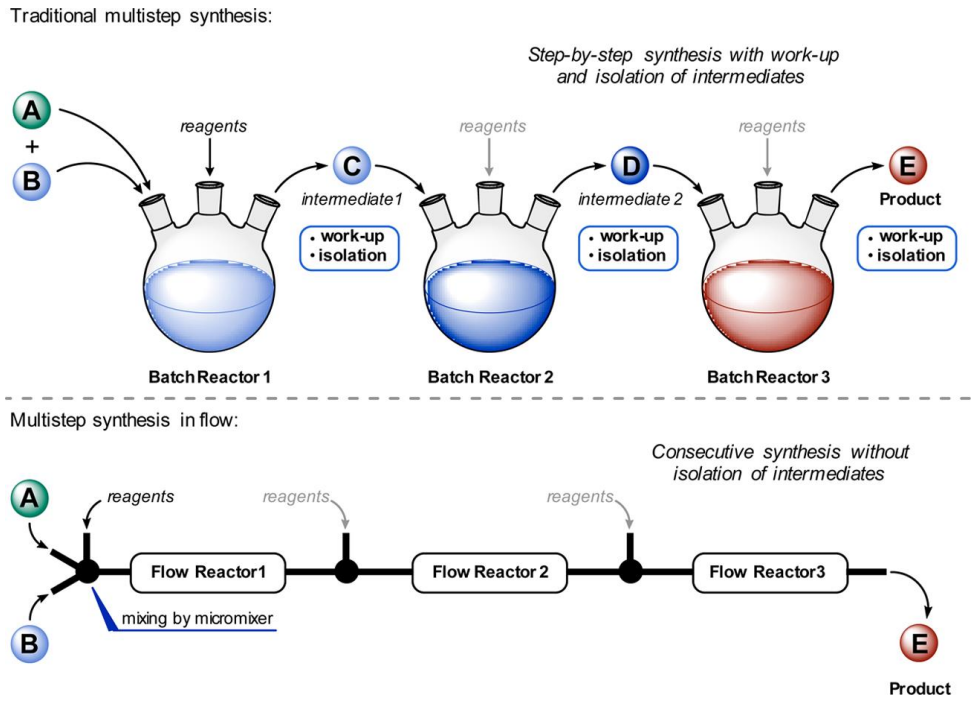

Figure 4.3. Multistep reaction in the batch and flow process. Reprinted with permission [4].

The hidden potential of continuous flow photochemistry for homogenous catalysis might be still explored, since a geometry of the microchannel reactor allows to control the flow dynamic and separate two miscible liquids. This strategy might be applied towards flash chemistry, in which the microreactors are used to perform extremely fast reactions ($t_p \leq$ milliseconds) [22,23]. The flash chemistry can serve to generate highly reactive species of photocatalyst (lifetime of excited state population ≤ nanoseconds) at interface of miscible solutions, in which the photocatalyst and reagents are homogeneously soluble in two different liquids.

4.1.3 Photochemical reactor materials selection

The selection of suitable materials for the flow reactor fabrication has a significant influence on the overall efficiency of the photocatalytic process. The chosen reactor material must meet some requirements such as optimal transparency properties (in the UV-Vis region), high physico-chemical stability (*e.g.* upon irradiation, reaction conditions) and high heat conductivity (*i.e*. faster heat transfer) [4]. For these reasons, a wide range of photoreactors is constructed from glass, silicon or polymers [15]. Nevertheless, since the polymer-based materials offer much better flexibility, they are more often applied to construct easy-to-assemble photomicroreactor than glass.

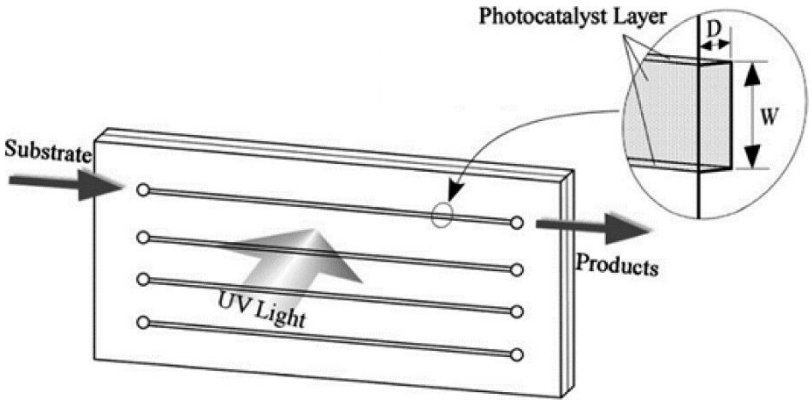

Figure. 4.4. Scheme of microfluidic device applied for the heterogeneous photocatalytic system. Reprinted with permission [23].

Furthermore, unlike inorganic materials, polymers are easy and low- cost to fabricate, and therefore have become the most-commonly used microfluidic devices materials (Figure 4.4) [16]. The most popular polymer applied for the prototyping of microfluidic devices is *polydimethylsiloxane* (PDMS), which allows to design a wide range of microchannel geometries using a simple soft-lithography technique. However, PDMS imposes some limitation on the photocatalytic system due to its propensity to swell in organic non-polar solvents and a high gas permeability (including oxygen) [24].

4.2 Experimental part

To expand the scope of photoredox catalysis towards the flow technologies, the previously discussed photocatalytic system based on T_3BTCH_3 (Chapter 2.3.6) was tested under dynamic conditions inside the microfluidic channels. The extensive study, performed at the liquid-liquid and the solid-liquid interfaces, intended to provide a microfluidic prototype for the photocatalytic transformation, which can work upon homogenous and heterogenous conditions.

4.2.1 Microfluidic channels

The microchannels applied for this study are made from the *polydimethylsiloxane* (PDMS) conformally sealed to the glass plate (Figure 4.5). The straight geometry channels were employed for heterogeneous reactions. Whereas, the Y-shaped and X-shaped channels were employed for homogeneous reactions.

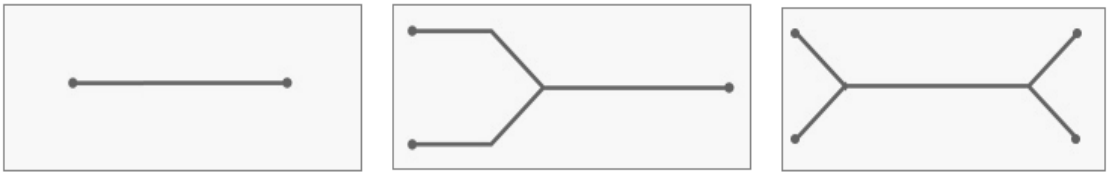

Figure 4.5. The PDMS microdevices possess different geometry (Straight channel: 500 µm width; 23 mm length; Y-shaped channel: 500 µm width; 23mm length (straight part without the arms: 11mm); X-shaped channel: 500 µm width; 24 mm length (straight par without the arms: 15mm)).

4.2.2 Liquid-liquid interface formation

The suitable design of microfluidic device allows to keep separated two reaction media inside the channel giving the possibility to regenerate photocatalytic reactive species and isolate the final product (Figure 4.6). In this reaction system, the photocatalyst (D-electron donor) and the reagents (A-electron acceptors) are introduced inside the channel as two individual solutions, which can be re-cycled until the maximum conversion is reached. However, the time required for the generation of the reactive species and their further interaction must be balanced with the diffusion process occurring in the channel.

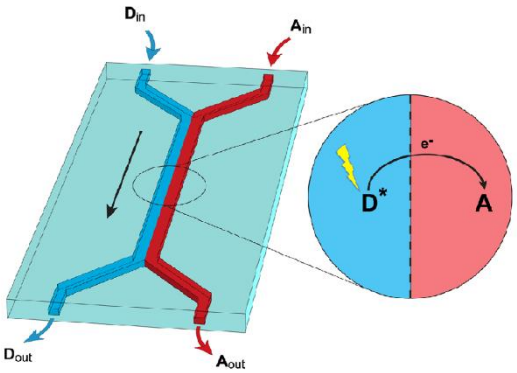

Figure 4.6. Scheme of photocatalytic reaction system formed at liquid-liquid interface.

In this respect, the study on the selected photocatalytic system, in which the efficient electron transfer takes place at liquid-liquid interface, was carried out. As first, the reaction conditions, in which both solutions are evenly fill up the microchannel volume were adjusted. Consequently, the solution of the photocatalyst (T_3BTCH_3) and the solution of the sacrificial agent (DIPEA) in acetonitrile were injected in two different arms of the Y-shaped channel (Figure 4.7). The flow behaviour of liquids under different pressure (25mbar-90mbar) was observed by the confocal fluorescent microscopy technique. The suitable reaction flow of both liquids, which provides their uniform distribution inside the channel, was set up at 70±5 mbar. As noticed, working under lower pressure (<30mbar) results in the expansion of the photocatalyst solution at the end of the channel (long residence time favours the diffusion process and mixing of the two liquids). Whereas, working under higher pressure (>90 mbar) provides too short residence time of the solutions inside the channel, which causes inconvenience during the measurement (not sufficient time to capture images). The confocal fluorescent images registered upon various pressure are presented in the Annex 4.1.

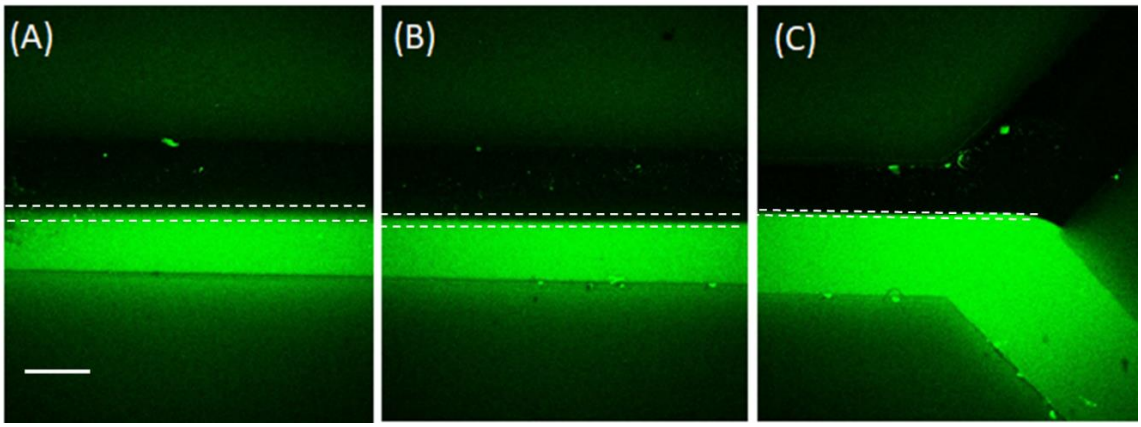

Figure 4.7. The confocal fluorescent images displayed the flow behaviour of quencher and photocatalyst solutions flowing through the microfluidic channel (A-end of the channel, B-middle of the channel, C-beginning of the channel) (Measurement conditions: Laser: λ_{ex}=405nm; Pressure: 70±5 mbar). Scale bar corresponds to 250 µm. Dashed lines correspond to diffusive mixing interface.

To prove an efficient electron transfer at liquid-liquid interface, the fluorescence lifetime imaging microscopy (FLIM) technique was employed. An active interface forming at liquid-liquid interface was evaluated by fluorescence lifetime measurements. The fluorescence lifetime repetition images were recorded respectively at the beginning, in the middle and at the end of the channel (Figure 4.8). The FLIM images display the gradual changes of the colour, which correspond to quenching of the lifetime and fluorescence intensity of T_3BTCH_3 at the interface between the two solutions, demonstrating an efficient electron transfer. Consequently, changes of the colour indicate formation of the active interface.

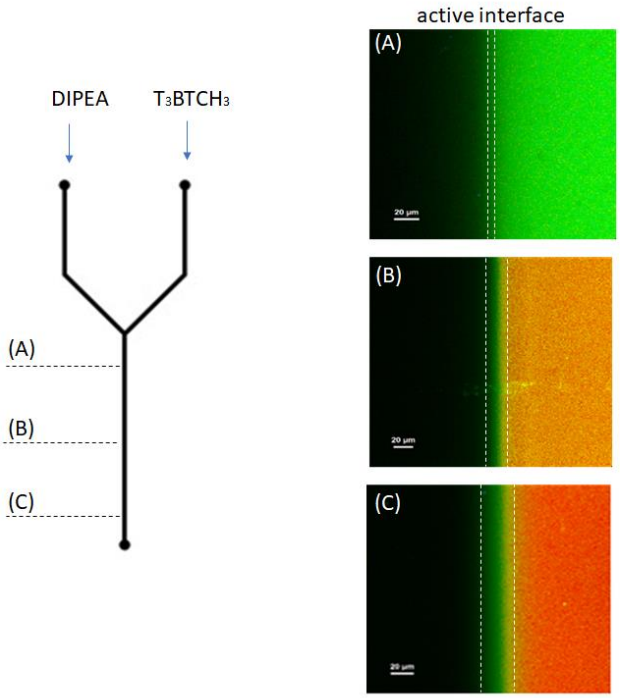

Figure 4.8. The FLIM images recorded along the length of the channel during flow of the DIPEA ($1x10^{-2}$ M) and T_3BTCH_3 ($1.6x10^{-4}$ M) in acetonitrile solution. The FLIM images, displayed at false colour scale, consist of overlapped images of the fluorescence lifetime and intensity. Presented pictures do not show a full width of the channel. The objective lens was focused on the centre of the channel, to capture changes occurred at the liquid-liquid interface in detail. (Measurement conditions: Laser: λ_{ex}=405nm; Pressure: 70mbar).

To estimate the active surface area, the changes of fluorescence lifetime and intensity related to the images presented in Figure 4.8, were plotted. The fluorescence lifetimes of T_3BTCH_3 were calculated based on the biexponential decay function (described in detail in Annex 4.2). The increasing degree of quenching along the length of the channel is clearly seen in Figure 4.9. The fluorescence lifetime decreases more at the end (Figure 4.9C) than at the beginning of the channel (Figure 4.9A). The changes of the lifetime profile (dashed line on the plot) indicate the formation of the active interface. For instance, the active interface at the beginning of the channel reaches approximately 50 microns, whereas at the end of the channel spreads to 150 microns (one pixel = approx. 1 micron). Similar behaviour is observed when the DIPEA is replaced by one of the reagents *i.e. 4,7-dibromobenzo[c][1,2,5]thiadiazole* (compound 7 act as quencher) (Annex 4.3).

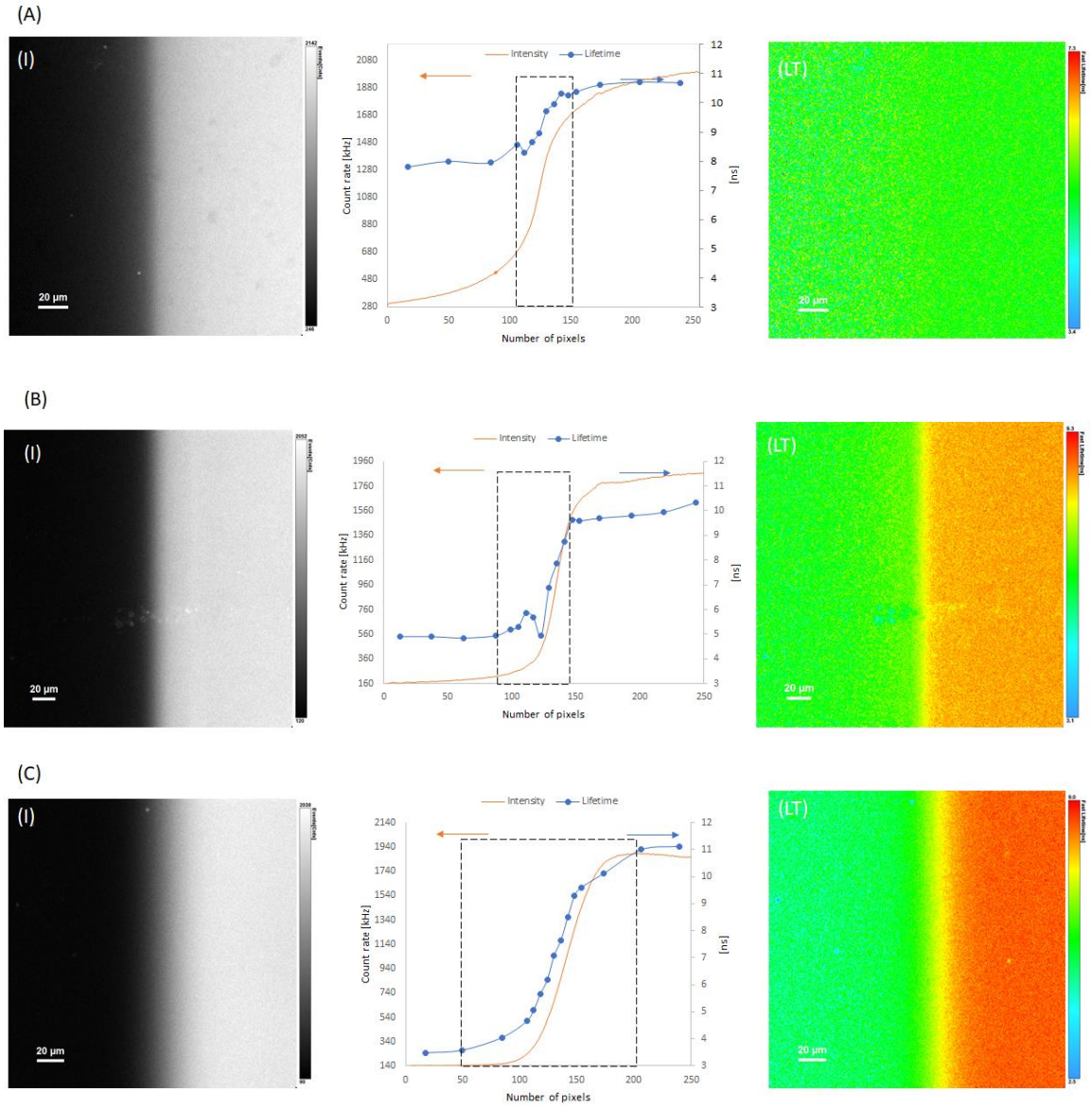

Figure 4.9. The profiles of fluorescent intensity (I) and lifetime (LT) corresponding to images capture (A) at the beginning (B) in the middle (C) at the end of channel.

In parallel, the fluorescence lifetime measurements were performed on the two immiscible solvents, where in the X-shaped channel simultaneously introduced the solution of DIPEA in water and T_3BTCH_3 in toluene. In this case, the sharp profile of the fluorescence intensity and constant profile of the fluorescence lifetime (Figure 4.10) is observed. Unchanged lifetime profile indicates non-quenching process that might be hindered due to the restricted diffusion of the reagents between two immiscible liquids. Therefore, one may suspect that an efficient electron transfer is boosted by the diffusion mixing. The noises signal of fluorescence lifetime related to quencher area, observed on the left part

of the plot, are most likely caused by diffuse reflection (coming from the chromophore area).

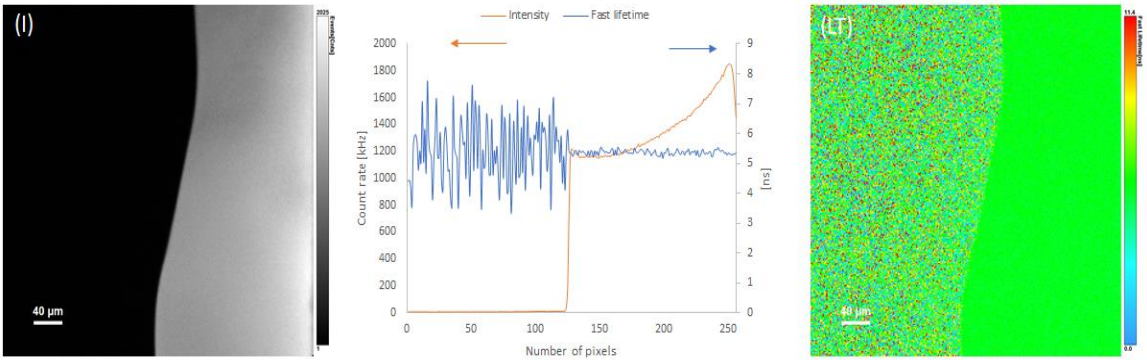

Figure 4.10. The FLIM images and plot corresponding to changes of the fluorescence (I) intensity and (LT) lifetime occur during flow two immiscible solution inside microfluidic channel. The DIPEA ($1x10^{-2}$M) in water and T_3BTCH_3 ($1.6x10^{-4}$M) in toluene were injected simultaneously. (Measurement conditions: Laser: λ_{ex}=405nm; Pressure: 70mbar).

Since in the former case, an efficient electron transfer at the liquid-liquid interface was demonstrated, the X-shaped microfluidic device was applied to perform photochemical reaction. Regrettably, all the attempts to perform debromination reaction of *4,7-dibromobenzo[c][1,2,5]thiadiazole* results in the partial mixing of reaction components (in both miscible and immiscible solvents). As noticed (Figure 4.11) the fluctuation of the flow occurs at the end of the channel (most likely caused by not suitable channel geometry) provides non-uniform separation of reagents. To overcome this limitation, the immobilization of photoactive organic molecules inside the microchannel, is proposed.

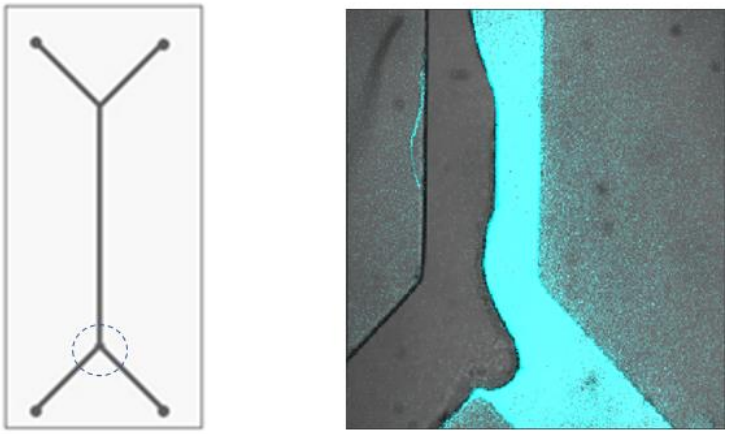

Figure 4.11.The confocal fluorescent images displayed the flow fluctuation inside the X-shaped channel.

4.2.3 Channel modification

Chemical binding of the photocatalyst on the internal surface of polydimethylsiloxane (PDMS) channels, requires functionalization of the inert polymer with a reactive linker molecule such as *(3-Aminopropyl)triethoxysilane* (APTES). The chemical interaction between APTES and PDMS surface occurs through hydrolysis of the ethoxy group of APTES and further formation of Si-O-Si bonds with the surface silanol group [25]. The formation of APTES cross-layer on the PDMS surface strictly depends on the reaction condition, especially on the solvent and reaction time. Since the hydrolysed APTES might undergo self-condensation reaction, if the reaction time is too long, and hence blocks the chemical interaction with PDMS surface [25]. Consequently, the selection of a suitable functionalization method is required to obtain a uniform amino-functionalized surface of PDMS (Figure 4.12). In this study, the functionalization of PDMS surface was carried out according to the procedure described by Arnold [14], where the hydrolysis of the ethoxy group of APTES is performed in the presence of a catalyst (base or acid) in ethanol.

Figure 4.12. Scheme of modification of PDMS surface by acid- or base-hydrolysis of APTES. Reproduced with permission [14].

In parallel, the amino-ending of the linker (*i.e.* APTES) can be successfully modified by covalent binding of selected chromophore (*i.e.* photocatalyst). The selection of chromophores, which should easily interact with amino groups, is crucial to avoid harsh reaction conditions and the use of additional reagents. Hence, *fluorescein 5-isothiocyanate* and *2,2-bithiophene-5'-succinimidyl ester* (Figure 4.13) were selected due to their higher reactivity towards -NH_2 group.

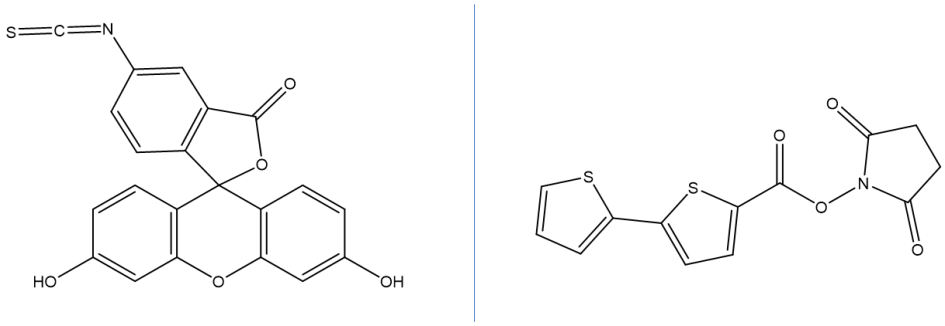

Figure 4.13. Chemical structure of selected chromophores: (A) *fluorescein 5-isothiocyanate* and (B) 2*,2-bithiophene-5'-succinimidyl ester*.

To find the optimal reaction conditions for the chromophore deposition, and hence obtain a uniform distribution of photocatalyst inside the channel, **three different modification approaches** (Table 4.1) were studied.

Initially, the reaction between APTES and the chromophore was performed outside the microchannel (Table 4.1;Entry 1). The **pre-synthesized APTES-chromophore molecule** was then introduced into a pristine PDMS microchip in the presence of a catalyst (base) to promote the hydrolysis of the ethoxy groups and consequently binding it on the PDMS surface. Unfortunately, the APTES-chromophore molecule, crossed the channel leaving it unaltered. This indicates that the reaction between APTES and the chromophore can deactivate the alkoxy groups present in the APTES and prevent their further hydrolysis inside the channel. Clearly, the APTES deposition on the surface of PDMS has to be performed before its reaction with the chromophore.

Table 4.1. Selection of the optimal modification method.

Approach	Pre-functionalization with APTES	Injection in the channel
1	No	pre-synthesized APTES-chromophore molecule
2	Yes	pre-synthesized APTES-chromophore molecule
3	**Yes**	**Sole chromophore**

On another approach, the modification of the channel was carried out in two steps consisting of: (i) pre-functionalization of PDMS surface with APTES and further (ii) coupling of the amino-ending with the chromophore (Table 4.1; Entry 2-3). Consequently, a solution of APTES, in the presence of a catalyst, was introduced in the channel and left there until

hydrolysis was completed (pre-functionalization step is described in Annex 4.4). This amino-functionalized channel was washed with ethanol and use for the chromophore immobilization (the reaction conditions for individual chromophores are described in Annex 4.4.) Two different modifications were attempt, a first one, where the sole chromophore was flown inside the channel (Table 4.1; Entry 3); and a second one, where the pre-synthesized APTES-chromophore molecule was flown inside the channel (Table 4.1; Entry 2). A uniform modification of microchip was obtained, when the solution of the sole chromophore was introduced inside the pre-functionalized channel and the reaction was performed inside the chip (preliminary results are shown in Annex 4.5). In the second case, uncontrolled self-condensation of APTES molecules resulted in its precipitation and local clogging of the channel. Therefore, further modification of the channels was performed according to method, which allowed to obtain a uniform distribution of photocatalyst (Table 4.1; Entry 3).

4.2.4 Solid-liquid interface

The modified channels were further characterised by confocal fluorescence microscopy technique. The fluorescence imaging allows to visualise the internal surface of the microfluidic channel before and after modification. As shown in Figure 4.14, microporous surface of the PDMS channel was successfully modified with both chromophores. As previously discussed, no-chromophore is observed on non-functionalized PDMS surface (pre-functionalization step with APTES is necessary). The pattern of chromophore immobilization (relative to green and blue lines) indicates the trajectory of crossed-linker layer created during APTES deposition. As suspected, functionalization of PDMS surface with APTES (*i.e.* silanization) is the crucial step, which defines the final chromophore immobilization. It is worth mentioning that, the silanization is much more efficient, when PDMS surface is previously activated by chemical or physical treatment (*e.g.* plasma treatment). This allows to introduce active -OH groups on the polymer surface and favours a chemical interaction between PDMS and APTES. Non-activated PDMS surface results in reduced number of active sites, where created cross-linked layer of APTES is rather anchored in the micropores of PDMS and strongly depend on the internal surface porosity. Therefore, on non-activated PDMS surface a

homogeneous APTES layer is difficult to achieve [14]. Nevertheless, the previously described modification method allows to obtain relatively uniform immobilization of chromophores across the channel (Figure 4.15) and provides an exemplar prototype of microfluidic device for the photochemical application.

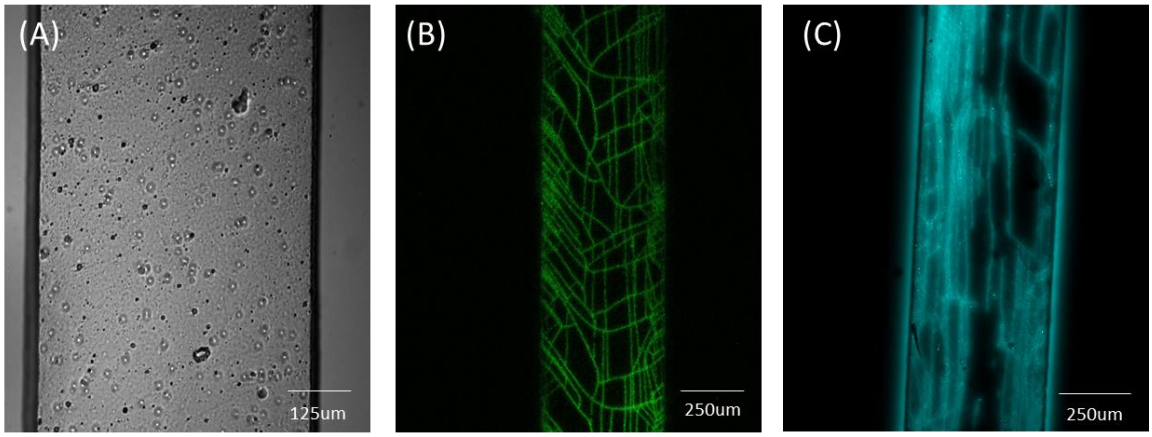

Figure 4.14. The confocal fluorescence microscopy images of (A) non-modified channel (bright field) and channel modified with (B) *fluorescein 5-isothiocyanate* (dark field, λ_{em}=488nm) (C) *2,2- bithiophene-5'-succinimidyl ester* (dark field, λ_{em}=405nm).

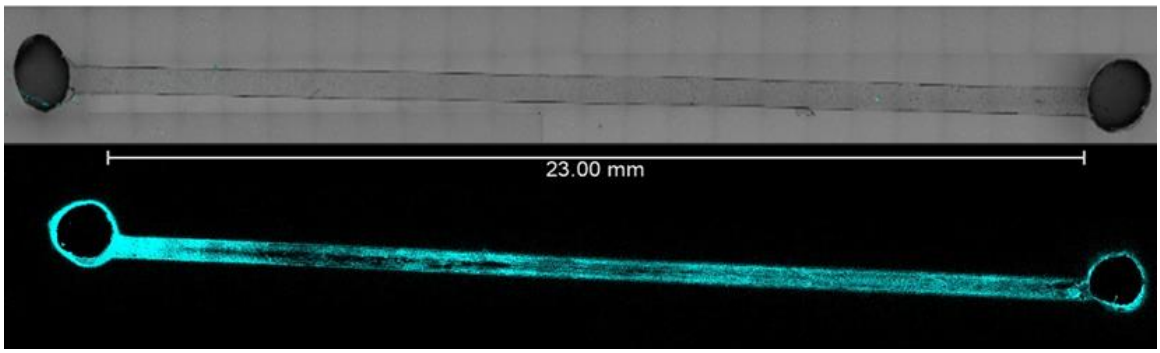

Figure 4.15. Merged confocal fluorescence microscopy images of (A) non-modified channel and (B) channel modified with *2,2-bithiophene-5'-succinimidyl ester* (dark field, λ_{em}=405nm).

To investigate the stability of the microfluidic prototype under dynamic conditions, modified channel was washed several times with acetonitrile. Collected samples of rinsing solvent were analysed by UV-Vis spectroscopy, whereas the microfluidic channel was further characterised by confocal fluorescence microscopy. No absorption bands of the chromophore are registered, and no sign of the chromophore leaching is observed (Figure

4.16A). This indicates that the photocatalytic device is stable under the flow conditions. Therefore, the examined channel was employed in the quenching measurement in the presence of DIPEA as a sacrificial agent. The injection of the amine into the microchannel results in the fluorescence quenching of the chromophore (Figure 4.16B). Given the fact that the fluorescence is restored after the passage and cleaning of the quencher, the same channel was further applied to perform the debromination reaction.

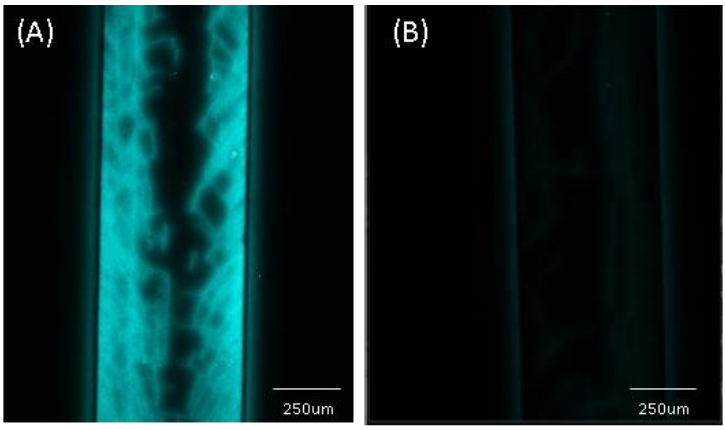

Figure 4.16. The confocal fluorescence microscopy images of channel modified with *2,2-bithiophene-5'-succinimidyl ester* (dark field, λ_{em}=405nm) (A) without the presence of DIPEA (B) in the presence of DIPEA.

4.2.5 Continuous-flow reaction in the bithiophene immobilized microreactor

Debromination reaction of *4,7-dibromobenzo[c][1,2,5]thiadiazole* (compound 7) (C_S =1.6x10^{-2}M) in the presence of DIPEA (C_A=1.3x10^{-1} M), was performed inside the straight microfluidic channel previously modified with *2,2-bithiophene-5'-succinimidyl ester* (Figure 4.15). The reaction mixture of compound 7 and DIPEA in acetonitrile was continuously pumping through the irradiated channel (150W, Xe lamp). The flow control system (Figure S2-S3; supplementary information) allowed to keep pressurized reaction mixture under inert atmosphere (*i.e.* nitrogen). Therefore, the high permeability of PDMS chips to oxygen did not impact in the performed reaction. It is assumed, that time required for the oxygen diffusion through the external PDMS layer is longer than the residence time of reaction mixture inside the channel.

In order to optimise reaction conditions different flow ratio (adjusted by pump pressure) was studied. Not surprisingly, the higher conversion rate is observed for the lowest pressure (12.5mbar), in which the residence time of reaction mixture inside the channel is prolonged (Table 4.2; Entry 1-3). Upon this reaction conditions, the debromination reaction afford 16% conversion, for a residence time of approx. 30 sec., whereas, the batch reaction provides 5% of conversion after 1 hour of irradiation (Table 4.2; Entry 5). To increase the conversion rate, the same sample was re-injected 2 times more through the channel, which results in a total conversion equal to 29% (Table 4.2; Entry 6). Moreover, performing the reaction in two different microfluidic channels, modified in the same way, led to reproducible results (Table 4.2;Entry 7-8).

Table 4.2. Conversion rate of debromination reaction*.

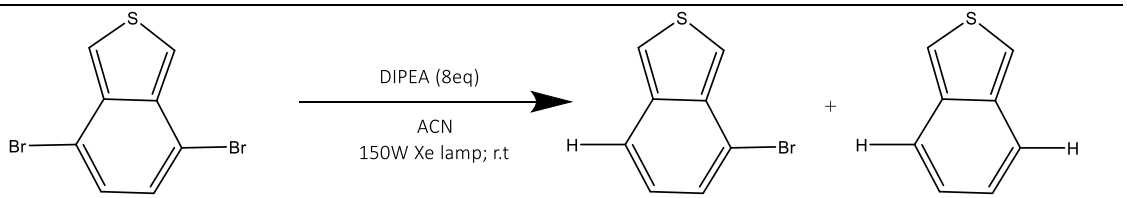

Entry	Pressure** [mbar]	Conversion rate***[%]	Residence time**** [sec]	Comments
1	50	5.2	7.5	
2	25	9.6	14	
3	12.5	16.0	28	
4	12.5	29.0	90	3-recycle
				Control experiments
5	12.5	2.0	28	non modified channel
6	-	5.1	3600	batch reaction
7	12.5	16.0	28	modified channel 1
8	12.5	13.7	28	modified channel 2****

* General scheme of the debromination reaction **pressure is the lowest which provide non-disorder continuous flow inside the channel *** conversion rate estimated based on GC spectroscopy **** residence time is the time of reagent inside the channel upon the irradiation; calculated based on the volume of the channel and time necessary to collect 1 mL of sample. ****- different channel modified in the same way

4.3 Conclusion

Performed spectroscopic studies on the photocatalytic system based on T_3BTCH_3, indicate that an efficient electron transfer (ET) process takes place at the liquid-liquid interface inside the microchannel and is reinforced by the diffusion. As demonstrated, in the case of two miscible liquids, the active interface increases along the channel, giving the possibility to trigger photochemical transformation. Therefore, the presented results disclose a new concept to perform reactions at liquid-liquid interface, where the suitable design of the microfluidic device and reaction conditions (*i.e.* selection of solvents and flow rate) allows the separation of the photocatalyst and the reagents.

Another approach, in which the photocatalyst was bond through a linker (*i.e*. APTES) to the channel walls, was developed, leading to a uniform distribution of the chromophore. Presented modified microfluidics devices are stable upon the reaction conditions (leaching of photocatalyst is not observed) and allow to perform several photocatalytic transformations. The debromination reaction carried out in the flow, afforded higher conversion rate in comparison to the reaction carried out in the batch reactor, reducing significantly the reaction time. Similar results obtained for two individual channels modified using the same method, indicates the reproducibility of the modification method.

In conclusion, these studies provide a prototype of microfluidic devices for the photocatalytic transformation, which can work upon homogenous and heterogenous conditions.

Acknowledgment

Presented studied were performed during 3-month internship at the Catholic University of Leuven in the framework of PHOTOTRAIN Project.

4.4 Inorganic photocatalytic system: perspectives

Ruthenium complexes are commonly applied towards photoredox catalysis due to their excellent photophysical and chemical properties (Chapter 1.6), including self-assembling properties. *The self-assembly is a process in which a system of pre-existing components, under specific conditions, adopts a more organized structure through interactions between the components* (IUPAC definition) [26]. The spontaneous organization is led by weak non-covalent interaction between reagents and hence is reversible.

In this light, the self-assembling properties might drive desired architecture of photocatalytic system (Figure 4.17A), inside the microfluidic devices, which provides short diffusion distances, low mass transport limit, and product removal favouring forward reactions.

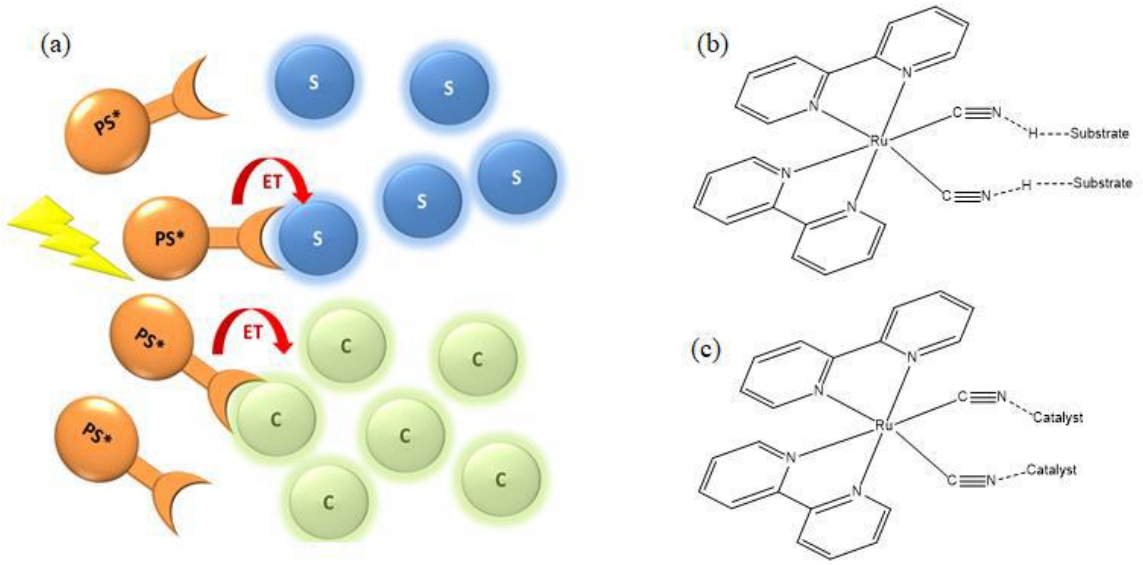

Figure 4.17. Scheme of (a) the self-assembling catalytic system. (PS*) photosensitizer, (S) substrate, (C) catalyst, (ET) electron transfer; (b) self-assembling catalytic system formed by hydrogen bonding between ligands and substrates; (c) self-assembling catalytic system formed between ligand and metal center of organometallic catalyst.

In this direction, the ruthenium metal complex *i.e.* $Ru(bpy)_2CN_2$, is proposed as a potential molecular module that may arrange self-organized architecture of the photocatalytic systems. The $Ru(bpy)_2CN_2$ complex possesses a high oxidation potential of

the excited state (E^*_{ox}=-1.32eV/E^*_{red}=0.37) and two available sites for self-assembling *i.e.* cyanide ligands (CN^-). The cyanide ligands might non-covalently interact with: (i) organic molecules *via* hydrogen bonds interaction (Figure 4.17B) or (ii) with metal center of organometallic complex (Figure 4.17C).

To demonstrate a non-covalent bonding between cyanide ligands and selected organometallic catalyst (*i.e*. palladium and nickel), a preliminary study was carried out. The absorption and emission spectra of ruthenium metal complex $Ru(bpy)_2CN_2$ were registered upon the addition of progressively increasing equivalents of two different organometallic catalysts (*i.e.* $Pd(PPh_3)_4$ and $NiCl_2x2H_2O$). As shown in Figure 5.18A, the addition of Pd metal complex leads to changes in the absorption and emission spectra of ruthenium metal complex, due to the interaction at the ground state between the CN^- ligands and the organometallic centre. In the case of Ni (Figure 5.18B), also an efficient quenching of the excited state is observed. This indicates that the interaction between $Ru(bpy)_2CN_2$ and organometallic complex provides an efficient electron transfer and hence modulates the oxidation states of metal complex catalyst (*i.e*. Ni). Therefore, an interesting perspective is to exploit the self-assembling properties of ruthenium metal complex to merge photoredox and organometallic catalysis.

(A)

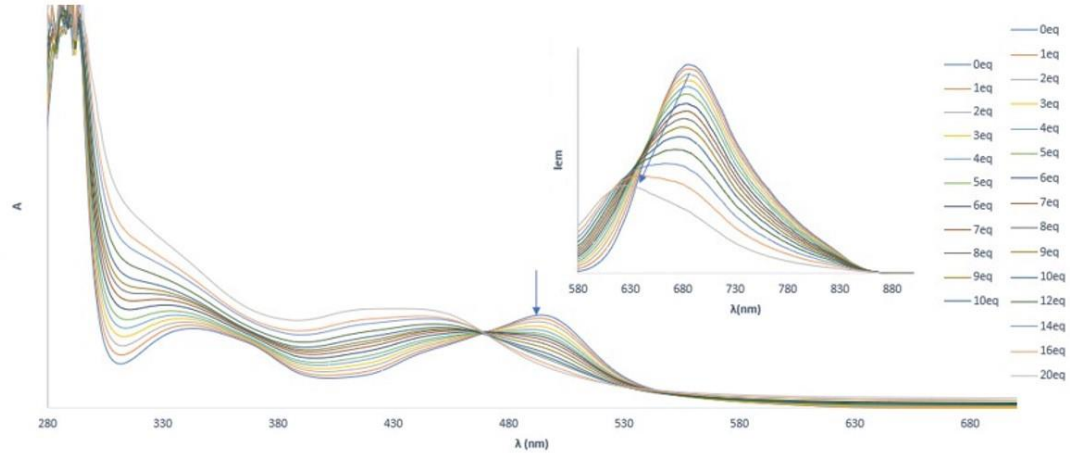

Figure. 4.18A. Changes observed in the absorption spectrum of ruthenium ($2x10^{-4}$M) in DMF solution at 298 K upon addition of $Pd(PPh_3)_4$.

(B)

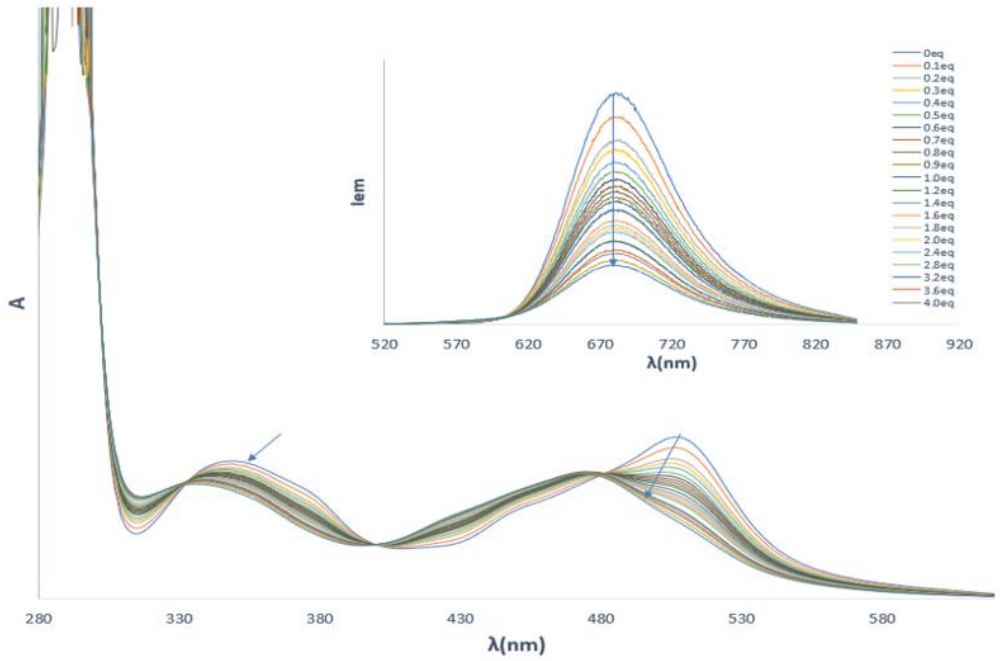

Figure. 4.18B. Changes observed in the absorption spectrum of ruthenium ($2x10^{-4}$M) in DMF solution at 298 K upon addition of $NiCl_2x2H_2O$.

The possibility to combine photocatalysis with organometallic catalysis may appear as a way of developing new synthetic strategies, in which the photocatalyst provides access to reactive radical species (oxidation and reduction process can act simultaneously) under mild reaction conditions without the necessity of using stoichiometric metallic reductants, generally applied in organic synthesis [27,28].

In this light, examined Ru-Pd complex was employed towards coupling reactions (*i.e*. Suzuki coupling reaction, Stille coupling reaction and Sonogashira coupling reaction) (Figure 4.19). As first, the Suzuki reaction was carried out according to the standard procedure, in which the presence of boronic acid, halides coupling agent (*i.e*. iodobenzene) and base (*i.e*. K_2CO_3) is required. Nevertheless, in this case, the addition of base results in the destruction of the catalytic complex and no coupling reaction is observed. Secondly, the Ru-Pd complex was applied to perform Stille coupling reaction. One difference between Stille coupling and Suzuki mechanism is that the boronic acid is replaced by stannane compound (Figure 4.19), which does not have to be activated by a base. Even if, in this case, the addition of a base was not required, the Ru-Pd complex was not stable during the

irradiation. Finally, upon the selection of stable reaction conditions, in the presence of phenylacetylene and iodobenzene (*i.e.* Sonogashira reaction), the C-C bond formation is observed.

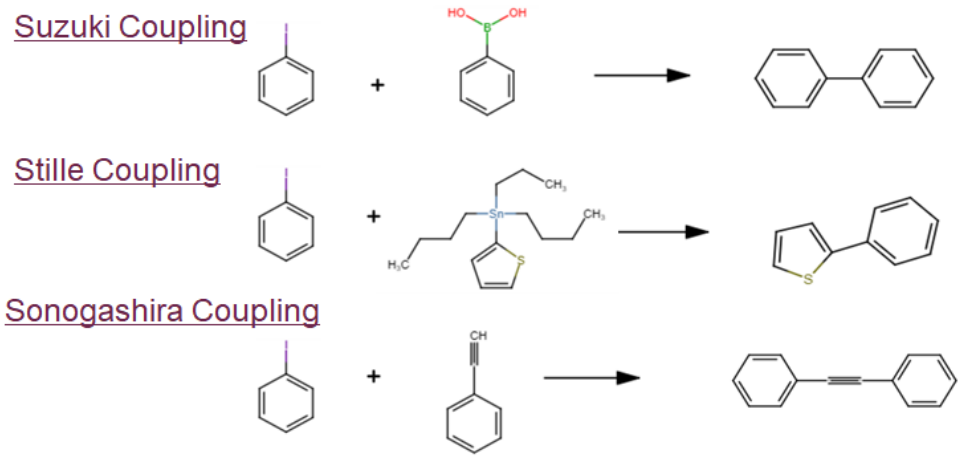

Figure 4.19. Scheme of performed coupling reactions in the presence of Ru-Pd complex as photo-organometallic catalyst.

Therefore, additional efforts might be made to optimize the reaction conditions and apply this photocatalytic system towards flow technology. Ideally, design a photocatalytic system inside the microchannel, in which the self-assembling properties of Ru metal complex provide more efficient energy transfer at liquid-liquid interface and hence increase the efficiency of the photocatalytic process upon dynamic conditions.

Reference:

[1] K. Gilmore, P.H. Seeberger, *Chem. Rec.,* 2014, 14, 410.

[2] J.P. Knowles, L.D. Elliott, K.I. Booker-Milburn, *Beilstein J. Org. Chem.,* 2012, 8*,* 2025.

[3] H.W. Hsieh, C.W. Coley, L.M. Baumgartner, K.F. Jensen, R.I. Robinson, *Org. Process Res. Dev.,* 2018, 22, 1045.

[4] D. Cambié, C. Bottecchia, N.J. Straathof, V. Hessel, T. Noël, *Chem. Rev.,* 2016, 116, 10276.

[5] Y. Su, N.J. Straathof, V. Hessel, T. Noël, *Chem. Eur. J.,* 2014, 20, 10562.

[6] R. Holger, R. Seliger, S. Werner, F. Wissmann, Patent: *Quartz Glass Micro-Photoreactors and Synthesis of 10-Hydroxycamptothecin and 7-Alkyl-10-Hydroxycamptothecin*. EP 2065387 A2, 2008/11/07 2009.

[7] T. Noël, *J. Flow Chem*., 2017, 7 (3-4), 87.

[8] C. Stephenson, T. Yoon, D.W. MacMillan, N.J. Straathof, T. Noël, (2018), *Accelerating Visible-Light Photoredox Catalysis in Continuous-Flow Reactors. In Visible Light Photocatalysis in Organic Chemistry*, Wiley-VCH Verlag GmbH & Co. KGaA.

[9] J.W. Tucker, Y. Zhang, T.F. Jamison, R. C.R.J. Stephenson, *Angew. Chem*., 2012, 51 (17), 4144.

[10] J. Gardiner, C.H. Hornung, J. Tsanaktsidis, D. Guthrie, *Eur. Polym. J*., 2016, 80, 200.

[11] A. Chemto, A. Rannée, L. Chalan, D. Fischer, S. Bistac, *Eur. Polym. J*., 2016, 80, 247.

[12] E.E. Coyle, M. Oelgemöller, *Photochem. Photobiol. Sci.*, 2008, 7, 1313.

[13] D. Cantillo, C.O. Kappe, *ChemCatChem*, 2014, 6, 3286.

[14] R. Munirathinam, J. Huskens, W. Verboom, *Adv. Synth. Catal*., 2015, 357 (6), 1093.

[15] K. Ren, J. Zhou, H. Wu Acc. *Chem. Res*., 2013, 46, 2396.

[16] J.C. Colmenares, V. Nair, E. Kuna, D. Łomot., *Ultrason. Sonochem*., 2018, 41, 297.

[17] V. Sunkara, D.K. Park, H. Hwang, R. Chantiwas, S.A. Soperac, Y.K. Cho, *Lab Chip*, 2011, 11, 962.

[18] J.H.L. Beal, A. Bubendorfer, T. Kemmitt, I. Hoek, W.M. Arnold, *Biomicrofluidics*, 2012, 6, 036503.

[19] J. Wahlen, D.E. De Vos, P.A. Jacobs, P.L. Alsters, *Adv. Synth.Catal.*, 2004, 346, 152.

[20] J. Yue, *Catal. Today*, 2018, 308, 3.

[21] F. Fanelli, G. Parisi, L. Degennaro, R. Luisi, *Beilstein J. Org. Chem.,* 2017, 13*,* 520.

[22] J. Yoshida, Y. Takahashia, A. Nagakia, *Chem. Commun.*, 2013, 49, 9896.

[23] Y. Matsushita, N. Ohba, S. Kumada, S. Suzuki, T. Ichimura, *Catal. Commun*., 2007, 8 (12), 2194.

[24] T. Yang, J. Choo, S. Stavrakis, A. de Mello, *Chem. Eur. J*., 2018, 24, 12078.

[25] B. Qiao, T.J. Wang, H. Gao, Y. Jin, *Appl Surf Sci*, 2015, 351, 646.

[26] R.G. Jones, C.K. Ober, P. Hodge, P. Kratochvíl, G. Moad, M. Vert, *Pure Appl. Chem*., 2013, 85, 85 (2), 463.

[27] K. Shimomaki, K. Murata, R. Martin, N. Iwasawa, *J. Am. Chem. Soc*., 2017, 139(28), 9467.

[28] J. Twilton, C. Le, P. Zhang, M.H. Shaw, R.W. Evans, D.W. C. MacMillan, *Nat Rev Chem*., 2017, 1(0052), 18.

ANNEX 4

Annex 4.1 Pressure influence

The confocal fluorescent images displayed the behaviour of quencher (DIPEA) and photocatalyst (T_3BTCH_3) solution flowing through the microfluidic channel (A-end of the channel, B-middle of the channel, C-beginning of the channel) upon various pressure. Pressure 70mbar reported Figure 4.7. Scale bar corresponds to 250 µm.

90mbar

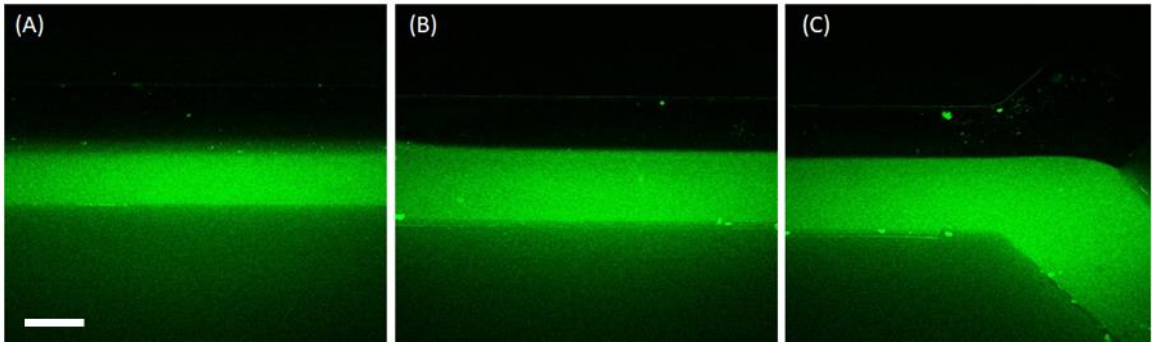

50mbar

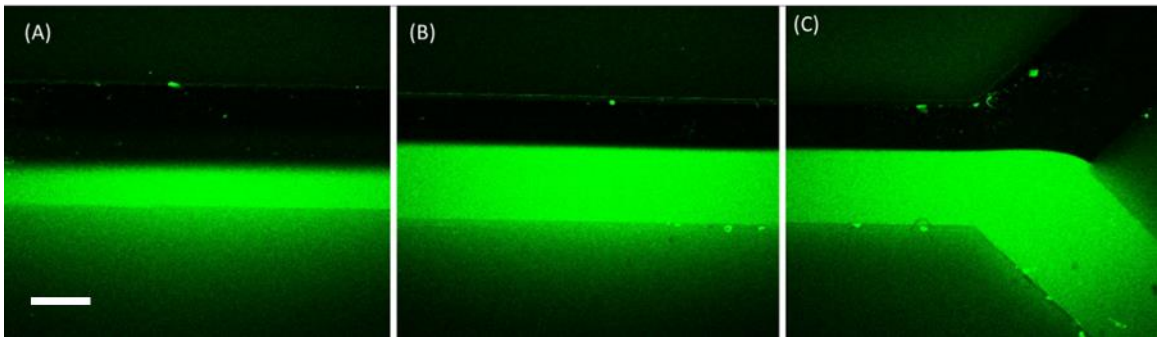

30mbar

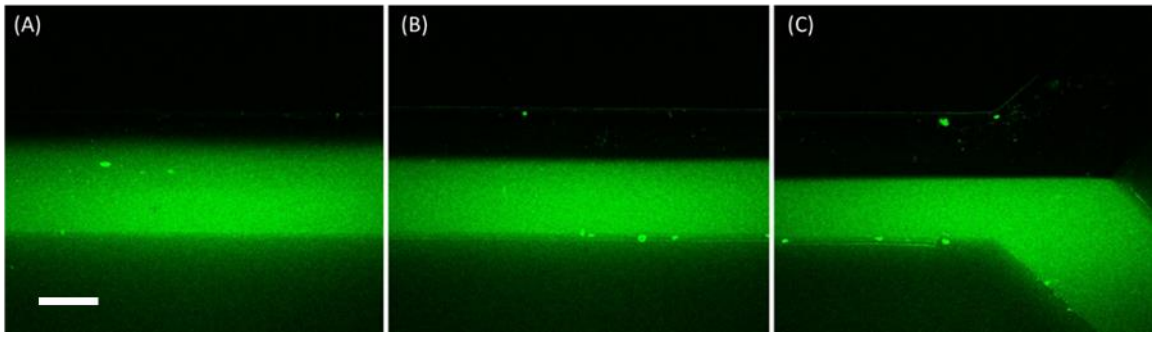

Annex 4.2 Fluorescence lifetime calculation

The profiles of fluorescent lifetime and intensity were plotted based on the FLIM images. The digital data was converted to raw data, consist of 256x256 pixels, one pixel on the graph corresponding to approx. 1 micron on the image. To plot profile of average fluorescent lifetime, the FLIM image was divided into small regions (A). For each region the individual lifetime decay was estimated (B). The lifetime was calculated based on the biexponential decay function according to equation

$$I = I_0 + A_1 e^{\frac{-t}{t_1}} + A_2 e^{\frac{-t}{t_2}} \tag{4.4}$$

where where I- is the intensity at time t, I_0- is the initial intensity, A- is the pre-exponential factor and t - is the time at which the intensity has decayed to $1/e$ of the original value. The instrument response function (for laser 405nm) was measured for LUDOX® HS-40 colloidal silica and has been considered for each calculation. The value of lifetime for each region presented in Table (C). Finally, the average lifetime was overlapped with the profile of fluorsecent intensity

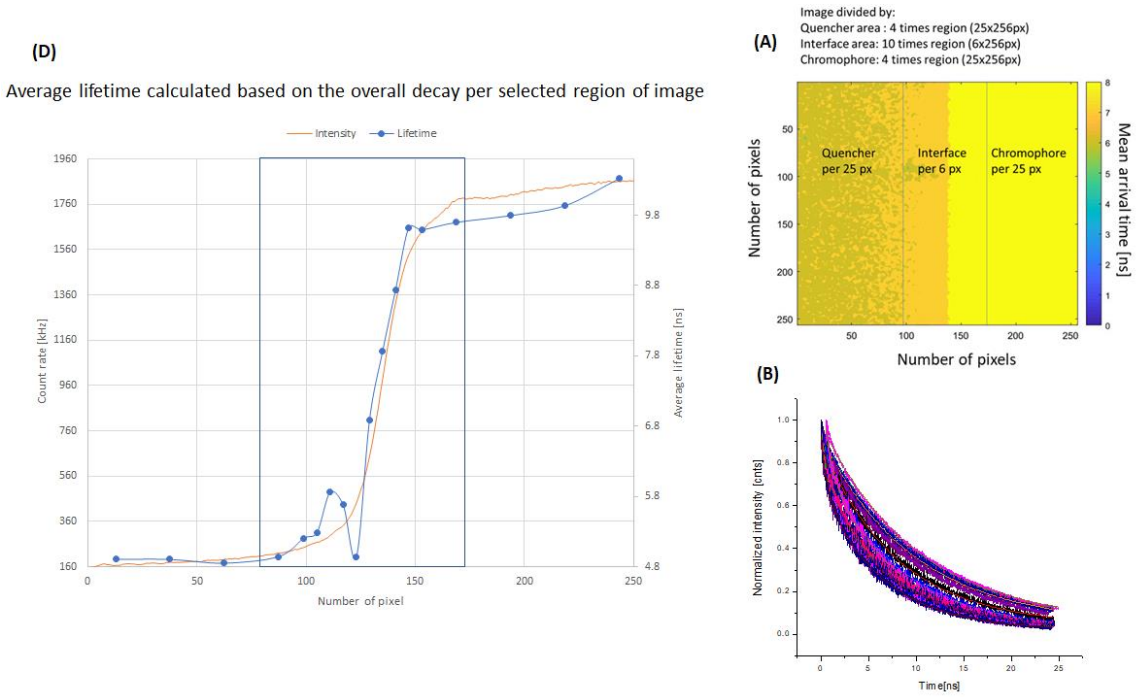

(C)

	AREA	y0	y0	A1	A1	t1	t1	A2	A2	t2	t2	Statistics	Statistics
		Value	Error	Value	Error	Value	Error	Value	Error	Value	Error	Reduced Chi-Sqr	Adj. R-Square
CHROMOPHORE	PIXEL 231-256	0.02317	0.00109	0.8724	7.78E-04	11.3316	0.045	0.09458	0.00144	1.05467	0.03194	1.83E-05	0.99963
	PIXEL 206-231	0.05322	0.0053	0.44297	8110.16	9.93781	9349.68	0.44297	8110.16	9.938	9350.05	7.68E-05	0.99847
	PIXEL 181-206	0.05474	--	0.46503	--	9.79656	--	0.46503	--	9.79656	--	8.33E-05	0.99832
	PIXEL 156-181	0.02307	0.00106	0.85675	8.43E-04	10.7765	0.04378	0.10561	0.00158	0.95527	0.02878	2.29E-05	0.99954
	PIXEL 150-156	0.05325	0.00642	0.42675	--	9.59471	135850	0.42675	--	9.59469	135849	1.49E-04	0.99682
	PIXEL 144-150	0.04635	0.00699	0.43918	--	9.62396	81356	0.43918	--	9.62398	81356.5	1.56E-04	0.99687
INTERFACE	PIXEL 138-144	0.02626	0.00203	0.85309	0.0018	9.71488	0.0773	0.10293	0.00386	0.68929	0.05231	1.36E-04	0.99725
	PIXEL 132-138	0.04132	0.00501	0.42829	16114.1	7.86144	6357.85	0.42829	16114.1	7.86122	6357.48	2.48E-04	0.99492
	PIXEL 126-132	0.01814	0.00159	0.80301	0.00292	7.96965	0.06918	0.14328	0.00452	0.78357	0.04987	1.69E-04	0.99646
	PIXEL 120-126	0.02158	0.00146	0.81731	0.0034	7.22131	0.06195	0.43304	0.02311	0.62852	0.0333	1.80E-04	0.99586
	PIXEL 114-120	0.02425	0.00146	0.74618	0.00323	7.06313	0.06562	0.20422	0.00544	0.61952	0.03332	2.34E-04	0.99451
	PIXEL 108-114	0.02077	0.00174	0.70695	0.00445	7.22327	0.08867	0.19087	0.00599	0.81759	0.05069	2.64E-04	0.99333
	PIXEL 102-108	0.01977	0.00145	0.65915	0.00319	7.07749	0.07379	0.25289	0.00542	0.61444	0.02659	2.33E-04	0.99339
	PIXEL 96-102	0.0214	0.00147	0.66529	0.00358	6.83359	0.07453	0.23642	0.00571	0.63128	0.03081	2.53E-04	0.99288
QUENCHER	PIXEL 75-100	0.02274	8.22E-04	0.68633	0.00204	6.5582	0.03924	0.2513	0.00365	0.53663	0.01556	9.84E-05	0.99733
	PIXEL 50-75	0.02199	7.72E-04	0.68921	0.00227	6.39627	0.03837	0.2519	0.00342	0.62228	0.01707	8.76E-05	0.99769
	PIXEL 25-50	0.01908	8.64E-04	0.66851	0.00286	6.35017	0.04611	0.23075	0.0038	0.71405	0.02344	1.02E-04	0.99715
	PIXEL 1-25	0.01908	8.64E-04	0.23075	0.0038	0.71405	0.02344	0.66851	0.00286	6.35017	0.04611	1.02E-04	0.99715

The instrument response function

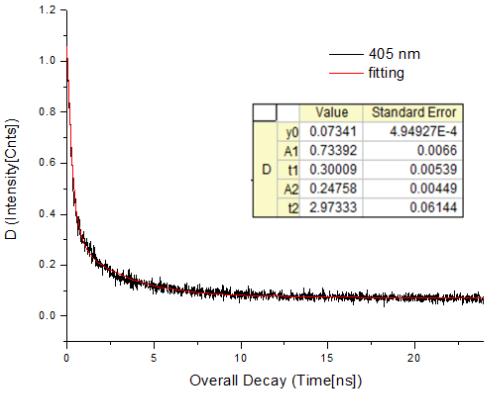

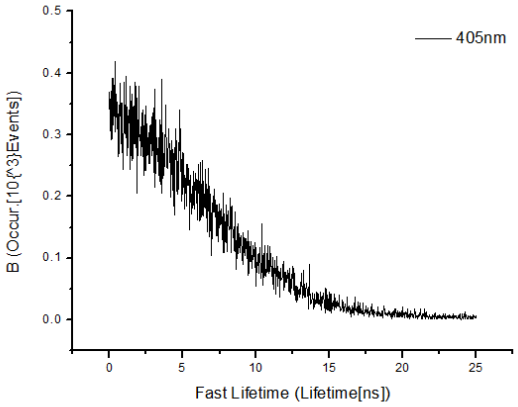

Annex 4.3 Profile of fluorescent lifetime and intensity

The profiles of fluorescent intensity (I) and lifetime (LT) corresponding to images capture: (A) at the beginning (B) in the middle (C) at the end of channel. The FLIM images were recorded along the length of the channel during flow of: the *4,7-dibromobenzo[c]-[1,2,5]thiadiazole* ($1.6x10^{-2}$M) (on the left side) and T_3BTCH_3 ($1.6x10^{-4}$M) (on the right side) in acetonitrile solution. (Measurement conditions: Laser: λ_{ex}=405nm; Pressure: 70mbar).

(A)

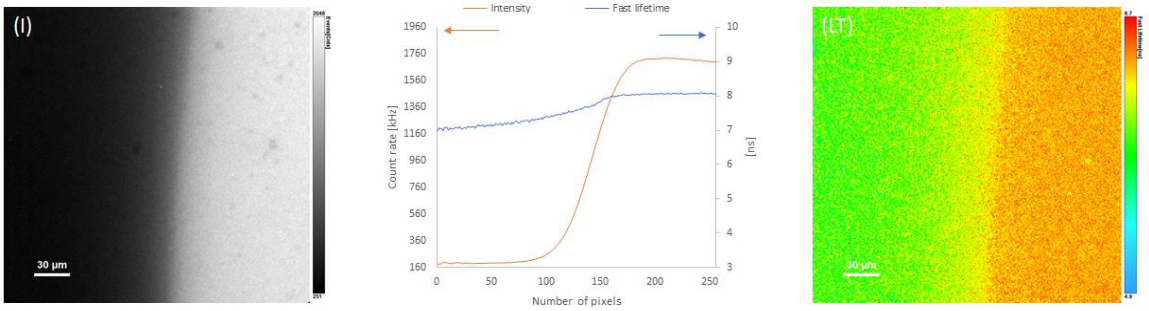

(B)

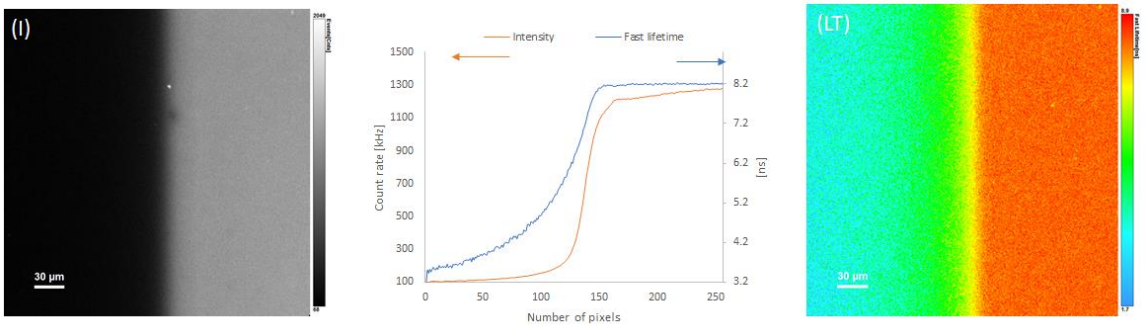

(C)

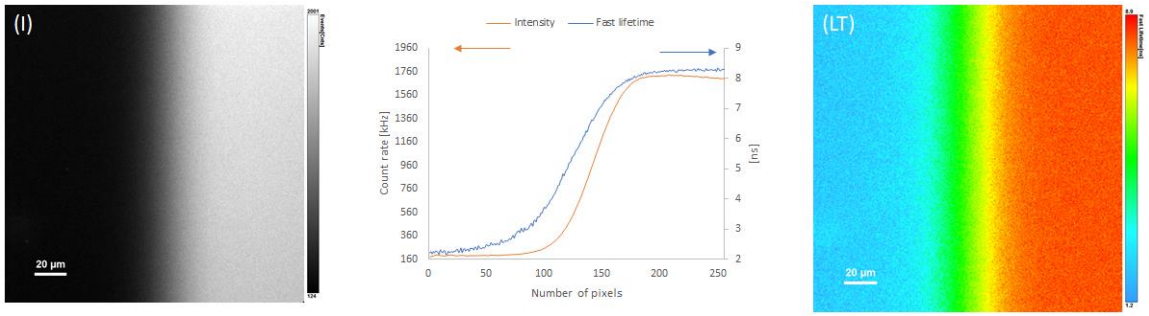

Annex 4.4 Channel modification

Channel modification was performed follow two-step procedure:

1. Pre-functionalization of PDMS surface with APTES: As first, the solution of APTES in ethanol (1:2 % v/v) was injected inside the channel and left for 5 minutes to allow APTES diffuse into the channel surface. The residual solution of APTES was removed using pressurised nitrogen. In the next step, the ammonia solution (in 2M ethanol) was introduced into the microchannel and left for the next 5 minutes. As previously, channel was purged with nitrogen and rinsed with the solvent until all residues were removed. Finally, pre-functionalized PDMS chips was left in the oven for 1h (100°C) and left for few hours to cool down.

2. The chromophore immobilization: The chromophore solution (1mg per 10mL of solvent) was inject into pre-functionalized channel. Solution of *fluorescein 5-isothiocyanate* in ethanol was left for 5min at room temperature. Solution of *2,2-bithiophene-5'-succinimidyl ester* in tetrahydrofuran (THF) required longer reaction time (up to 3h) and higher temperature 60℃. Afterwards, the chromophore solution was removed. The channel was purged with nitrogen and then rinsed with the solvent (x 3 times). At the end, modified channel was dried in the oven for 1h (100°C).

Annex 4.5 Selection of chromophore immobilization method

Channels modified by three different approaches (Table 4.1) are presented in Figure 4.21.

Table 4.1. Selection of the optimal modification method.

Approach	Pre-functionalization with APTES	Injection	Results
1	No	pre-synthesized APTES-chromophore molecule	No fluorescence
2	Yes	pre-synthesized APTES-chromophore molecule	Figure 4.20 A
3	Yes	Sole chromophore	Figure 4.20 B

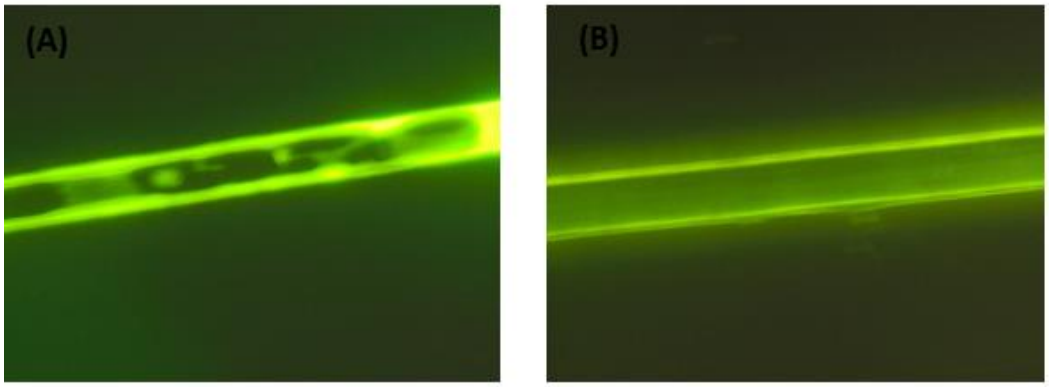

Figure 4.20. The fluorescence microscope images of modified channels.

SUMMARY

This doctoral dissertation described the process of selection and formation of an integrated photocatalytic system for organic synthesis. Particular attention has been paid to demonstrate all the requirements, which have to be met to perform an efficient photoredox transformation, and to overcome the main limitation of the photoredox catalysis. Consequently, a comprehensive study highlights, which parameters have to be considered during the selection of a suitable photocatalyst and substrates, and which factors influence the photocatalytic activity of the reaction system towards desired transformations. Moreover, the presented work demonstrates the possibility to: (i) create an integrated photocatalytic system at liquid-solid and liquid-liquid interface inside the microfluidic channel and (ii) transfer the performed organic transformation from standard batch reactor system towards flow technology.

Detailed UV-Vis spectroscopic characterization performed on several photoactive molecules allowed to select an efficient metal-free photocatalyst (*i.e*. T_3BTCH_3), which further was applied towards reductive dehalogenation reaction (of *4,7-dibromobenzo[c]-[1,2,5]thiadiazole*), coupling reaction (of *4,7-dibromobenzo[c][1,2,5]thiadiazole and 2-methylthiophene)* and polymerization reaction (of *methyl and lauryl methacrylate).* Furthermore, spectroscopic studies on the selected photocatalytic system, carried out inside the microfluidic channels, has helped to design a prototype of microfluidic devices that might be applied for the photocatalytic transformation (*e.g.* presented here debromination reaction) performed upon homogenous and heterogenous reaction conditions. Finally, spectroscopic study on the self-assembling properties of inorganic photocatalytic system (ruthenium metal complex) disclosed an interesting approach for organic synthesis, which might be supported by the photoredox catalysis and the microfluidic technology.

Chemicals

Photocatalyst

The potential organic photocatalysts examined in this work was synthesized and provided by the CNR-ISOF (Bologna, Italy) research group: **Dr. Giovanna Barbarella** and **Dr. Francesca Di Maria** (CNR-ISOF, Bologna, Italy).

Table 1. List of photocatalyst

	Photoactive organic dyes
C1	4,7-bis(5-methylthiophen-2-yl)benzo[c][1,2,5]thiadiazole
C2	5,5'''-dimethyl-2,2':5',2'':5'',2'''-quaterthiophene
C3	2-(5-(hydroxymethyl)thiophen-2-yl)-3,5-dimethyl-6-phenyldithieno[3,2-b:2',3'-d]thiophene 4,4-dioxide
C4	2,3-di([2,2'-bithiophen]-5-yl)benzo[b]thiophene 1,1-dioxide
C5	2,2- bithiophene-5'-succinimidyl ester

Reagents

The reagents employed in this work are commercially available and were supplied by Sigma Aldrich.

Table 2. List of chemical reagents

Entry	Name	CAS Number	Purity
1	2-bromothiophene	1003-09-4	98%
2	2-bromo-5-methylthiophene	765-58-2	95%
3	5-bromothiophene-2-carboxaldehyde	18791-79-2	98%
4	5-bromothiophene-2-carboxylic acid	7311-63-9	97%
5	5,5'-dibromo-2,2'-bithiophene	4805-22-5	99%
6	5,5''-dibromo-2,2':5.5'-terthiophene	98057-08-0	97%
7	4,7-dibromobenzo[c][1,2,5]thiadiazole	15155-41-6	99.5%
8	1,3-dibromo-5-octyl-4H-thieno[3,4-c]pyrrole-4,6(5H)-dione	566939-58-0	≥99.5%
9	N,N-Diisopropylethylamine	7087-68-5	≥99%
10	N,N,N',N'-Tetramethylethylenediamine	110-18-9	≥99%
11	Triethylamine	121-44-8	≥99%
12	Quinuclidine	100-76-5	≥97%
13	Methyl methacrylate	80-62-6	≥99%
14	Lauryl methacrylate	142-90-5	96%
15	Fluorescein isothiocyanate	27072-45-3	≥90%
16	3-Triethoxysilylpropylamine	919-30-2	≥98%

17	Ammonia water 28%	1336-21-6	≥99%
18	Formic acid	64-18-6	≥95%

Solvents

The solvents employed in this work are commercially available and were supplied by Sigma-Aldrich.

Table 3. List of solvents

Abbreviation	Name	CAS Number	Purity
ACN	Acetonitrile-d; anhydrous	75-05-8	99.8%
ACN-D	Acetonitrile; CD_3CN	2206-26-0	99.8%
TOL	Toluene; anhydrous	108-88-3	98%
MeOH	Methanol	67-56-1	≥99.9%
EtOH	Ethanol	64-17-5	≥99.8%
CDCl3	Chloroform-d; $CDCl_3$	865-49-6	≥99.8
THF	Tetrahydrofuran	109-99-9	≥99.9%
DMF	N,N-Dimethylformamide	68-12-2	99.8%

Instruments and photocatalytic reaction setup

Irradiation sources:

Photocatalytic reactions were carried out using LED lamp (λ_{ex}=460nm; LZ4 emitter; 10W) provide by LED Engin company, where the excitation light was modulated by the adjustment of the photon flux.

Photocatalytic reaction setup:

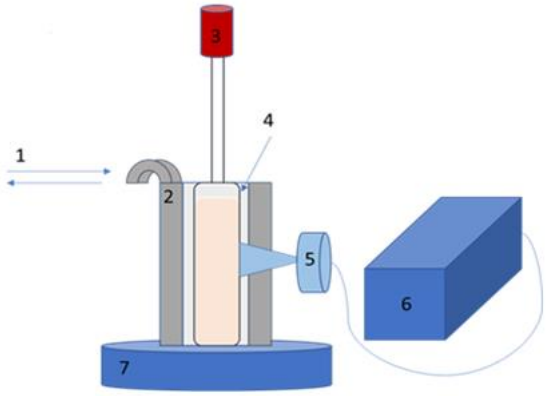

S1. Scheme of the photoreaction batch processing: (1) water cooling system (2) cuvette holder (3) quartz cuvette - photoreactor (4) mirror (5) LED light (6) power supply (7) magnetic stirrer.

Microfluidics reaction:

Flow experiments were performed using microfluidic flow control system OB1 MK3 (with the working pressure range 0-200mbar) provide by Elvesys company.

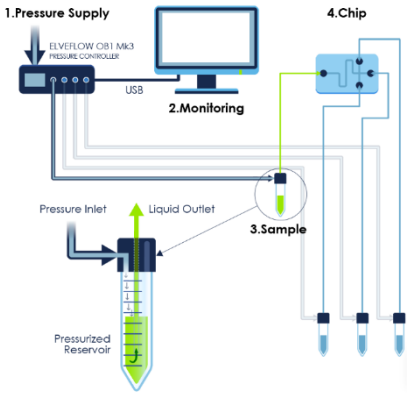

S2. Scheme of microfluidic step-up [www.elveflow.com].

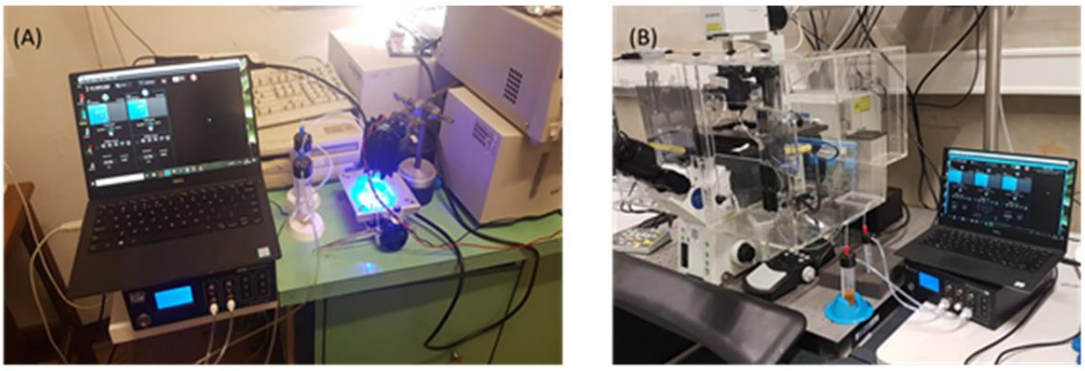

S3. Microfluidics reaction system was applied to carry out (A) the photocatalytic reaction and (B) fluorescence lifetime measurement.

Photophysical measurement applied in this study:

Ultraviolet-visible (UV-Vis) spectroscopy: The UV-Vis absorption spectra were recorded by Perkin Elmer 650 double-beam spectrophotometer at room temperature, using standard or degas quartz cuvette (Hellma®) with selected optical path length 0.1-1cm. Molar absorption coefficient values were estimated based on the Lamber-Beer law. The experimental error may be caused due to inaccuracies in the weighting of compounds and should not excess 5%.

Fluorescence spectroscopy: Fluorescence emission and excitation spectra were registered in the range of 200-900nm by Perkin Elmer LS55 spectrofluorometer equipped with Hamamatsu R928 photomultiplier using (Suprasil) quartz cuvette.

Singel photon lifetime measurement (TCSPC): Fluorescence lifetime were measured with the Edinburgh spectrometer using time corellated single-photo counting technique. Pulsed diod laser (300nm or 405nm) provide by Picoquant were used as a exciation source.

Fluorescence lifetime imagine microscopy (FLIM): were performed using confocal microscope (Leica TCS SMD) integrated with The SymPhoTime 64 software for lifetime measurement. The Leica TCS system were equipped with HC PL APO CS2 10.0 DRY

objective. Diode laser (λ=405nm) with modulated frequencies (20MHz/40MHz) were used as an excitation light. Internal detector with spectral detection range between (410-600 nm) and acquisition time up to 2000 photon/pixel were applied.

Nuclear magnetic resonance spectroscopy (^{1}H NMR): spectra were recorded on a Varian Mercury-400 spectrometer. Chemical shifts were calibrated using the internal CD_3CN or $CDCl_3$ resonance which was referenced to TMS (Tetrametylosilan).

Gas chromatography and mass spectrometry (GC-MS): Spectra were taken by EI-electron ionization at 70 eV on a Hewlett-Packard 5971 with GC injection. LC-electrospray ionization mass spectra (ESI-MS) were obtained with Agilent Technologies MSD1100 single-quadrupole mass spectrometer. They are reported as: *m/z* (rel. intense).

The gel-permeation chromatography (GPC): The molecular weights were obtained by gel-permeation chromatography (GPC) using a1100 HPLC system (Agilent Technologies, USA) equipped with PL gel 5-µm MiniMIX-C column(Agilent Technologies, USA) (length = 250 mm, internal diameter = 4.6 mm). A refractive index was employed as detector. In all cases, chloroform was used as eluent with a 0.3 mL/min flow.
The GPC measurements were performed by **Prof. Chiara Gualandi** - Department of Polymer Chemistry "Giacomo Ciamician – University of Bologna" .